Dynamique de l'adaptation de Cryptococcus neoformans à l'hôte

Alexandre Alanio

UNIVERSITE PARIS DIDEROT (Paris 7)

INSTITUT PASTEUR

ECOLE DOCTORALE : BIOCHIMIE, BIOTHÉRAPIE, BIOLOGIE MOLÉCULAIRE ET INFECTIOLOGIE (B3MI)

DOCTORAT BIOLOGIE GENETIQUE ET IMMUNOLOGIE DES INFECTIONS PARASITAIRES

spécialité Microbiologies procaryote et eucaryote

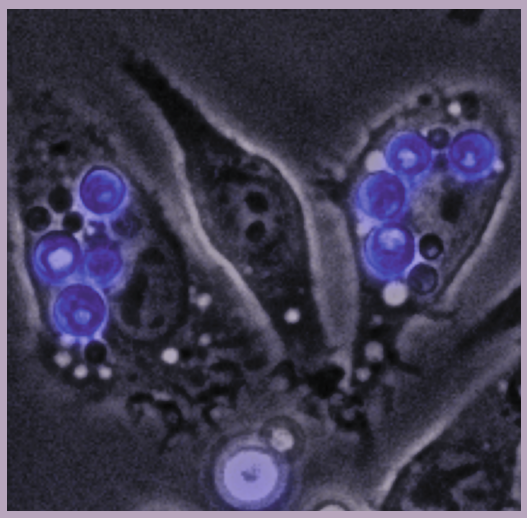

ALEXANDRE ALANIO

DYNAMICS OF *CRYPTOCOCCUS NEOFORMANS* ADAPTATION TO HOST

Thèse dirigée par le Pr Françoise Dromer

Soutenue le 16 décembre 2013

JURY

Pr Olivier Dussurget, Président

M. Oscar Zaragoza, Rapporteur

Pr Patrice Le Pape, Rapporteur

M. Guilhem Janbon, examinateur

Mme Priscille Brodin, examinateur

Pr Françoise Dromer, examinateur

Je dédie de cette thèse à ma grand-mère Anna Nikiforovna Karpova Alanio cette petite dame de Leningrad qui a traversé brillamment le 20ème siècle,

A mes parents et mon frère bien-aimés,

A ma femme et mes enfants adorés,

A mes beaux-parents, beaux-frères et belles-soeurs,

A toutes les personnes qui ont fait de moi l'homme que je suis,

A ma troisième famille du laboratoire de mycologie moléculaire et du centre National de référence mycologie et antifongiques.

A mes 'mentors' Françoise Dromer, Stéphane Bretagne et Olivier Lortholary,

« On n'a que peu de reconnaissance pour un maitre quand on reste élève»

FRIEDRICH NIETZSCHE
Ainsi parlait Zarathoustra, 1883
De la vertu qui donne

A Jordi Savall, Monserrat Figueras et Hesperion XXI,

A Fedor Dostoievski et Friedrich Nietzsche qui m'ont accompagnés ces années durant,

«Les jours humides et sombres, la solitude, les paroles sans amour que l'on nous adresse, font naitre en nous des conclusions *semblables à des champignons : nous les voyons apparaitre devant nous, un matin, sans que nous sachions d'où elles viennent et elles nous regardent, grises et moroses. Malheur au penseur qui n'est pas le jardinier, mais seulement le terrain de ses plantes !»*

FRIEDRICH NIETZSCHE
Aurore, Pensées sur les préjugés moraux,1881
Livre quatrième

Abbreviations:

AFLP: Amplified fragment length polymorphism

APC: Allophycocyanin

BF: Bright field

BsH2: Baseline at 2 hours

CALCO: Calcofluor

CD: Cluster of differentiation

CFU: Colony forming unit

ClinCn: clinical isolates of *C. neoformans*

CMFDA: 5‘chloromethylfluorescein diacetate

$CMFDA^{sur}$: surrounded CMFDA

$CMFDA^{intra}$: intracellular CMFDA

Cn: *Cryptococcus neoformans*

CNS: Central nervous system

CSF: Cerebrospinal fluid

Cy3: Cyanine 3

DAPI: 4′,6-diamidino-2-phenylindole

DiEM; Diethyl maleate

DMEM: Dulbecco’s modified Eagle medium

DMSO : Dimethylsulfoxide

FCS: Fetal calf serum

FITC: Fluorescein isocyanate

FSC: Forward scatter

IgG: Immunoglobulin G

iH2: Intracellular at 2 hours

IPH2: Intracellular proliferation at 2 hours

IPH48: Intracellular proliferation at 48 hours

J774: J774.16 macrophage cell-line

KO: Knock-out

KOG: Eukaryotic orthologous groups

mAb: monoclonal antibody

MAT: Mating type

MLST: Multi locus sequence typing

MO: Mouse

MP: Macrophage

OD: Optical density

OR: Odds ratio

PBS: Phosphate buffer saline

PCA: Principal component analysis

PE: R-Phycoerythin

PFA: Paraformaldehyde

PI: Phagocytic index

rcf: Relative force centrifugation

rpm: Revolutions per minutes

RT-PCR: Real-time polymerase chain reaction

SAGE: Serial analysis of gene expression

SD: Standard deviation

SSC: Side scatter

sSTAT: Stained stationary phase yeasts

STAT: Stationary phase

TOPRO: TO-PRO-3 iodide

YNB: Yeast nitrogen base medium

YPD: Yeast extract peptone glucose medium

YPDps: YPD+10% Penicillin/Streptomycin

Summary in French:

Cryptococcus neoformans (*C. neoformans*) est une levure opportuniste basidiomycète cosmopolite de l'environnement. Ce champignon a la particularité de survivre à la phagocytose de nombreux organismes allant des protozoaires unicellulaires aux cellules immunitaires spécialisées des mammifères (macrophages, cellules dendritiques, neutrophiles). Il s'agit d'un microorganisme intracellulaire facultatif, ce qui lui confère notamment la possibilité d'échapper au système immunitaire et d'utiliser les cellules hôtes comme véhicules (stratégie du cheval de Troie) pour franchir les barrière épithéliales de l'organisme.
Cette levure est responsable de la cryptococcose qui est une infection opportuniste survenant le plus souvent à un stade avancé du déficit immunitaire lors de l'infection par le VIH ou à l'occasion d'autres déficits immunitaires cellulaires (greffe d'organe solide, déficit lymphoïde chronique, corticothérapie au long cours, …).
Les isolats responsables de la cryptococcose chez l'homme sont divers en terme de sérotypes, de mating-type et de ploïdie. Les différentes espèces/variétés capables de provoquer la cryptococcose sont *C. neoformans* var. *grubii* (sérotype A), *C. neoformans* var. *neoformans* (sérotype D) et *Cryptococcus gattii* (sérotype B et C) [1]. *Cryptococcus neoformans* se multiplie par bourgeonnement (mode asexué) mais est également capable d'une reproduction sexuée impliquant des mating-types de signes opposés (MATa et MATalpha) mais également de même signe sexuel qui contribue de façon importante à la variabilité des populations même si la reproduction asexuée est le mode d'expansion principal [1]. Une variabilité de ploïdie existe également chez cette levure majoritairement haploïde, avec la possibilité d'aneuploïdie, de diploïdisation. Au final, les isolats cliniques à l'échelle mondiale sont majoritairement des souches de *C. neoformans* var. *grubii*, MATalpha et haploïde.
Le Center for Diseases Control (CDC, Atlanta, USA) a récemment estimé à 1 million/an le nombre de cas de cryptococcose neuro-méningée et 700 000 décès associés, ce qui fait de cette entité une pathologie aussi préoccupante que la tuberculose en termes de santé publique mondiale [2]. La cryptococcose est une infection le plus souvent disséminée, au cours de laquelle la localisation méningo-encéphalique est la plus fréquente et la plus grave. La méningo-encéphalite est toujours mortelle en l'absence de traitement, et reste fatale dans environ 20% des cas malgré un traitement antifongique [3]. L'atteinte pulmonaire est la deuxième localisation viscérale. Chez l'homme, l'infection commence par l'inhalation de particules infectantes que l'on suppose être des basidiospores ou des levures desséchées présentes dans le milieu extérieur. La primo-infection a lieu dans l'enfance et passe le plus souvent inaperçue ou sous la forme d'une pneumonie non étiquetée. Le système immunitaire est habituellement efficace pour contrôler la maladie mais des levures persisteraient ensuite dans l'organisme dans les macrophages alvéolaires et/ou dans un granulome tissulaire pulmonaire pendant une phase dite de latence. A ce stade, on suppose que les levures sont dormantes. La notion de dormance a été démontrée épidémiologiquement [4] mais aucune preuve biologique n'existe à ce jour. L'infection survient si, à la faveur d'une immunodépression (principalement cellulaire), les levures se réactivent, pour ensuite se multiplier puis disséminer via la circulation sanguine dans l'organisme [5]. La traversée de la barrière hémato-encéphalique va alors conduire à une méningo-encéphalite qui est la présentation clinique la plus commune et la plus grave.
D'un point de vue général, on sait que les déterminants des maladies infectieuses dépendent de facteurs d'hôtes et de facteurs spécifique au pathogène. Certains facteurs

de virulence ont déjà été bien identifiés dans des modèles expérimentaux murins mais aussi chez l'homme et *in vitro* au cours de l'interaction avec les macrophages.
Bien que la diversité des isolats de *C. neoformans* soit relativement bien établie en terme de génotypes [6], la diversité de l'adaptation de la levure à divers environnements n'est que partiellement connue. En particulier, il n'est toujours pas définitivement établi comment la variabilité d'évolution de la maladie chez l'homme pourrait être reliée au statut immunitaire ou au patrimoine génétique du patient, à des facteurs fongiques ou à leur combinaison. Ces facteurs fongiques sont d'ailleurs habituellement étudiés à partir de souches de référence et des mutants qui en sont générés mais rarement à partir de souches cliniques. Récemment, il a été montré pour *C. gattii*, qu'un génotype spécifique (VGII, responsable d'une épidémie sur l'Ile de Vancouver en Colombie Britannique, Canada) était associé à un phénotype particulier avec une augmentation de la capacité de prolifération intracellulaire des levures *in vitro* mais également un plus grande virulence chez la souris [7]. Pour *C. neoformans*, l'influence d'un génotype ou d'un phénotype particulier sur l'évolution de la maladie n'a pas encore été mise en évidence.

L'objectif de mon travail était de comprendre comment la diversité des isolats cliniques de *C. neoformans* pourrait influencer l'évolution et les caractéristiques de l'infection. Pour répondre à cette question, nous avons exploité (i) les souches et les données cliniques collectées au cours de l'étude CryptoA/D (étude clinique multicentrique coordonnée dans le laboratoire) (ii) un modèle de cryptococcose disséminée murine cliniquement pertinent (iii) un modèle d'interaction avec le macrophage *in vitro* et nous avons mis au point de nombreux outils permettant une quantification précise de différents paramètres. Nous nous sommes ensuite orientés vers l'étude de l'adaptation de *C. neoformans* dans ces mêmes modèles expérimentaux.

Dans un premier temps nous avons mis au point un modèle d'interaction entre les levures et les macrophages en utilisant la lignée cellulaire J774 de macrophage murin et la souche de référence de *C. neoformans* H99. Nous nous sommes particulièrement intéressés à l'indice de phagocytose (nombre de levures internalisées pour 100 macrophages) et la prolifération intracellulaire des levures (taux de levures générées après une durée d'incubation définie). Pour cela, nous avons mis au point des méthodes basées sur des marqueurs fluorescence [anticorps anti-capsule couplés à des anticorps secondaires fluorescents et un marqueur fluorescent spécifique de la chitine (Calcofluor)] et avons quantifié ces paramètres en cytométrie de flux quantitative (MacsQuant analyser). Le calcofluor permet de marquer en fluorescence (bleu) la paroi des levures (cellules mères) qui en se multipliant vont transmettre une partie de leur fluorescence à la paroi des levures filles. Les levures filles vont donc être marquées plus faiblement que les levures mères. Il est ainsi aisé de différencier les levures mères et filles et de calculer la prolifération des levures en cytométrie de flux. Nous avons ensuite validé le modèle et les outils à l'aide de mutants (KO) de différents gènes de virulence bien caractérisés, générés dans le fond génétique de la souche de référence H99 [*lac1Δ* (KO pour la laccase 1, Lac1), *vps34Δ* (KO pour la PI3 kinase, Vps34), *vad1Δ* (KO pour la DEAD-box RNA helicase, Vad1) and *app1Δ* (KO pour l'antiphagocytic protein, App1), *ipc1Δ* (pour lequel l'inositol-phosphoryl ceramide synthase, Ipc1, est sous-exprimée)] et dont le phénotype d'interaction avec le macrophage était bien connu.
Après ces mises au point, nous avons criblé 54 souches cliniques *C. neoformans* var. *grubii* MATalpha haploïdes isolées de liquides céphalorachidiens de 54 patients immunodéprimés (VIH et non-VIH) et comparé les données à celles obtenues avec la souche

de référence H99 dans les mêmes conditions. Les 54 souches ont été sélectionnées dans la collection issue de l'étude CryptoA/D et nous disposions donc des données cliniques associées.
Nous avons pu montrer que les souches cliniques étaient diverses intrinsèquement en terme de production de mélanine, d'uréase, et de capacité de multiplication (courbes de croissance). Il existait également une diversité importante de leur interaction avec les cellules J774 mesurée par l'indice de phagocytose (PI, variation de 30 fois), et les indices de prolifération intracellulaire à 2 heures (IPH2, 50 fois) et à 48 heures (IPH48, 16 fois). Grâce aux données cliniques associées à ces souches, nous avons pu mettre en évidence que deux phénotypes particuliers étaient associés à des évolutions cliniques défavorables. Les souches fortement phagocytées (ratio ≥ 0,5 par rapport à H99) et qui avaient un indice de prolifération important à 2 heures (ratio > 1 par rapport à H99) avaient été isolées de patients pour lesquels l'évolution avait été plus souvent fatale (p=0.05) et les souches peu phagocytées (ratio < 0.5) et avec un indice de prolifération faible (ratio ≤ 1) avaient été plus souvent isolées de patients en échec du traitement d'induction (15 jours de bithérapie antifongique). Sur les 54 souches cliniques initiales, nous avons ensuite sélectionné 9 souches cliniques aux phénotypes extrêmes et variables et avons approfondi l'étude de leur virulence à l'aide du modèle murin d'infection et en analysant l'expression de différents gènes de virulence dans le modèle d'interaction avec le macrophage. La virulence de ces isolats était variable, certains isolats étant plus (AD2-82a) et d'autres moins virulents (AD1-07a, AD1-95a) que H99. D'autre part, il existait également une corrélation inverse entre l'expression du gène *APP1* de la levure (connu pour son action anti-phagocytaire) et l'indice de phagocytose des souches cliniques, et une corrélation entre expression des gènes de virulence *IPC1*, *VAD1*, *APP1*, *COX1* (PCR quantitative en temps réel), et la prolifération intracellulaire à 48H des souches cliniques.
Ces résultats suggèrent fortement que les souches cliniques sont différentes intrinsèquement en terme de phénotype d'interaction avec les macrophages, ce qui avait été montré avec quelques souches et des polynucléaires neutrophiles humains [8], et que ce phénotype pourrait influencer l'évolution de la maladie et la réponse au traitement chez l'homme, ce qui en revanche n'avait jamais été démontré. Les souches de phénotype "forte phagocytose/forte prolifération" pourraient être responsable de la plus grande mortalité en raison des dégâts qu'elles pourraient causer aux macrophages sensés contrôler la maladie après phagocytose, aboutissant à leur lyse et au relargage ultérieur de nombreuses levures dans le milieu extérieur. Par ailleurs, les cellules de phénotype "faible phagocytose/faible prolifération" pourraient être plus résistantes au traitement d'induction en raison de leur faible prolifération ou d'un potentiel état "dormant". L'hypothèse que nous soulevons ici provient des données générées au cours de l'interaction avec le macrophage. En effet, après 48 heures d'interaction avec le macrophage, il persiste une population de levures mères (environ 30%), donc supposée ne pas s'être divisée, alors qu'en condition de croissance maximale *in vitro*, cette proportion est très faible. La proportion de ces cellules supposées dormantes est également variable d'une souche à l'autre.

Pour mettre en évidence ce phénomène de dormance, nous avons mis en place de nombreux autres outils basés sur une analyse morphologique et en cytométrie de flux en nous focalisant sur les modèles de cryptococcose murine et d'interaction avec le macrophage. Nous avons utilisé le calcofluor pour suivre la prolifération des levures *in vivo* et dans les macrophage associé à un marqueur de viabilité des levures (TOPRO) et un marqueur de stress intracellulaire (CMFDA [9], associé au taux de glutathion in-

tracellulaire) après avoir testé ces marqueurs dans différentes conditions de stress (incubation dans l'eau, dans l'eau oxygénée, dans le milieu de culture cellulaire). Nous avons ensuite étudié l'évolution de ces marqueurs au cours de l'infection dans les poumons des souris et au cours de l'interaction avec les macrophages. Il est apparu qu'au cours des premières heures après infection ou internalisation dans les macrophages, la fluorescence CMFDA augmentait dans les levures suggérant une bonne adaptation au stress, mais après quelques heures d'incubation supplémentaires, une population de cellules avec une faible fluorescence CMFDA apparaissait. Ce phénomène concernait un faible nombre de cellules et d'abord les levures mères puis les levures filles.

Ainsi, pour explorer cette population faiblement marquée au CMFDA et minoritaire, nous avons du infecter un nombre important de souris. Nous avons ensuite analysé les levures issues du broyat de tous ces poumons à l'aide d'une machine appelée Imagestream^X, permettant d'analyser la morphologie (photos de chaque évènement) de 10 000 cellules dans plusieurs canaux de fluorescence en flux et de mettre ainsi en parallèle l'intensité de la fluorescence avec la morphologie de la cellule. Cet outil nous est apparu comme essentiel pour détecter les artéfacts de fluorescence et les éliminer, et ainsi interpréter correctement les données générées par l'analyse des levures extraites des broyats de poumons. Sept jours après infection dans les poumons des souris et 24 heures après l'interaction avec les macrophages, nous avons constaté la présence de populations ayant respectivement une fluorescence élevée, modérée ou faible au CFMDA. La répartition des différentes populations était variable en fonction de la souche étudiée (souches cliniques AD1-07a, AD1-83a) en comparaison à la souche de référence H99. En analysant plus finement la population ayant une fluorescence CMFDA élevée, nous avons ainsi pu constater qu'une grande proportion de cette population correspondait à des levures mortes. Ceci a été possible grâce à l'utilisation de différents marqueurs cellulaires permettant l'analyse de la quantification des ARN totaux, de l'activité mitochondriale, et de la morphologie des membranes plasmiques et du noyau. Ensuite, nous avons pu mettre en évidence à l'aide des algorithmes d'analyse d'image disponibles dans le logiciel Imagestream^X, qu'une population de levures faiblement fluorescentes en CMFDA avait une morphologie particulière par rapport aux autres populations.

Nous avons ensuite entrepris de trier les levures issues des poumons et après interaction avec le macrophage pour analyser les capacités de croissance et l'expression de certains gènes de ces différentes populations en comparaison aux levures en fin de croissance in vitro (phase stationnaire). Nous avons pu montrer que les levures faiblement fluorescente au CMFDA issues des poumons de souris avaient une capacité de croissance inférieure à celle des autres populations et étaient dépendantes de la présence de sérum de veau fœtal pour stimuler leur croissance. Après analyse (single-cell PCR quantitative en temps réel) l'expression de différents gènes impliqués dans les phénomènes de résistance à la restriction en nutriment, d'entrée en phase stationnaire, d'autophagie ou de la synthèse de la paroi ou de la capsule, nous avons pu montrer que les populations de cellules faiblement fluorescente au CMFDA (provenant de poumons de souris ou de macrophages) sur-exprimaient un gène mitochondrial (*COX1*) et d'autophagie (*ATG9*) et sous-exprimait les gènes impliquées dans la néoglucogenèse (*PCK1*) à l'inverse des autres populations.

Ainsi, grâce à la mise en place de nouveaux outils, nous avons des arguments pour penser que la population de levures faiblement fluorescente au CMFDA pourrait être une population composée de levures dormantes. Le gène mitochondrial *COX1* et les protéines associées à l'activité respiratoire sont connues pour être sur-exprimées en

réponse à l'hypoxie à l'inverse de ce qui se peut se passer avec *Saccharomyces cerevisiae*, *Schizosaccharomyces pombe* ou *Candida albicans* [10]. Pour valider ce phénomène, il est maintenant indispensable de pourvoir générer un grand nombre de levures ayant ce phénotype dans des conditions standardisées. Nous sommes actuellement en train de tester différents milieux et conditions de culture pour répondre à ce besoin. Si ces expériences se concrétisent, nous aurions le moyen d'étudier la biologie de la dormance chez *C. neoformans*, et ainsi les moyens d'éradiquer ces levures dormantes chez les patients immunodéprimés à risque de cryptococcose.

Références :

1. Lin X, Heitman J (2006) The biology of the *Cryptococcus neoformans* species complex. Annu Rev Microbiol 60: 69–105. doi:10.1146/annurev.micro.60.080805.142102.
2. Park BJ, Wannemuehler KA, Marston BJ, Govender N, Pappas PG, et al. (2009) Estimation of the current global burden of cryptococcal meningitis among persons living with HIV/AIDS. AIDS 23: 525–530.
3. Dromer F, Mathoulin-Pélissier S, Launay O, Lortholary O, Group F (2007) Determinants of disease presentation and outcome during cryptococcosis: the CryptoA/D study. Plos Med 4: e21.
4. Garcia-Hermoso D, Janbon G, Dromer F (1999) Epidemiological evidence for dormant *Cryptococcus neoformans* infection. J Clin Microbiol 37: 3204–3209.
5. Dromer F, Casadevall A, Perfect J, Sorrell T (2010) *Cryptococcus neoformans*: Latency and Disease. *Cryptococcus*: From Human Pathogen to Model Yeast. ASM Press. p.429.
6. Litvintseva AP, Thakur R, Vilgalys R, Mitchell TG (2006) Multilocus sequence typing reveals three genetic subpopulations of *Cryptococcus neoformans* var. *grubii* (serotype A), including a unique population in Botswana. Genetics 172: 2223–2238.
7. Ma H, Hagen F, Stekel DJ, Johnston SA, Sionov E, et al. (2009) The fatal fungal outbreak on Vancouver Island is characterized by enhanced intracellular parasitism driven by mitochondrial regulation. Proc Natl Acad Sci USA 106: 12980–12985.
8. Kozel TR, Pfrommer GS, Guerlain AS, Highison BA, Highison GJ (1988) Strain variation in phagocytosis of *Cryptococcus neoformans*: dissociation of susceptibility to phagocytosis from activation and binding of opsonic fragments of C3. Infect Immun 56: 2794–2800.
9. Nicola AM, Robertson EJ, Albuquerque P, Derengowski LDS, Casadevall A (2011) Nonlytic Exocytosis of *Cryptococcus neoformans* from Macrophages Occurs In Vivo and Is Influenced by Phagosomal pH. MBio 2: e00167–11–e00167–11.
10. Chun CD, Liu OW, Madhani HD (2007) A link between virulence and homeostatic responses to hypoxia during infection by the human fungal pathogen *Cryptococcus neoformans*. PLoS Pathog 3: e22.

Introduction

Cryptococcus neoformans (*C. neoformans*) is basidiomycetous opportunistic yeast that is widely present in the environment. This fungus can survive the predation of various organisms ranging from protozoans to metazoans through ready-made virulence traits [1]. *Cryptococcus neoformans* interacts closely with uni- or multicellular organisms that are natural predators in nature (amoeba, paramecium, nematodes) [2-4] and with cells dedicated to innate immune response of metazoans (macrophages, dendritic cells, natural-killer lymphocyte) with various propensity to phagocytose and kill the yeasts [5,6]. Intracellular persistence in immune cells provides advantages to the fungus by allowing escape of the immune response and later dissemination through epithelial barriers [7,8].

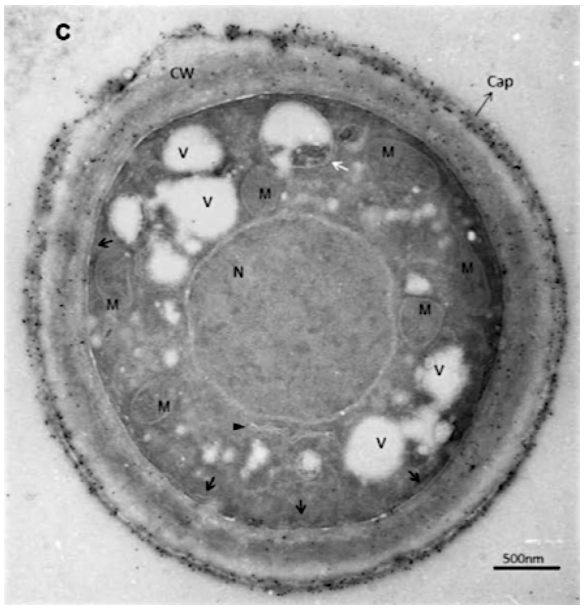

Cryptococcus neoformans ultrastructure (adapted from Oliveira et al. 2009)
(N: nucleus, M: mitochondria, V: vacuoles, CW: cell wall, Cap: capsule)

With 1 million cases per year and 700,000 annual deaths, cryptococcosis is one of the most frequent invasive fungal infection, worldwide [9]. It occurs mostly in patients with immune defects, especially those with AIDS, but also non-HIV immunocompromised patients (sarcoidosis, solid organ transplantation, steroid or other immunosuppressive therapy) [10]. Cryptococcosis is a multifaceted pathology in terms of clinical presentation and outcome, with meningoencephalitis being the most frequent and severe presentation. Despite three months of adequate antifungal treatment, 15-20% patients will die from cryptococcosis [11]. In humans, the infection begins after inhalation of basidiospores or desiccated yeasts [12]. Primo-infection occurs in childhood with unrecognized pneumonia [13]. Yeasts are then controlled by the immune system through granuloma formation [14] and adaptive immunity with production of antibodies against *C. neoformans* antigens [13]. From this point on and until immunosuppression occurs, yeasts remain invisible. The disease is latent [15] and the yeasts are dormant as demonstrated epidemiologically [16,17]. When/if immunodeficiency occurs, yeasts reactivate and replicate probably in the lung and disseminate through the bloodstream to different organs. Crossing of the brain blood barrier leads to meningoencephalitis, the most common and more severe clinical presentation [12,18-20].
From an experimental point of view, the pathophysiology of the infection has been mainly studied in rats that are naturally controlling *C. neoformans* lung infection and more

extensively in mice that are susceptible to infection. Characteristics of the infection depend on both hosts and microbial factors. Fungal factors described as virulence factors influence the outcome of infection according to data obtained in the mouse model of cryptococcosis [21], but also *in vitro* [22] and in humans [23]. Microbial adaptation to the hosts is complex and had been studied globally in lungs using histopathology [24] and global transcriptome analysis upon amoeba [3] and macrophage [25] ingestion or upon early infection of mice and rabbits [26,27].

Isolates responsible for cryptococcosis are diverse in terms of species, serotype, mating type, and ploidy. This includes *Cryptococcus neoformans* variety *grubii* (serotype A) or variety *neoformans* (serotype D), and *Cryptococcus gattii* (serotype B and C). *Cryptococcus neoformans* propagates by budding and is also capable of sexual multiplication and same-sex mating, which contributes to the high diversity of the overall population even if asexual expansion is the predominant feature [28]. Haploid *C. neoformans* serotype A *MAT*α isolates represent the most prevalent clinical isolates worldwide. Clinical isolates can be haploid or diploid, mating type alpha (*MAT*α) or a [29]. In addition, single (one strain) or mixed (mixture of isolates belonging to various serotypes, mating types, genotypes and/or ploidies) infections have been described [30]. *Cryptococcus* spp. is present in the environment especially in soil, trees (Eucalyptus tree in Australia and mopane trees in Africa) and decaying wood [29]. A strong association between *C. neoformans* var. *grubii* and guano from *Columba livia* (feral pigeons) was found in the 1950s [31,32]. The relation with pigeons was also evidenced based on serological studies of pigeon fanciers that revealed a higher cryptococcal antibody compared to controls [33,34]. Genetic relatedness between environmental (pigeon droppings) and clinical isolates is observed [35-37]. It is demonstrated that *Columba livia*, that was domesticated 5,000 years ago and spread globally from Africa over the last 400 years, is responsible for the worldwide distribution of *C. neoformans* var. *grubii* during the past centuries. Indeed, genetic divergence between cosmopolitan (low genetic diversity) and African (higher genetic diversity) is observed in environmental isolates and dated around 5,000 years ago [38,39]. Overall, clinical and environmental isolates harbor a huge diversity in terms of genotype [38] and phenotype [40,41]. From a evolutionary point of view, this gives advantage to the fungus to survive various complex environments ranging from soil or trees to mammalian hosts.

1. Surviving humans

Cryptococcosis is one of the most frequent fungal invasive infection in humans worldwide [9]. It occurs mostly in patients with immune defects, especially those with AIDS, but also in patients exposed to immunosuppressive therapy [10]. The pathophysiology of cryptococcosis is reminiscent of that of tuberculosis with a phase of latency. Reactivation can be observed years after primary infection usually through the respiratory route [15]. Upon immunosuppression, reactivation and dissemination can occur and the infection can be hard to control and treat despite active antifungal drugs [11].

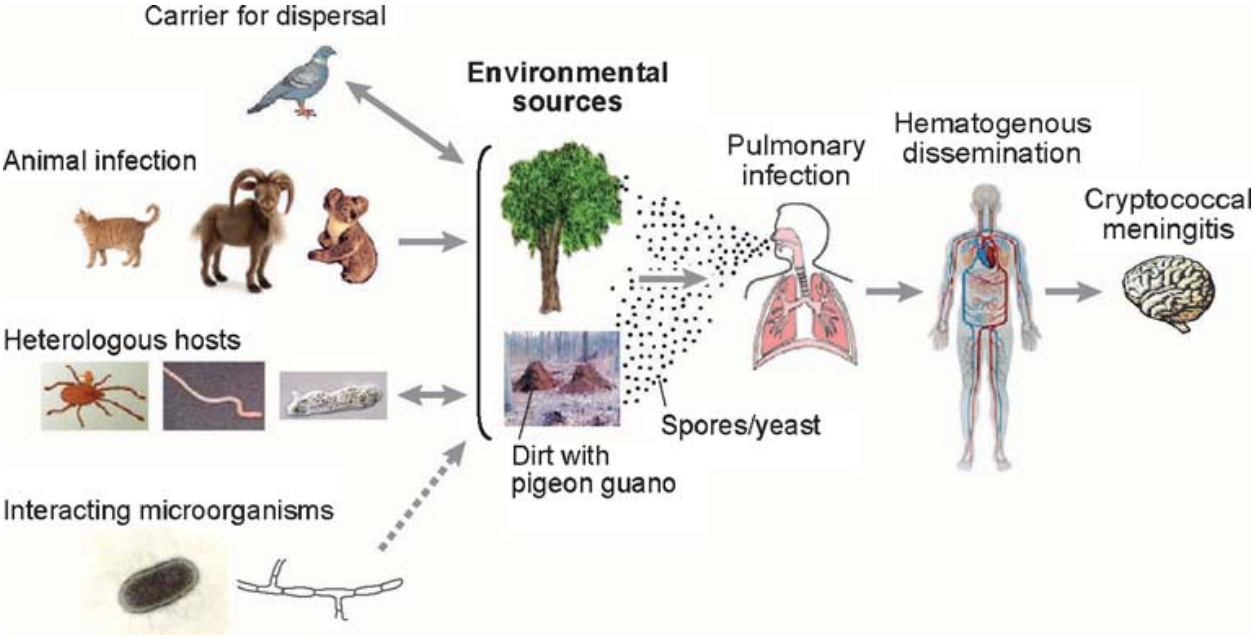

Schematic representation of the route of infection for cryptococcosis in humans (adapted from [29])

1.a. The earlier, the longer

Inhalation of aerosolized particles from soil (desiccated yeasts or basidiospores) is thought to be the major route of infection in humans [12]. Primoinfection with *C. neoformans* occurs mainly in immunocompetent children as demonstrated by serological studies with unrecognized (asymptomatic) infection as the main clinical presentation. The proportion of children immunized against *C. neoformans* increases with age. Acquisition of cryptococcal antibodies begins very early (1 year) with minimal reactivity of the sera. After 5 years, 70% of the children reacts with *C. neoformans* antigens [13]. However, the acquisition of anti-cryptococcal humoral immunity varies among geographic areas. Cryptococcal antibodies are very common in Bronx children but not in another New York areas (Dutchess County) or in Manila (The Philippines), another densely populated urban area [95]. Environmental exposure may depend on climatic and environmental factors (temperature, humidity, pigeon density), but also on human sociological factors (habitat conditions, financial resources). These findings supports epidemiological data revealing that cryptococcosis in immunocompromised individuals is more prevalence in some areas of the world, especially in Africa [9].

Of note, *C. gattii* exposure and primoinfection does not follow the same epidemiological trends than *C. neoformans* based on studies realized in endemic areas in animals and humans [15].

1.b. Waiting for better days

Serologic evidence of early cryptococcal immunity in immunocompetent hosts without recognized infection seems paradoxical with the very low frequency of cryptococcosis in immunocompetent hosts. However, immune control of the yeasts by immunocompetent hosts following primoinfection is possible with latency of the disease or complete clearance of the fungus as a consequence. Immunocompetent adults frequently exposed to *C. neoformans* had positive skin test but did not develop clinical disease [96]. Autopsy studies have raised the hypothesis that pulmonary granulomas could be the place for persistence since *C. neoformans* is observed in sub-pleural nodules and draining lymph nodes in immunocompetent and immunocompromised hosts [14]. Analysis of clinical isolates of *C. neoformans* var. *grubii* recovered in France from patients born in Africa (median of 110 months) prior to moving to France, revealed that genotypes from these patients clustered together, apart from those recovered from patients born in Europe [16]. This study is the main epidemiological evidence for dormancy of *C. neoformans*. The same conclusion is also drawn based on a serologic survey of solid organs transplant recipients (immunocompromised hosts) with analysis of sera obtained prior to transplantation and at the time they developed cryptococcosis. Indeed, early cryptococcosis after transplantation is observed preferentially in patients exhibiting serologic evidence of cryptococcal infection before transplantation [97]. Additionally, report of *C. gattii* infections in patients who travelled endemic areas years or month before, provides another evidence for dormancy before the Vancouver Island *C. gattii* outbreak [17].
However, symptomatic infection following primoinfection with or without further dissemination exists [98-100]. These acute infections occur mainly in immunocompromised or immunocompetent patients who were recently exposed to environmental sources of yeasts via massive inhalation or skin injury, leading to acute pulmonary [101,102] or to primary cutaneous [103] cryptococcosis, respectively.

1.c. Wake up and spread

The first manifestation of reactivation is observed in HIV-infected individuals for which asymtomatic cryptococcal antigenemia is detected [104-106]. Viable yeasts are not recovered from clinical sample at this step but treatment is mandatory to prevent symptoms and dissemination [107]. Pulmonary cryptococcosis is a well-described clinical entity that can evolve differentially depending on the immune status of the hosts. In immunocompetent hosts, *C. neoformans* does not usually disseminate, whereas the possibility of dissemination in immunocompromised patients is high. It is likely that dissemination occurs after reactivation of lung-persistent yeasts, crossing the lung epithelial barrier and disseminate through capillary blood [12]. However, pulmonary symptoms are not the principal clinical manifestation of cryptococcosis in immunocompromised patients. Indeed, most are diagnosed at the stage of dissemination or meningoencephalitis [11].

1.d. A thick-skinned fungus

Cryptococcosis is characterized by a high frequency of central nervous system (CNS) involvement with positive cerebrospinal fluid (CSF) and dissemination through blood. Cryptococcosis is more severe in male, HIV-positive patients, and those infected with serotype A [11]. Acute cryptococcal meningoencephalitis is always fatal without antifungal therapy [20]. It requires an antifungal therapy induction based on amphotericin B and flucytosine for a minimum of 2 weeks [108]. Mycological failure after 2 weeks of induction is recognized as a factor of bad prognosis, which requires continuation of the induction therapy [108]. Mycological failure is independently associated with initial dissemination, high serum antigenemia (>1:512) and lack of initial flucytosine treatment [11]. The three-months mortality rate during the management of acute cryptococcal meningoencephalitis approximates 20% despite adequate treatment. It is still not clear whether this mortality rate is due to individual's immune status, genetic factors [109], fungal determinants or a combination of them.

2. Surviving host cells

Cryptococcus neoformans is a facultative intracellular pathogen [24]. Interaction of *C. neoformans* with host cells can lead to phagocytosis, with occasional escape to the extracellular space (vomocytosis), and possible yeast transfer between phagocytic cells [28,42]. *Cryptococcus neoformans* is capable of replication within the phagolysosome, sometimes associated with host cell lysis [29,42]. These phases have been well studied in different models of interaction with host cells but mainly within macrophages.

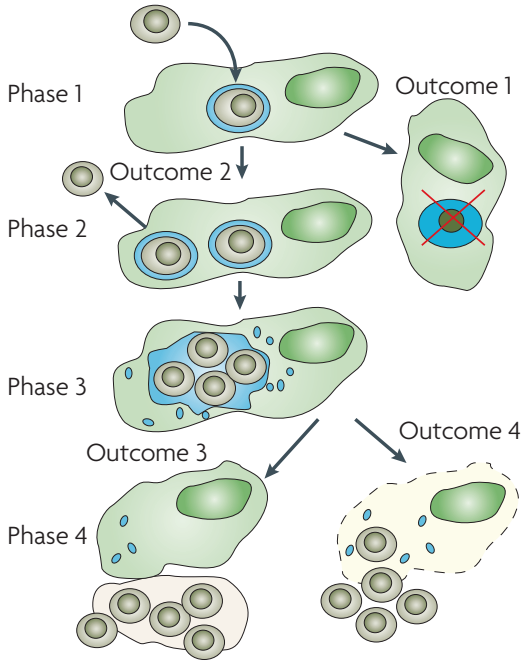

Schematic representation of the different phases and outcomes during Cn/host cell interaction (adapted from [42])

2.a. To be or not to be...phagocytosed (Phase 1)

The uptake of *C. neoformans* cells is assumed by professional phagocytes. Immune cells have various propensities to phagocytosis. Neutrophils [43,44], monocytes/macrophages [45] and dendritic cells [46] are well known professional phagocytes that are able to deal with *C. neoformans* as well as the drosophila S2 cells [47]. The phagocytic capacities of these cells vary [47]. Various phagocytic capacities in rat macrophages originated from various sites (pleural, peritoneal, alveolar macrophages) [48] or in mice macrophages (alveolar or peritoneal) [5] are observed when challenged with a given *C. neoformans* strain. Intracellular yeasts have been observed in lungs. Fungal uptake depends on the equilibrium between host factors mainly present at the surface of immune cells and microbial factors that are produced by the yeasts to escape phagocytosis.

Phagocytosis is mediated by receptor activation that allows cytoskeletal modifications of the host cell to internalize the yeasts. Receptors are opsonic, such as Fc receptors or complement receptor family, or non-opsonic, such as Dectin-1, CD11b, or

mannose receptors. The latter recognize the pathogen through pathogen associated molecular patterns (PAMPs) present at the fungal surface. In vitro, phagocytosis is inefficient in the absence of opsonin [49] making necessary the adjunction of an opsonin to study phagocytosis of *C. neoformans*. Antibody-mediated opsonization appears to be most efficient [50] compared to complement-mediated opsonization. Interestingly, surfactant protein D and A produced in the lung acts as an opsonin in vitro in poorly encapsulated yeasts [51,52] but seems to be less efficient in fully encapsulated yeasts [53,54]. Paradoxically, surfactant protein D facilitates infection [55].
Non-opsonic receptors and their role in cryptococcosis are still not well established. When dealing with basidiospores, phagocytosis by alveolar macrophages takes place though interaction between beta-glucan, Dectin-1 or CD11b receptors [56]. However, Dectin-1 deficient mice are similar to wild type mice in terms of clinical course of the infection and cytokine production, suggesting that Dectin-1 plays a minor role for the development of protective immunity against *C. neoformans* [57]. At the opposite, the mannose-receptor plays a role in adaptive immunity against *C. neoformans* by stimulation of CD4 T cells proliferation, but it is not involved in *C. neoformans* uptake by dendritic cells [58].

Fungal factors that make *C. neoformans* resistant to phagocytosis are multiple. Polysaccharide capsule is the main one. Glucuronoxylomannan (80-90%) as the main component of the capsule is not recognized by the phagocyte [59,60] and dissimulates PAMPs to the phagocytic cells acting as a physical barrier [61,62]. Other factors are involved in resistance to phagocytosis. The secreted anti-phagocytic protein (App1) blocks complement-mediated and not antibody-mediated phagocytosis [63]. App1 binds to the CD11b receptor and blocks complement binding to the receptor [64]. Though the screening of a library of 1201 gene knock-out *C. neoformans* mutants, the transcription factor Gat201 (GATA family transcription factor 1) is identified as a capsule independent anti-phagocytic protein [65]. Gat201 plays a pleiotropic role in *C. neoformans* as it participates to the formation of capsule and melanin. Gat201 regulates Gat204 (a transcription factor) and Blp1 (Barwin like protein 1) to maintain anti-phagocytic activity [66]. Yeast size is important for phagocytosis. Indeed, yeasts called titan cells with 25-30 µm for cell body size and 50-100µm with capsule, that are generated in lungs, are resistant to phagocytosis [67-69].

Cryptococcus neoformans obtained from lung homogenates (mice)
have variable size ranging from Titan cells (big size, enlarged cell wall, left)
to normal size (budding yeast, right)

2.b. The less you have, the more you will be (Phase 2/3)

The ability of *C. neoformans* to multiply intracellularly has been known for a long time. In vitro, intracellular yeast in human macrophages grow faster than extracellular yeasts [45]. In vitro, replication is observed in activated J774.16 macrophages as soon as 2 hours after ingestion and is associated with accumulation of vesicles filled with polysaccharide within the macrophage cytoplasm and phagosome membrane disruption leading to increased phagosomal pH [70]. Th2 cytokine enhanced intracellular proliferation compared to Th1 or Th17 ones [71]. In vivo, this phenomenon appears 24 hours after mice inoculation with increasing number of yeasts per phagosome. Budding is also more frequent within alveolar macrophages than in the extracellular space. Intracellular replication is associated with cytotoxicity and intracellular polysaccharide production [24].

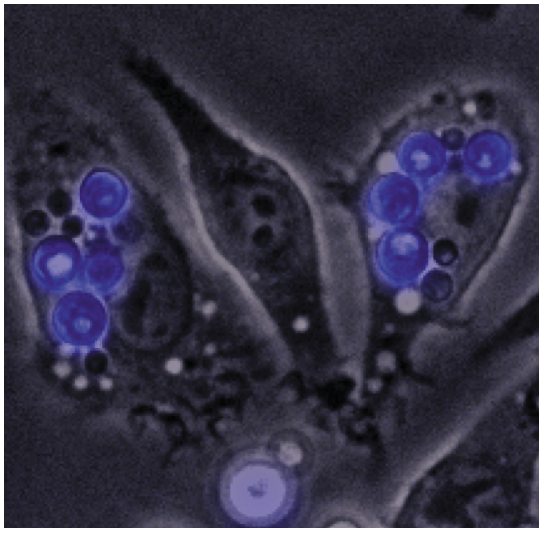

Cryptococcus neoformans proliferates within J774 macrophages
6 hours after after phagocytosis
(Mother yeast cells are bright blue and daughter yeast cells are less fluorescent)

2.c. Dead end (outcome 1)

Killing is the natural role of professional phagocytic cells. The maturation process leading to the acidification of the initial single-membraned phagosome by fusion of phagosome with lysosomes happens after *C. neoformans* phagocytosis [72] as observed by lamp1 (CD107a, type I transmembrane glycoprotein) recruitment [73]. Interestingly, *C. neoformans* cells replication is enhanced by acidification and antifungal activity is observed after alkalization of the phagosome. Many virulence factors, such as melanin production via laccase activity, protect yeasts against antifungal activity of macrophages. Despite that *C. neoformans* expends numerous mechanisms based on anti-oxidative enzymes to avoid killing [74], dead yeasts are still observed and can be measured by colony forming unit (CFU) counts or flow cytometry upon macrophages internalization [75-77]. Indeed, apart from pH acidification, antimicrobial activity is also achieved by production of respiratory burst with generation of reactive oxygen species (ROS), addition of anti-microbial peptides, proteases and nutrient starvation leading to a global

antimicrobial activity [73,78]. Alveolar macrophages are able to kill *C. neoformans* cells by non-oxidative mechanisms, paradoxically, preferentially in encapsulated rather than acapsular yeasts [79]*. Cryptococcus neoformans* killing occurs also extracellularly after contact with IFNγ-activated macrophages suggesting secretion of antifungal peptides by macrophages [80].
In nature, *C. neoformans* cells encounter unicellular or multicellular predators such as *Paramecium*, amoebas or *Caenorhabditis elegans*. The proportion of killed *C. neoformans* cells is higher in *Paramecium* [4] than in amoebas [81] or nematodes [82].

2.d. An emetic yeast (outcome 2/3)

Expulsion of yeasts without lysis or dramatic damages of macrophages is observed in vitro [83-85] and demonstrated in vivo [86]. This non-lytic exocytosis phenomenon was initially called vomocytosis. It has also been observed with *Candida albicans* [87]. The mechanisms that support this phenomenon are not completely understood. Release of the *C. neoformans* cells could results from stochastic fusion between phagosome and plasma membrane plasma and phagosome membranes fusion [88], since vomocytosis occurs preferentially when the phagosome is filled with multiple yeasts [85]. However, vomocytosis is rarely observed with mutants deficient in Plb1 secretion (*plb1Δ*) [89], killed yeasts or intracellular beads suggesting an active phenomenon that depends on physiological characteristics of some strains [85]. Vomocytosis is also dependent on the activation state of the macrophage with a reduced occurrence in Th2 cytokine-treated macrophages compared to TH1 or Th17 treated cells [71]. On the opposite, alkalization of phagosomes induced increased rate of vomocytosis [84,86]. Although host actin cytoskeleton is not required for vomocytosis, a possible mechanisms based on repeated cycles of actin polymerization (called actin flashes) regulated by the WASH-Arp2/3 pathway could explain this phenomenon [88]. Apart from exocytosis, cell to cell transfer of *C. neoformans* between two macrophages has also been observed *in vitro* [90,91].

2.e. A toxic marble bag (outcome 4)

As observed in vivo, extracellular yeast are associated with cell debris within the first 24 hours after inoculation suggesting that intracellular yeasts that began to replicate 2 hours after inoculation are able to lyse the phagocytic cells with release of living yeasts into the extracellular space as a consequence [24]. Replication followed by cell lysis is also reported in vitro in human macrophages [45] or human microglia [92]. Polysaccharide vesicles accumulation and phagosomal membrane disruption could lead to instability and finally disruption of the cellular membrane. Macrophage killing could also result from apoptosis since galactoxylomannan is shown to induce Fas/FasL-mediated apoptosis in macrophage [93] as well as B lymphocytes [94].

3. Adapting to hostile environments

Cryptococcus neoformans and *C. gattii* are able to survive in, to adapt to and to lyse the host cell or disseminate into infected organisms. Theses features are the result of fungal factors selected during the evolution due to the selection pressure in *Cryptococcus* environment. Three main virulence contributes to the infectivity of these yeasts: the production of a polysaccharide capsule [110], the ability to grow at 37°C [111], and the production of melanin by laccase [112]. The capsule provides anti-phagocytic [60] and immunomodulatory properties [113]. Key enzymes are involved also in the virulence: phospholipase B [114], urease [115], superoxide dismutase [116], proteases [117]. Cryptococcal cells have a specific delivery system for excreting virulence factors via vesicles called 'virulence factors delivery bags' [118]. The release of these bags is the first cryptococcal armamentarium to prevent adapted immune response [119]. Apart from well-identified virulence factors, global transcription analysis identified the global mechanisms that support fungal adaptation to hostile environments.

3.a. Adapting to natural predators

Natural predators of *C. neoformans* in nature are unicellular (Amoebas, *Paramecium*) or multicellular (nematodes or insects) organisms. Amoebas of the genera *Acanthamoeba* feed on bacteria or fungi [120,121]. They are present in soil and fresh water and were initially identified as cryptococcal culture contaminant. *Cryptococcus neoformans* can be phagocytosed [122] and can replicate in *Acanthamoeba castellanii* [2] or the social amoeba *Dictyostelium discoideum* [81], leading at the end to the killing of the amoeba. In comparison, these features are not observed with *Candida albicans* and *Saccharomyces cerevisiae*. Virulence factors such as capsule, melanin or phospholipase are needed to resist phagocytosis and oxidative burst and to replicate in amoebas. At the opposite, *Paramecium tetraurelia* or *Paramecium aurelia* are organisms that are able to ingest and to kill *C. neoformans* within the first 24 hours of incubation [4]. Other *Paramecium* species such as *Paramecium multimicronucleatus* has a fungistatic but not fungicidal effect on *C. neoformans* [4].

Multicellular invertebrate hosts can interact in theory with *C. neoformans* in nature. The free-living nematode *Caenorhabditis elegans* can use *Cryptococcus* spp. as the sole source of food [82]. *Cryptococcus neoformans* and not *Cryptococcus laurentii* or *Cryptococcus kuetzingii* (species that are known to interact with *C. elegans* in nature) is able to kill the nematode by accumulation within the gastrointestinal tract of the nematode. This phenomenon is dependent of virulent factors. The caterpillar of the greater wax moth (*Galleria mellonella*) model has also been developed to easily study virulence at room temperature. It appears that *C. neoformans* can proliferate inside the hemocoel and kill the caterpillar even if *C. neoformans* are phagocytosed by *G. mellonella* hemocytes.

Drosophila melanogaster has also been challenged with *C. neoformans* [123]. Interestingly, flies are resistant to *C. neoformans* when inoculated in the hemolymph, whereas they are susceptible when ingested [124]. This is explained by the differential expression of the toll-like receptors in fly tissues.

C. neoformans adaptation to predators has been analyzed upon *Acanthamoeba castellanii* ingestion in terms of whole transcriptome modifications [3]. Genes encoded well-known virulence factors are up regulated, as well as genes involved in nutrient transporters, in general metabolism and stress response. Genes involved in transcription and translation and ergosterol biosynthesis are down regulated. Parallel analysis of the

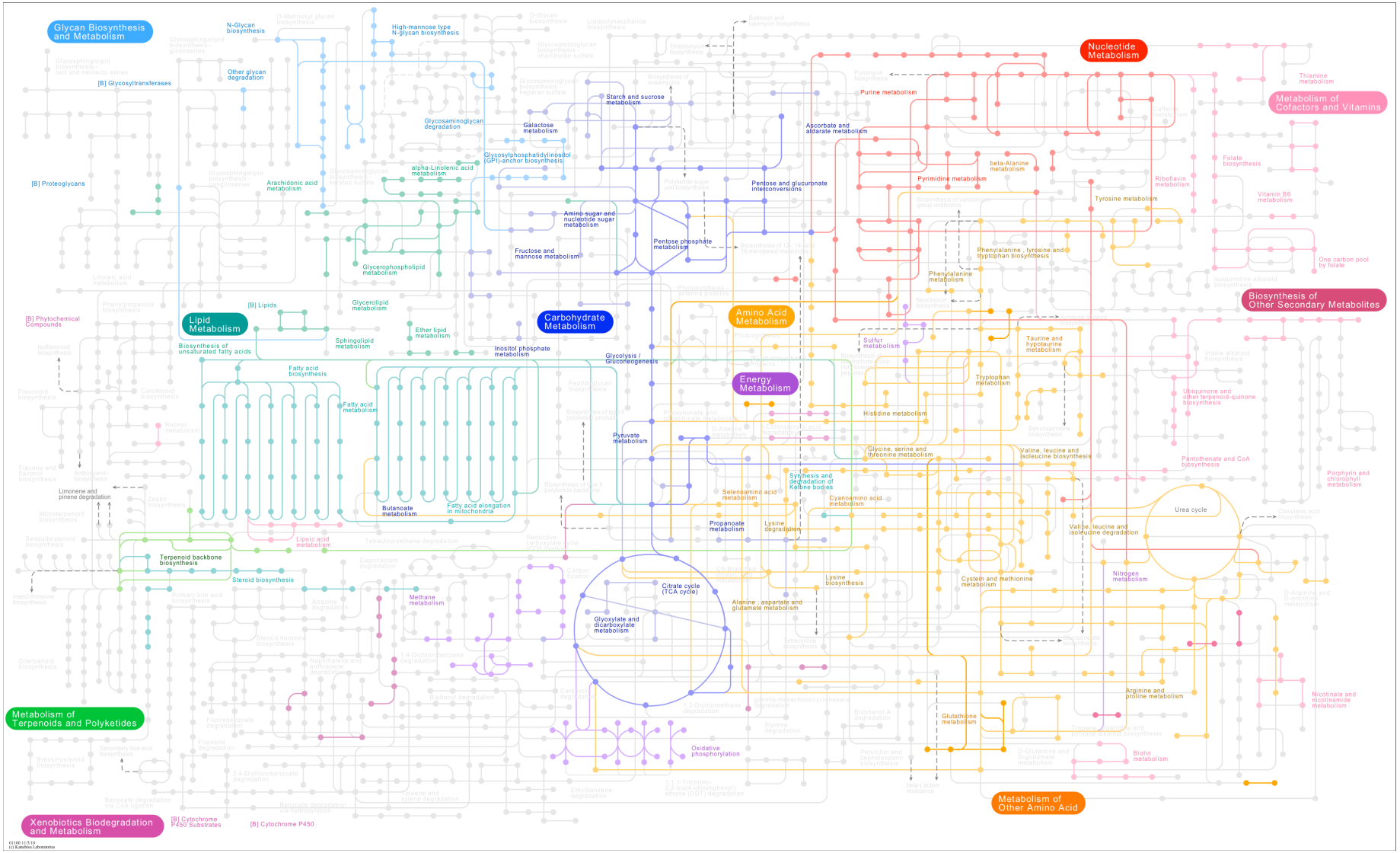

Schematic representation of the relations that exists between metabolic pathways in *C. neoformans* based on KEGG database (http://www.kegg.jp/kegg/atlas/?01100)

transcriptional modification upon amoeba or macrophage internalization revealed that 83.8% of yeasts genes are modulated similarly. The metabolic modifications are very similar between both conditions with a switch towards gluconeogenesis, fatty acids degradation, and glyoxylate cycle. Furthermore, *PTP1* (Polyol transport protein 1) gene involved in 5,6-carbon polyol transport is up regulated upon macrophages and amoeba internalization. This study reinforces the hypothesis in which the virulence in mammalians originated from interaction of yeasts with environmental protozoan predators [3].

3.b. Adapting to mammalian hosts

Immunity against *C. neoformans* is different from a mammalian host to another. Rats has been demonstrated to be naturally resistant to cryptococcal infection [125]. For mice, the genetic background is influencing the course of the infection. For example the pathophysiology of cryptococcosis in BALB/c and CBA/J inbred mice is different [126]. Outbred mice can also be used with the idea to mimic the natural diversity of the host to study immune response to infection [127].
The *C. neoformans* (H99 strain) translational modifications have been studied in the lungs of A/Jcr mice after early infection (8 – 24 hours) [26] and in the central nervous system (CNS) of New Zealand White rabbits, both using the SAGE (serial analysis of gene expression) methodology [27].
In lungs, a remodeling of the yeast central carbon metabolism is observed with particular stimulation of the glyoxylate pathway, gluconeogenesis, ß-oxidation and amino acids biosynthesis [26]. Indeed, *C. neoformans* seems to adapt to glucose-limited environment by exploiting alternative sources of energy such as acetate, lactate, fatty acids or amino acids. Transporters for monosaccharides, iron, copper and acetate and stress response proteins are also over-expressed suggesting nutrient restriction and hostile host environment.
At the opposite, the *C. neoformans* transcriptional patterns in the CNS, is directed toward protein biosynthesis (ribosomal proteins, translation elongation, translation initiation), protein degradation (proteasome pathway, secreted proteases) and response to stress (heat shock proteins). Up-regulation of gene involved in energy production is also observed [27].
Overall, *C. neoformans* seems to adapt well in CNS with a typical translational patterns of multiplication compared to lungs where up-regulation of genes involved in resistance to nutrient-limitation is predominant.

3.c. Adapting to immune response

Whole gene expression analysis using homemade microarrays chips was used to examine *C. neoformans* (H99 reference strain) adaptation to the intracellular environment of the murine J774 macrophages [25]. The up-regulated genes are involved in membrane transport for hexoses, amino acids, iron, ammonium, nicotinic acids and phosphates. Genes implicated in the metabolism of lipids, autophagy, and peroxisomes are also elevated. Response to oxidative stress is observed by up-regulation of flavohemoglobin. Components of the cAMP signal transduction pathway are also more expressed. Down-regulation of translational initiation, elongation and ribosomal RNA processing proteins are observed. Comparable results are obtained using serial analysis gene expression (SAGE) [128] and upon phagocytosis of rat peritoneal macrophages with induction of the same metabolic pathways in *C. neoformans* [129]. This is also consistent with what is

found in *Candida albicans* in response to macrophage environment [130].
The adaptation to humoral immune response as also been studied. Anti-cryptococcal antibody response plays a role in the immune response during cryptococcosis [131,132]. Binding of protective antibodies to the cryptococcal surface (capsule) induced up-regulation of the fatty acids biosynthesis pathway and ergosterol synthesis, and down-regulation of protein involved in translation functions [133]. The translational response is different depending on the type of antibody and the location of the epitope. This suggests that *C. neoformans* could develop strategies to escape adaptive immunity during infection.

4. Diversity: a powerful force for *C. neoformans* survival

Confronted with the need to survive different hosts in different environments, *C. neoformans* has selected ready-made virulence traits [1]. From a deterministic point of view, *C. neoformans* population needs also diversity to survive predators harboring different killing propensity. The plasticity of the genome *C. neoformans* could lead to this diversity [134]. *Cryptococcus neoformans* and *C. gattii* are haploid organisms that can be found as diploid organisms both in nature and in hosts [30,135]. Generation of hybrids is possible between the varieties *grubii* (serotype A) and *neoformans* (serotype D) [135,136] but also between *C. neoformans* and *C. gattii* illustrating again this plasticity [137].

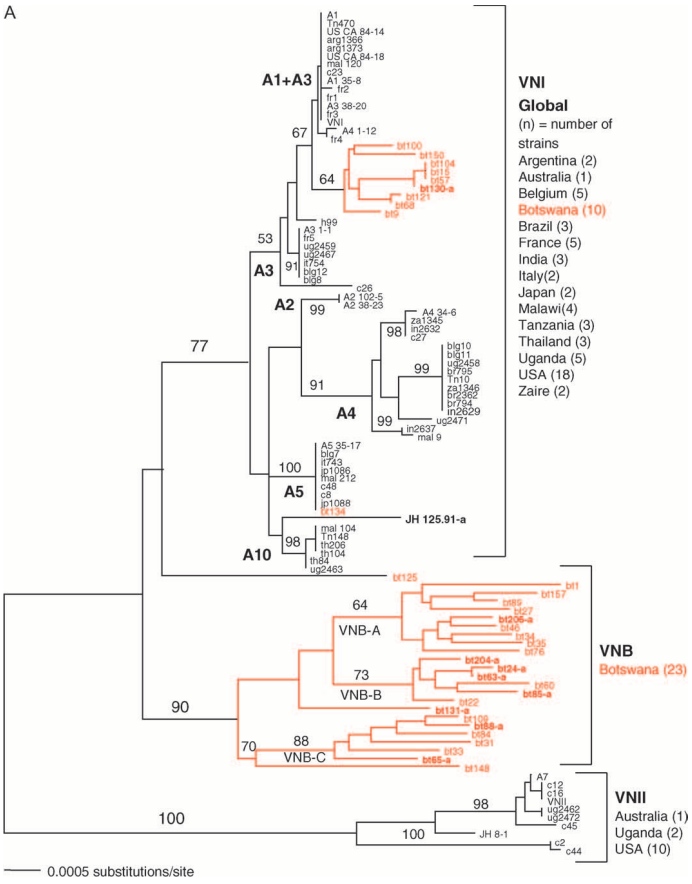

Phylogenetic tree representing the genetic diversity of *C. neoformans* isolates (serotype A) obtained from various countries (adapted from [139])

Diploidization of serotype A or D is also possible and can be recovered from clinical specimens [30,138]. Clinical and environmental isolates of *C. neoformans* are highly diverse and can be classified in 3 genetic subpopulations based on AFLP and MLST methods including VNI, VNII, VNB with VNI as the most prevalent and ubiquitous subtype [139,140]. Overall, this diversity impacts the interaction between various hosts and *C. neoformans* isolates. Experimental data are mostly obtained using reference strains such as H99 (serotype A) or JEC21, JEC20 or NIH52D (serotype D). However, the few studies that use clinical isolates in addition to reference strains suggest even more diversity.

4.a. Facing predators in nature

Diversity of *C. neoformans* phenotype upon interaction with various predators is observed. Phagocytosis [141] and killing [2] of *A. castellanii* varies among isolates (clinical and reference strains). The same features are observed upon interaction with the social amoeba *Dictyostelium discoideum* [81]. Vomocytosis can also been observed with *Acanthamoeba castellanii* with a rate that is dependent on the strain and the viability of the yeasts [141]. Upon interaction with *Paramecium*, the sensitivity of *C. neoformans* strains to this organism vary in comparison with H99.
Cryptococcus neoformans and not *Cryptococcus laurentii* or *Cryptococcus kuetzingii* (species that are known to interact with *Caenorhabditis elegans* in nature) is able to kill *C. elegans* [82]. Virulence in this model varies among *C. neoformans* isolates regardless of the serotype [82]. Of note, environmental strains of *C. neoformans* are also pathogenic for *C. elegans*. In the caterpillar of the greater wax moth (*Galleria mellonella*) model, although all strains tested are able to kill the caterpillar, H99 is more virulent [142]. Killing of *D. melanogaster* is also more important for H99 compared to clinical isolates of serotype A or serotype D [123].

4.b. Facing various mammalian hosts

In mice lungs, the proportion of yeasts in the intracellular or extracellular spaces varies with the duration of infection and the strain inoculated [24]. The nature of the infecting particles inoculated to hosts is important. Basidiospores from a serotype D strains are 100 fold more infective that the yeasts form [143]. This had not been reproduced using serotype A strains [144]. Indeed, basidiospores compared to yeasts inoculation lead to lower CFU in lungs at early time points after inoculation [56].
The nature of the strain of *Cryptococcus* spp. used to inoculate mice will also influence the course of the infection, as observed with two environmental strains of *C. neoformans* [145]. Differences of virulence have been observed when isolates of serotypes A, B, C, D are compared [146]. Thus, the pathophysiology of the infection between *C. neoformans* H99 and *C. gattii* R265 is different. H99 is more prone to induce meningoencephalitis and less to induce lung injury compared to R265 [147]. Variation of CFU in lungs is also observed in different *C. gattii* strain [22,148]. Difference in virulence is observed comparing clinical isolates of *C. neoformans* recovered from AIDS patients [40], or environmental strains [149] or comparing clinical to environmental strains with clinical isolates harboring higher virulence than environmental isolates [37].

4.c. Facing immune cells

When challenged with various *C. neoformans* strains, variation of phagocytic index is observed using single macrophage cell-line of rats [150] or mice [49], or human neutrophils [151]. Phagocytic index of human neutrophils varies from 0.7 to 98 ingested yeasts per 100 neutrophils considering various clinical isolates. In comparison, phagocytic index of different donors facing the same *C. neoformans* strain does not vary in the same proportion [44]. As a result of variation in the phagocytic index, killing of various *C. neoformans* clinical isolates is different [76,152]. Direct activity of T lymphocytes and natural killers against *C. neoformans* is different in two different isolates [153].
Variation in the intracellular proliferation rate in J774 mouse macrophages is also

observed in different strains of *C. gattii*, with the clonal VGII isolates (responsible for the Vancouver island outbreak) harboring higher proliferation ratio compared to *C. gattii* from other genotypes [22]. The authors associated this phenotype with a higher mitochondrial activity. This study did not demonstrate if higher mitochondrial activity is the origin or the consequence of the observed phenotype. Isolates from VGIIa and VGIIc *C. gattii* genotypes have higher IPR than those from VGIIb genotypes with additional variation of IPR between isolates within the VGIIb population [154]. In addition, vomocytosis is observed preferentially with some specific strains [155].

Objectives

Species, serotype, genotype diversity of *C. neoformans* is established, but the diversity of adaptation of the yeasts to various environment is partially understood. It is still not clear whether the variable clinical presentation and outcome of cryptococcosis is related to the individual's immune status, some genetic factors [109], fungal determinants or a combination of them. The role of fungal determinants in the outcome of cryptococcosis is usually studied using mutants generated from reference strains, and rarely with clinical isolates. For *C. gattii*, a specific genotype (VGII, responsible for the Vancouver Island outbreak) is associated with increased intra-macrophagic yeast proliferation and virulence in mice compared to other genotypes [22]. However, for *C. neoformans*, the influence of genotypes or phenotypes diversity on pathogenesis has not yet been established.
Our objective was here to understand how fungal diversity could impact the pathophysiology of the infection by *C. neoformans*. We took advantage of the well-characterized collection of clinical isolates and corresponding clinical data (CryptoA/D study) [11], a clinically relevant murine model of disseminated cryptococcosis and developed new tools to address this question. We then focused on *C. neoformans* adaptation to host during infection with the hypothesis that a specific population representing dormant cells could be identified.

Materials and Methods

Cell line.
The J774.16 cell line (J774) was purchased from the American Type Culture Collection to study the interaction of Cn clinical isolates with macrophages. J774 is a murine macrophage-like cell line derived from a reticulum sarcoma. Cells were maintained at 37°C in the presence of 5% CO_2 in DMEM supplemented with 10% heat-inactivated fetal calf serum (FCS) and 1% penicillin/streptomycin (fresh medium) (all from Invitrogen). Cells were used between 10 and 35 passages.

***C. neoformans* strains.**
A panel of 54 *C. neoformans* clinical isolates was selected. All isolates were recovered from cerebrospinal fluids and responsible for single infection (one isolate/one genotype/ one infection), as opposed to mixed infection [30]. All isolates were collected during the CryptoA/D prospective study [11]. This study was approved and reported to the French Ministry of Health (registration # DGS970089). For each isolate, the patient's background, clinical presentation, outcome of infection, and various biological parameters were available (Table 1). One single colonies (ClinCn) from each clinical isolate was frozen in glycerol 40% at -80°C and used thereafter. All ClinCn were characterized as haploid, serotype A MAT using previously described methods [30]. Before each experiment, yeasts were first cultured on Sabouraud dextrose agar (SDA) medium and then subcultured in liquid yeast extract-peptone-glucose medium at 30°C at 150 rpm for 22 hours (standard YPD culture). All isolates were tested blind to the clinical parameters. Two ClinCn isolates (AD1-83a and AD1-07a) were selected based on their various virulence characteristics [23] for specific experiments.
Mutant strains (all derived from H99) *lac1Δ* (lacking laccase 1, Lac1) [156], *vps34Δ* (lacking the PI3 kinase, Vps34) [157], *vad1Δ* (lacking the DEAD-box RNA helicase, Vad1) [158] (kindly donated by P. Williamson, NIH, Bethesda, MD), and *app1Δ* (lacking the antiphagocytic protein, App1 [63], that binds the CR3 and CR2 receptors on phagocytic cells [64]), *ipc1Δ* (in which inositol-phosphoryl ceramide synthase, Ipc1, is down-regulated) [159] (kindly donated by M. Del Poeta, Charleston, SC), were also used. The reference strain H99 (serotype A, MATalpha, haploid) (kindly donated by J. Heitman, Duke University, NC) was used as reference in all experiments.

Reagents and *C. neoformans* labeling.
Calcofluor white dye (CALCO) (Fluorescent brightener 28, Sigma) specifically stains chitin contained in the cell wall of some eukaryote microorganisms, and was used to label yeasts. Yeast cells were collected from standard YPD culture, washed twice and resuspended in phosphate buffered saline (PBS) (Invitrogen) at $5x10^6$ to $2x10^7$ per ml. The cells were then incubated with CALCO at 10µg/ml in PBS for 10 min in the dark at room temperature and then washed twice in PBS. In preliminary experiments, we checked that the in vitro growth curves strains were similar (identical slopes) for CALCO-stained and unstained yeasts, except for *lac1Δ* for which growth decreased after CALCO staining (data not shown). To assess the evolution of CALCO-fluorescence during multiplication, CALCO-stained *C. neoformans* (10^6/ml) cultured in standard YPD were analyzed using fluorescence microscopy (Zeiss Axioscope A1, 4′,6-diamidino-2-phenylindole (DAPI) filter) and flow cytometry at various incubation times. E1, a murine IgG1 monoclonal anti-capsular polysaccharide antibody (E1 mAb) was used as an opsonin [160]. Fluorescein isothiocyanate (FITC)-labeled horse anti-mouse IgG (anti-IgG–FITC) (Vector Laboratories) and allophycocyanin (APC)-labeled goat anti-mouse IgG (anti-IgG–APC) (BD Pharmingen) were used at 1:100 for 20 min-incubation.

5-chloromethylfluorescein diacetate (CMFDA) (CellTracker Green CMFDA, Life Technologies) is a dye that needs two enzymatic steps and glutathione to acquire fluorescence (FITC) properties. It is commonly used to quantify glutathione in mammalian cells [161,162], and has been employed for long terms tracking of *C. neoformans* in vivo [86]. The stock solution in anhydrous dimethyl sulfoxide (DMSO) was diluted at 10µM in PBS.
TO-PRO-3 iodide (TOPRO), (Invitrogen), diluted at 10µM in PBS, was used to stain nucleic acids of yeasts with disrupted membrane (dead yeasts) and then analyzed in the allophycocyanin (APC) channel.
Preliminary experiments showed that combining TOPRO and CMFDA for 30 min-incubation at 37°C without agitation was efficient over yeasts concentrations ranging from 10^6 to 10^7/mL and in the presence of tissue debris. CALCO staining was always performed on living cells prior to all other stimuli whereas CMFDA/TOPRO assay followed them. These stainings did not alter yeasts viability (data not shown).
In specific experiments, yeasts were subjected in vitro to various stimuli to test the glutathione-mediated stress response and then subjected to CMFDA/TOPRO assay at different time points. The stimuli included (i) pure water; (ii) hydrogen peroxide (Sigma) adjusted to 2 mM in water [163]; (iii) fresh medium or yeast nitrogen base medium (YNB) that represents a non optimal culture media for yeasts based on preliminary experiments (data not shown); (iv) heat at 65°C for 2 hours that results in 99.9% of dead yeasts. All stimuli were tested in duplicates. Diethyl maleate (DiEM) (Sigma) adjusted to 100µM in sterile water was used to deplete the yeast's glutathione stock [162] and assess the glutathione-dependent CMFDA staining.
Polyclonal rabbit anti-capsular antibodies together with cyanine3 (Cy3) or R-phycoerythrin (PE)-labeled goat anti-rabbit IgG (Anti-IgG-Cy3 or Anti-IgG-PE) (Invitrogen) were used to stain the capsule of yeasts at 1:100 for 30 min-incubation. The polyclonal sera were obtained after immunization of rabbits with whole heat-killed yeasts adapted from published procedures [164].
Additional dyes were used to characterize metabolic activities or yeast cell organization: (i) mitochondrial activity with Mitotracker Orange CMTMRos (Invitrogen) at 40nM (30 min incubation at 37°C) [22]; (ii) RNA content with SYTO85 (Invitrogen) at 5 µM (30 min-incubation at 37°C); (iii) lipid membrane layers staining with MDY64 (Invitrogen) at 10µM (3 min-incubation at room temperature (RT) [67]; (iv) nucleus morphology with DAPI (Invitrogen) at 1:5000 (5 min incubation at RT) [67].

Baseline genotypes and phenotypes characterization of the clinical isolates.
The genotype of each ClinCn was determined by Multi-Locus Sequence Typing (MLST) on 7 loci, as previously described [140]. Morphological aspect (smooth or mucous) was assessed after 72 hours of culture on SDA at 30°C. Growth curves were determined in 96-well plates starting at 10^6/ml without agitation in liquid YPD at 30°C (triplicate wells). The optical density (OD) was recorded at 600 nm up to 140 hours of incubation (LabSystems Multiskan). The regression line (y=ax+b) was determined and results expressed as the ratio between the slopes ("a" value) for the ClinCn compared to H99. Cell and capsule sizes were determined after standard YPD culture. Cells suspensions were made at 10^6/ml in PBS. An aliquot was observed in India ink suspension using a microscope Axioscan (Carl Zeiss, Germany) and the camera AxioCam ICc1 (Carl Zeiss, Germany). Cell size, delineated by the cell wall, as well as capsulated cell size, delineated by the white exclusion zone around the cells, were measured for 10 cells randomly-selected of each ClinCn and H99 using the Zeiss AxioVision software (Carl Zeiss,

Germany). Results were expressed as the average size ratio for ClinCn/H99. The binding of E1 mAb to the capsule surface was determined. Yeasts were cultured on SDA for 24 hours at 30°C, for each ClinCn, washed in PBS and suspended at a concentration equivalent to 0.1 OD at 600 nm. Then, 300µl of the suspension were centrifuged and pellets were resuspended in 100µl of PBS containing E1 mAb (0.5µg/ml) and FITC anti-IgG for 20 min in the dark at room temperature. Then, 400µl of PBS-PFA 1% was added to fix cells before cytometry analysis. The results were expressed as the ratio between the geometric mean of the FITC-fluorescence intensity for the ClinCn and H99. The chitin content was determined after standard YPD culture and standard calcofluor-staining by quantification of the geometric mean of the calcofluor fluorescence intensity for the ClinCn and H99 using flow cytometry (see below).
To study the variability of the s9-ClinCn, urease activity and melanin formation were quantified using urea agar base medium [165] and asparagine agar containing 1mM of L-Dopa [25]. Urease activity and melanin formation of 10^5 to 10^7 yeasts cells after 24 hours of incubation at 37°C and 72 hours of culture at 30°C, respectively, were quantified by measuring the diameter of the pink halo (urease), and the RGB content of colonies (laccase) using ImageJ software. The mating assay used Murashige and Skoog medium [166] and fertility was assessed after 7 days of incubation at room temperature in the dark with KN99a (serotype A, mating type a), KN99alpha (serotype A, mating type alpha) and JEC20 (serotype D, mating type a).

Interaction with macrophages.
J774 cells suspension (10^5 in fresh medium per well of a 24-well culture plate) were incubated at 37°C in 5% CO_2 for 48 hours. The day of the experiment, E1 mAb (250µl) and CALCO-stained yeasts suspension (250µl) both in fresh medium at the desired concentrations were added to the J774 cell monolayer and incubated at 37°C and 5% CO_2 for 2 hours (phagocytosis assay, Cn:J774 ratio = 5:1). Non-adherent extracellular yeasts were then removed by PBS washings, and incubation stopped to assess phagocytosis or protracted to determine intracellular proliferation. Phagocytosis was determined after staining residual extracellular yeasts using anti-IgG–FITC, additional PBS washings and macrophage lysis using distilled water (Fig. 2A). The samples were then centrifuged, resuspended in 1% paraformaldehyde (PFA) in PBS (PFA-PBS), vortexed and sonicated for 3 minutes before analysis.
To assess intracellular proliferation of ClinCn using flow cytometry (proliferation assay, Cn:J774 ratio = 2.5:1), the incubation was protracted in fresh medium for 48 hours. Residual extracellular yeasts were stained by addition of E1 mAb (0.5µg/ml) and anti-IgG–FITC, PBS-washed and J774 were lysed by water (Fig. 2B). In order to differentiate potentially unstained yeasts from cell debris an additional step was done using E1 mAb and APC anti-IgG. All yeasts were APC^{pos} while only extracellular yeasts were APC^{pos} $FITC^{pos}$.
Intracellular proliferation was determined for each ClinCn at the end of the phagocytosis step (H2) and at 48 hours (H48). Phagocytosis and proliferation were analyzed in two independent experiments. As a control, viable $CALCO^{high}$ H99 cells present intracellularly after 48 hours-incubation with macrophages were compared to freshly labeled yeasts (without coincubation) based on $CALCO^{high}$ events before (T_0) and after 24 hours-YPD culture (T_{24}). The total number of $CALCO^{high}$ events was recorded by flow cytometry.

Flow cytometry analysis of yeasts/macrophages interaction (FACS-YMI).
Flow cytometry analyses were performed using MacsQuant Analyzer and the

MacsQuantify Software 2.0 (Miltenyi) to provide absolute quantification. Samples were analyzed using FlowJo 8.7 software (Tree Star, Inc.). Aggregates were excluded by gating relevant events in the Forward scatter/Side scatter (FSC/SSC) contour plot. Three parameters were calculated:

- Phagocytic index (PI) as the number of events in the $CALCO^{high}FITC^{neg}$ gate at H2.
- Intracellular proliferation at H2 (IPH2) as the ratio between daughter cells ($CALCO^{low}$ + $CALCO^{med}$) and mother cells ($CALCO^{high}$) at H2.
- Intracellular proliferation at H48 (IPH48) as the ratio between daughter cells ($CALCO^{low}$ + $CALCO^{med}$) at H48 and mother cells ($CALCO^{high}$) at H2.

Results were expressed as the ratio of the given parameter for the ClinCn/mutant strains compared to H99 parameter determined in the same run. We assessed that results obtained during the 2 independent experiments were reproducible for PI, IPH2, IPH48 ($P<0.0001$ for each parameter), and mean of replicates were then used for subsequent analyses.

Dynamic imaging.

The evolution of fluorescence intensity from mother to daughter intracellular yeasts was assessed by dynamic imaging (Nikon Biostation). J774 were cultured and incubated with CALCO-stained yeasts (2.5:1) in dishes (Hi-Q4 35 mm, Nikon) at 37°C and 5% CO_2. Series of images were taken by phase contrast and fluorescence microscopy (DAPI filter) every 5 minutes for 24 hours at x40 magnification. Merging and inverting the look-up table were done using ImageJ software (http://rsb.info.nih.gov/ij/). The movie was generated from the 289 modified pictures using iMovie software v8.0.6 (Apple Inc).

Virulence in mice.

Outbred OF1 male mice (age 6–8 weeks) (Charles Rivers Laboratoires) were housed 7 per cage in our animal facilities and received food and water ad libitum. The inoculum was prepared in sterile saline from standard YPD culture. The yeasts suspension (10^5/mouse) was inoculated intravenously to 7 mice. Survival was recorded once daily until day 60 after inoculation. Animals about to die (unable to reach their food) were systematically euthanized by CO_2 inhalation. Animal studies were approved by the Institut Pasteur Animal Care Committee (#03/144).

Real-time PCR.

RNA extraction was performed on the s9-ClinCn and H99 coincubated with J774 cells (intracellular condition (iH2)) or in fresh medium (baseline condition (BsH2)) for 2 hours at 37°C in 5% CO_2. For iH2, J774 cells were washed twice with PBS, scraped, lysed in 2 mL 0.05% SDS ice-cold water, vortexed and the pellet was collected after 3 min centrifugation at 2000 relative centrifugal force (rcf). RLT Lysis Buffer (500µl, Qiagen) + 1:100 beta-mercaptoethanol (Sigma) was added to the yeasts pellets. The suspensions were transferred to ceramic MagNa Lyser Green beads tubes (Roche Diagnostics), homogenized 3 times (MagNa Lyser Instrument, 30 sec, 7,000 rpm), centrifuged (3 min, 10,000 rcf). RNA extraction was performed on 350 µl supernatant using the RNeasy Mini kit (Qiagen). RNAs were quantified and qualified using the Nanodrop® spectrometer (ThermoFisher Scientific Inc.).

cDNA was generated from TurboDNase (Ambion)-treated RNA using the Transcriptor First Strand cDNA Synthesis Kit (Roche Diagnostics). Quantitative RT-PCR using 10µl of LightCycler 480 SYBR Green I Master, 2 µl of cDNA, and specific primers (**Primer table 1**) in a LightCycler® 480 (Roche Diagnostics) consisted in a denaturation step at 95°C, 45

cycles of amplification (95° for 5 sec, 60°C for 5 sec and 72°C for 5 sec). Each cDNA was analyzed in duplicate and normalized with the corresponding *GAPDH* gene expression [167], *ACT1* gene (actin 1) expression being variable function of experimental conditions (data not shown). Fold changes for each s9-ClinCn (iH2 and BsH2 conditions) were assessed compared to H99 in the same conditions, according to Pfaffl [168]. Two independent RNA extractions for each condition were analyzed blindly, and an internal calibrator consisting in an iH2 cDNA of H99 was used in each RT-PCR run as recommended [169].

In vitro and in vivo models to study yeast adaptation to host.

Fungal cell isolation after yeasts/macrophages interaction

J774 cells suspension (10^5 in fresh medium per well of a 24-well culture plate) were incubated at 37°C in 5% CO_2 for 48 hours. The day of the experiment, E1 mAb and CALCO-stained yeasts suspension both in fresh medium at the desired concentrations were added to the J774 cell monolayer and incubated at 37°C and 5% CO_2 for 2 hours (Cn:J774 ratio = 5:1). Non-adherent extracellular yeasts were then removed by PBS washings, and incubation was stopped (iH2) or protracted for 24 hours (iH24). At the end of the incubation time, non-adherent yeasts were removed by PBS washings and intracellular yeasts were recovered after use of a cell scrapper and 0.05% Sodium Dodecyl Sulfate (SDS, Sigma) ice-cold RNAse-free water (Invitrogen) (lysis solution) over the macrophage layer. The yeast suspension was then centrifuged, washed twice in PBS.

Fungal cell isolation from organs of infected mice

Experimental infections were performed with 6 to 8 weeks outbred OF1 (Charles Rivers Laboratoires) or BALB/c (Janvier) male mice. Animals were housed 7 per cage in our animal facilities and received food and water *ad libitum*. Animal studies were approved by the Institut Pasteur Animal Care Committee (#03/144).

The inoculum was prepared in sterile saline from CALCO-stained yeasts after standard YPD culture. A 10^6/ml yeasts suspension (10^5/mouse) was inoculated intravenously. Mice were euthanized 7 days after inoculation by CO_2 inhalation. For specific experiments, mice were sacrificed at early time points (30 min, 7, 15 and 30 hours) after inoculation. After sacrifice, the lungs, spleen and brain were aseptically removed. Tissues were then homogenized by grinding fresh tissue in a Potter homogenizer with 2 mL lysis solution. The suspension was transferred in a 2ml tube, centrifuged at 2,000 rcf and washed twice in lysis solution and once in PBS. The pellet was then filtered in a 40µm cell-strainer (BD biosciences) in PBS over a sterile Petri dish to remove the largest tissue debris. The filtrate was then centrifuged and washed once with PBS.

Stress response staining protocol (CMFDA/TOPRO assay)

After washings the yeasts pellet, a solution of CMFDA (10µM) and TOPRO (10µM) in PBS was added, and incubated for 30 min at 37°C. Three PBS washings were then performed to remove extra dyes. For specific experiments, the pellet was then incubated 30 min at RT in a 1:100 solution of polyclonal rabbit anti-capsular antibodies together with anti-IgG-Cy3 or anti-IgG-PE and washed twice in PBS. Just before flow cytometry analysis, an additional filtration step (35µm cell-strainer) was requested to remove newly formed aggregates.

Analysis of *C. neoformans* populations upon host interaction.

Microscopy techniques

Interferential contrast microscopy (DM LB2 microscope, Leica) and epifluorescence microscope (Axioscan, Carl Zeiss) were used to analyze morphology and fluorescence features of the yeasts recovered from lungs homogenates before and after stainings and pictured with the camera AxioCam MRm (Carl Zeiss).

Yeast multiplication was assessed by dynamic imaging (Nikon Biostation). Yeasts recovered from lung homogenates were suspended in YPD at 30°C without CO_2. Series of images were taken by phase contrast and fluorescence microscopy (DAPI filter) every 10 minutes for 48 hours at x40 magnification.

Classical flow cytometry analysis

To better characterize the yeast populations in terms of multiplication and stress response, fluorescence intensity was quantified using MacsQuant Analyzer with the MacsQuantify Software 2.0 (Miltenyi) and analyzed using FlowJo 8.7 software (Tree Star, Inc.). Aggregates were excluded by gating relevant events in the forward scatter/side scatter (FSC/SSC) contour plot. PE^{high} (yeasts) and APC^{low} (viable yeasts) population was then gated and the DAPI/FITC channels dot plot was analyzed for multiplication (CALCO/DAPI channel) and stress response (CMFDA/FITC channel).

Multispectral flow cytometry analysis

To connect cell morphology and fluorescence feature we used ImageStream^X with the INSPIRE software (Amnis Corporation). Cell suspensions were adjusted to 10^7 in 80 µL and 10,000 cells were recorded at 40-fold magnification in 5 different channels including the right field channel (BF) and 4 fluorescence channels (channel 3: 560-595nm [E1-Cy3, yeasts], channel 2: 470-560nm [CMFDA], channel 7: 430-505nm [CALCO], channel 11: 660-720nm [TOPRO]). Data analysis was performed using the IDEAS software (Amnis Corporation) after fluorescence compensation procedures. The first step consisted in the definition of a mask that delineated the relevant pixels in each picture. Then, 54 algorithms (calculations made for each event within a defined mask) were used to analyze size, texture, location, shape or signal strength.

Using basic algorithms, unfocused events, tissue debris, yeasts aggregates and dead yeasts were excluded (**Figure 16**). For multiplication and stress response analysis, gates were determined based on the CALCO/CMFDA dot plot considering the intensity algorithm and optical control of the events pictured in the gates. For each population of interest, the geometric mean was calculated using the IDEAS software. From the whole dataset and each algorithm, data were then normalized between 0 and 1, with 0 as the minimal value and 1 as the maximal value. Schematic representation was performed using the open-source genomic analysis software MeV v4.6.1 (The TM4 Development Group) obtained from www.tm4.org [170]. Hierarchical clustering was performed using complete linkage clustering and Pearson correlation.

Analysis of specific *C. neoformans* populations.

Sorting of the yeasts cells population based on CMFDA fluorescence intensity

Based on the discovery of variable yeasts stress responses upon host interaction, cell sorting was decided to better characterize the phenotypes of these populations using the FACS Aria II (BD biosciences).

Yeasts obtained after 24hours-incubation within macrophages were sorted based on CALCO/CMFDA dot plot while yeasts obtained from 21 to 42 pooled mice inoculated 7

days before, were sorted based the SSC/CMFDA dot plot. Aggregates, cell debris (PE^{low} population), and dead yeasts (APC^{high} population) were then excluded. Three populations were sorted as $CMFDA^{high}$, $CMFDA^{med}$, $CMFDA^{low}$ for both conditions, with an additional population of $CMFDA^{high}/CALCO^{low}$ for the yeasts recovered after macrophage interaction. Independent duplicate experiments were performed and used for growth kinetics determination and gene expression analysis.
A yeast sample, harvested from a standard YPD culture, stained at the same time and stored in the same conditions than the experimental samples was used as a control (stained stationary control, sSTAT).

Growth curves determination
The growth kinetics of each population was analyzed. After sorting and centrifugation at 2000 rcf, the populations were ressuspended in sterile YPD containing 10% penicillin/ streptomycin (YPDps) at the desired concentration based on the absolute count provided by the cell sorter.
Each sample was studied in duplicate in the presence or absence of 10% FCS supplementation (100µL final volume) in parallel with sSTAT control and medium alone. The plates were incubated in a thermomixer (Eppendorf) at 30°C and 700 rpm. Optical density (OD) was recorded at 600nm at different time points. Analysis of the growth curves was performed using Prism Software 5.0 (GraphPAD Software) and the Weibull algorithm [171].

Sample preparation for quantitative real-time PCR
After sorting, the different yeasts populations were washed carefully in RNAase-free water to remove PBS salts, flash-frozen in liquid nitrogen and stored at -80°C. sSTAT control were processed in parallel. All experiments were performed with the SuperScript™ III Platinum® CellsDirect One-Step qRT-PCR Kit (Invitrogen) that is classically used for single-cell PCR analyses. The day before RNA extraction, the samples were lyophilized overnight. One microliter of lysis enhancer and 10µL of resuspension buffer were added to the lyophilisates and incubated 10 min at 75°C. Then, 1.6µl of DNAse buffer and 5µL of DNAse I were added and incubated 5 min at 25°C and then inactivated using 4µL of EDTA and incubation at 70°C for 10 min. RNA samples were then stored at -80°C.

One step quantitative real-time PCR
We based our selection on the genes that were homologues between H99 and *Saccharomyces cerevisiae* [172]. All H99 genes for which the gene description for *S. cerevisiae* contained the keywords ‘growth’, ‘stationary phase’, ‘starvation’, ‘oxidative stress’, were first selected. Additional H99 genes involved in capsule and cell wall formation and some regulated during early pulmonary infection [26] were added. The coding sequence of the selected H99 genes was then retrieved from the Broad Institute website (http://www.broadinstitute.org). The sequence of 90 different pre-designed Locked Nucleic Acids octamer probes of human Universal ProbeLibrary set (Roche) were used as the probe library. If a probe matched the selected gene, the corresponding primers were designed using the dedicated ProbeFinder Software (Roche, http:// www.universalprobelibrary.com). At the end, 37 assays were implemented for real-time quantitative PCR, including 33 for nuclear genes (**Primer Table 2**), 1 for ribosomal RNA genes (*18S rRNA*), 1 for a mitochondrial gene (*COX1*) and 2 for reference genes (*ACT1* and *GAPDH*).
Quantitative RT-PCR that allows primer specific reverse transcription (50°C for 15min) and

quantitative PCR amplification based on probe detection (95°C for 2 min and 45 cycles of 95°C 15 sec and 60°C 30 sec) was performed in a total volume of 10µL including 2µL of 1:10 dilution of each RNA samples.
Each RNA sample was normalized with geometric mean of the Cq of the corresponding *ACT1* and *GAPDH* gene expression [167]. Fold changes for each sample were calculated according to Pfaffl [168]. For hierarchical clustering analysis using MeV v4.6.1, the data were normalized as described above.

Statistical analysis.
Graph and Pearson's index (R^2) calculation, exact Fisher's test and one-way ANOVA test were performed using Prism 4.0 (GraphPAD Software). STATA 10.0 software (Stata Corporation) was used to compare the ClinCn/macrophages interactions' phenotypes with clinical outcome for the corresponding patients. For the multivariate analysis, logistic regression was used to determine factors independently associated with non-sterilization of CSF at week 2 (45 patients with available information). Only 2 variables were entered in the model because of the limited number of events (n=24). Odds ratios (OR) and their 95% confidence intervals (95% CIs) were determined.
Schematic representation of fold changes was performed using the open-source genomic analysis software MeV v4.6.1 (The TM4 Development Group) obtained from http://mev.tm4.org [170]. Complete linkage clustering and Pearson correlation were chosen to perform hierarchical clustering. The principal component analysis (PCA) analysis was performed based on 3 interaction parameters (PI, IPH2 and IPH48) and 5 mycological parameters (cell and capsule size, E1 binding, growth and chitin content) using the open-source genomic analysis software MeV v4.6.1 (Manhattan distance, mean centering mode and 10 neighbors for KNN imputation). Variables were compared using the Student's t test. P values ≤0.05 were considered significant.

Results

New flow cytometry assays are implemented to assess the dynamics of yeasts/ macrophages interactions

To estimate whether the interaction between ClinCn and host cells interactions was variable, we developed original quantitative flow cytometry assays using J774 murine macrophage cell line. Calcofluor (CALCO) is a basic fluorescent dye used to stain fungal cell wall. Preliminary studies using calcofluor staining revealed that fluorescence is transmitted from mother to daughter cells during multiplication in various conditions (YPD, within macrophages or in vivo) (**Figure 1A**). Immediately after staining, mean fluorescence intensity (MFI) was high for all cells. In YPD, after 3 hours of culture, an emerging population with a decreased MFI was detected while budding cells harboring decreased fluorescence were seen using fluorescence microscopy. This suggested that CALCO-labeled chitin was transferred from mother to daughter cells during budding. During protracted incubation, several populations with decreased MFI progressively appeared while the high CALCO-fluorescent initial population progressively disappeared over 24 hours. This phenomenon was confirmed using dynamic imaging of yeasts proliferating inside J774 cells (**Figure 1B-D**). The decrease in CALCO fluorescence intensity observed in yeasts cells recovered from the lungs (**Figure 1A**, right panel) as soon as 30 minutes after inoculation was attributed to quenching and not multiplication (data not shown).

Based on these observations, we decided to assess the dynamics of yeasts/ macrophages interactions by flow cytometry (FACS-YMI) assays using the MacsQuant® analyzer (**Figure 2**). Preliminary experiments (**Figure 3**) using the reference strain H99 helped us define optimal opsonin quantity (E1 mAb) and yeasts:macrophages ratio using microscopy. Two E1 concentrations and ratio were fixed as 5µg E1 mAb and 5:1 ratio for phagocytosis assay and 1µg E1 mAb and 2.5:1 ratio for proliferation assay (**Figure 3A**).

In the phagocytosis assay, three distinct populations were observed on the CALCO/FITC dot plot, the intracellular yeast population being $CALCO^{high}FITC^{neg}$, the extracellular yeast $CALCO^{high}FITC^{pos}$, and cell debris $CALCO^{neg}FITC^{neg}$ (**Figure 4A**). This allowed us defining a phagocytic index (PI) (103.7 for H99). In the proliferation assay, three distinct intracellular yeast populations ($APC^{pos}FITC^{neg}$ gate) were observed, the mother yeast cells population being $CALCO^{high}$, and 2 populations of daughter cells $CALCO^{med}$ and $CALCO^{low}$ (**Figure 4A**), the lowest fluorescent cells (daughter cells) being the smallest in size, as determined based on the Forward scatter (FSC, **Figure 3B**). After 48hours of incubation, the FSC values of the $CALCO^{high}$ and $CALCO^{med}$ populations were higher than after 2 hours of incubation. Intracellular proliferation indexes were then calculated based on the number of $CALCO^{high}$, $CALCO^{med}$ and $CALCO^{low}$ populations after 2 (IPH2) and 48 (IPH48) hours of incubation (1.00 and 1.20, respectively for H99).

Results obtained with H99 mutants validates the FACS-YMI assays

To validate the assays, mutant strains derived from H99 and known for increased phagocytosis (*app1Δ*, *lac1Δ*) and decreased proliferation (*vad1Δ*, *vps34Δ*, *ipc1Δ* and *lac1Δ*) were screened in comparison to H99. The FACS-YMI assays allowed discrimination between mutant strains based on PI, IPH2 and IPH48 ($P<0.0001$ each, **Figure 5**). For the mutants, the PIs were categorized in 2 groups (similar to H99 [ranging from 0.8 to 1.2] for *vps34Δ*, *ipc1Δ*, *vad1Δ* or higher [1.5 to 1.9] for *app1Δ*, *lac1Δ*). Three categories were also delineated for IPH2 (very low [0.02-0.04] for *vad1Δ* and *vps34Δ*, intermediate low [0.35] for *lac1Δ*, and low [0.7] for *app1Δ* and *ipc1Δ*), and for IPH48 (very low [0.02-0.2] for *vps34Δ* and *vad1Δ*, low [0.8] for *lac1Δ*, and high [2.9-3.1] for *app1Δ* and *ipc1Δ*).

Interactions of *C. neoformans* clinical isolates with J774 macrophages are highly diverse

Based on these validated FACS-YMI assays, we then studied 54 ClinCn recovered from the CSF of HIV-positive or -negative unrelated patients (**Table 1**). An important diversity in terms of genotypes (11 MultiLocus Sequence Types) and baseline phenotype characteristics (colony morphology, cell and capsule sizes, growth rate, E1 mAb binding level, chitin content, urease activity and melanin production) was observed (**Figure 6**).

We then established the diversity of the ClinCn/macrophages interactions. A 30-fold variation in PI (**Figure 7A and Figure 8**), 50-fold variation in IPH2 and 16-fold variation in IPH48 (**Figure 7B and Figure 8**) were found. The E1 mAb binding level is inversely correlated with PI (P=0.006). The ClinCn exhibiting high (≥ 0.5) PI and low (<1.0) E1 mAb binding level were mostly smooth (26/30, 86.7%), as compared to those exhibiting low PI and high E1 binding which were mostly mucous (9/10, 90%, P<0.0001, **Figure 9**). There was no significant association between genotypes and baseline phenotypes or phenotypes of ClinCn/macrophages interaction using principal component analysis (PCA, data not shown).

ClinCn/macrophages interactions phenotypes are associated with variable outcome of cryptococcal meningoencephalitis in humans

Given the high variability of ClinCn/macrophages interaction phenotypes, we then wondered if these parameters (PI, IPH2, IPH48) correlated with outcome of infection in the corresponding patients. Four categories of isolates were defined according to PI (<0.5 and ≥0.5) and IPH2 (≤1 and >1). Based on univariate analysis, non-sterilization of CSF despite 2 weeks of antifungal therapy was associated with a population of isolates harboring decreased PI and IPH2 (**Figure 10 and Table 2**). The proportion of parameters previously [11] associated with non-sterilization of CSF (gender, dissemination, or high CSF antigen titer) did not significantly differ among the four categories of isolates. Death at months 3 was significantly associated with a population of isolates harboring high PI and IPH2 (**Figure 10**). Parameters previously [11] associated with death at month 3 (abnormal neurology or brain imaging) did not significantly differ among the four categories. In the multivariate analysis, the risk of non-sterilization of the CSF at week 2 was independently associated with low PI and IPH2 (Odds Ratio (OR) [95% CI]= 15.5 [1.3-184.4], P=0.030) and with HIV infection (OR=25.2 [1.8-348.6], P=0.016) (**Table 2**).

Expression of some virulence factors correlates with ClinCn/macrophages interaction phenotypes

Considering that in a standardized in vitro model, variations in ClinCn/macrophages interaction phenotypes were associated with different outcomes in humans, we further explored known virulence factors in relation with these phenotypes. We selected 9 ClinCn (s9-ClinCn) based on various combinations of their ClinCn/macrophages interaction phenotypes (**Figure 11A**), genotypes and related patient's outcomes. All s9-ClinCn were fertile (data not shown), with variable virulence in mice as shown by median survivals (expressed as a ratio for each s9-ClinCn to H99) ranging from 0.57 (AD2-82a) to 3.3 (AD1-07a) (**Figure 11B**, p <0.0001). The 2 hours-intracellular (iH2) and baseline (BsH2) relative expressions of 6 virulence factors (*LAC1*, *URE1*, *APP1*, *VAD1*, *IPC1*, *PLB1* genes [63,114,115,158,159,173]) and one mitochondrial gene (cytochrome oxidase 1, *COX1* [22,174]) were quantified with *GAPDH* as the reference gene and H99 as the control. High BsH2 *APP1* expression (>5 fold) was significantly associated with low PI (P=0.028).

IPH48 and iH2 expression were significantly correlated for *IPC1* (R^2=0.73, P=0.003), *APP1* (R^2=0.66, P=0.008), *COX1* (R^2=0.66, P=0.008), *VAD1* (R^2=0.65, P=0.009) (**Figure 11C**), and *PLB1* (R^2=0.55, P=0.021). PI and iH2 expression of *LAC1* (R^2=0.59, P=0.016) were also correlated. No correlation was found for *URE1* gene expression.

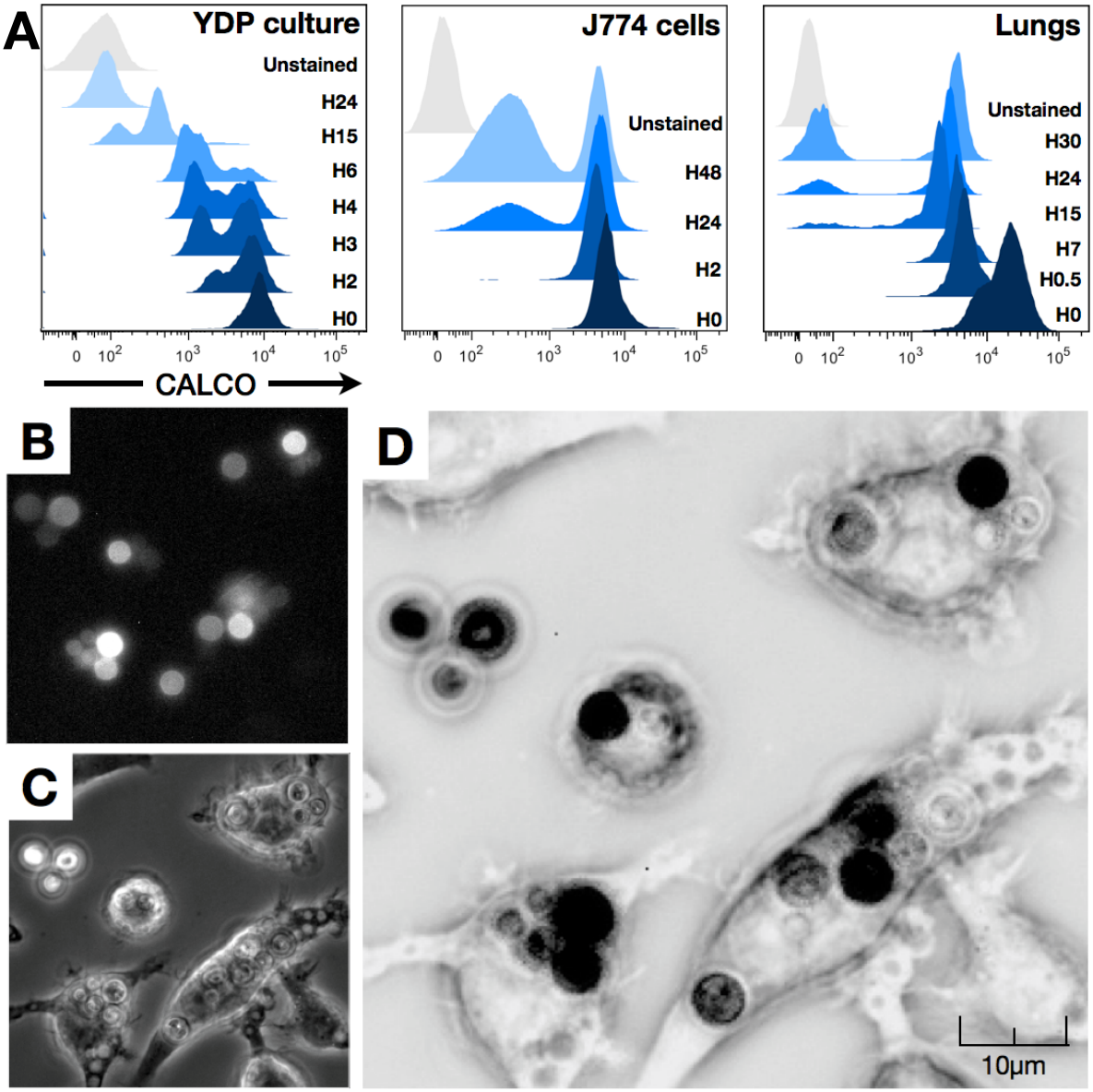

Figure 1: Decrease in fluorescence in calcofluor-labeled *C. neoformans* (reference strain H99) during multiplication.

(A) Yeast multiplication in vitro was evaluated after yeasts staining with calcofluor prior to incubation at 30°C in liquid YPD, interaction with murine macrophages or inoculation to OF1 outbred mice. The yeasts were recovered from different environments (YPD culture, J774 cells, and Lungs) at different time points, and compared to unstained yeasts using flow cytometry (MacsQuant analyzer). The appearance of a population with lower CALCO fluorescence (daughter cells) was visualized over time during incubation in the three conditions. Of note, the decrease in CALCO fluorescence intensity observed in yeasts cells recovered from the lungs as soon as 30 minutes after inoculation was attributed to quenching and not multiplication (data not shown). **(B-D)** Visualization of H99 multiplication inside macrophages assessed by dynamic imaging. Yeasts were stained with calcofluor prior to incubation with J774 cell line at a 2.5:1 ratio in the presence of E1 anti-capsular polysaccharide monoclonal antibody (E1mAb) (10^6 yeasts/1µg E1mAb). Dynamic imaging using the Nikon Biostation was performed starting after one hour of coincubation (images obtained at 16 hours 45 min are shown). **(B)** DAPI fluorescence filter. **(C)** Transmitted light. **(D)** Decreased fluorescence of daughter cells assessed after image treatment using ImageJ software (merging pictures B and C and inverting the look-up table. Mother yeast cells appear black whereas daughter cells look medium to light grey (original magnification x40).

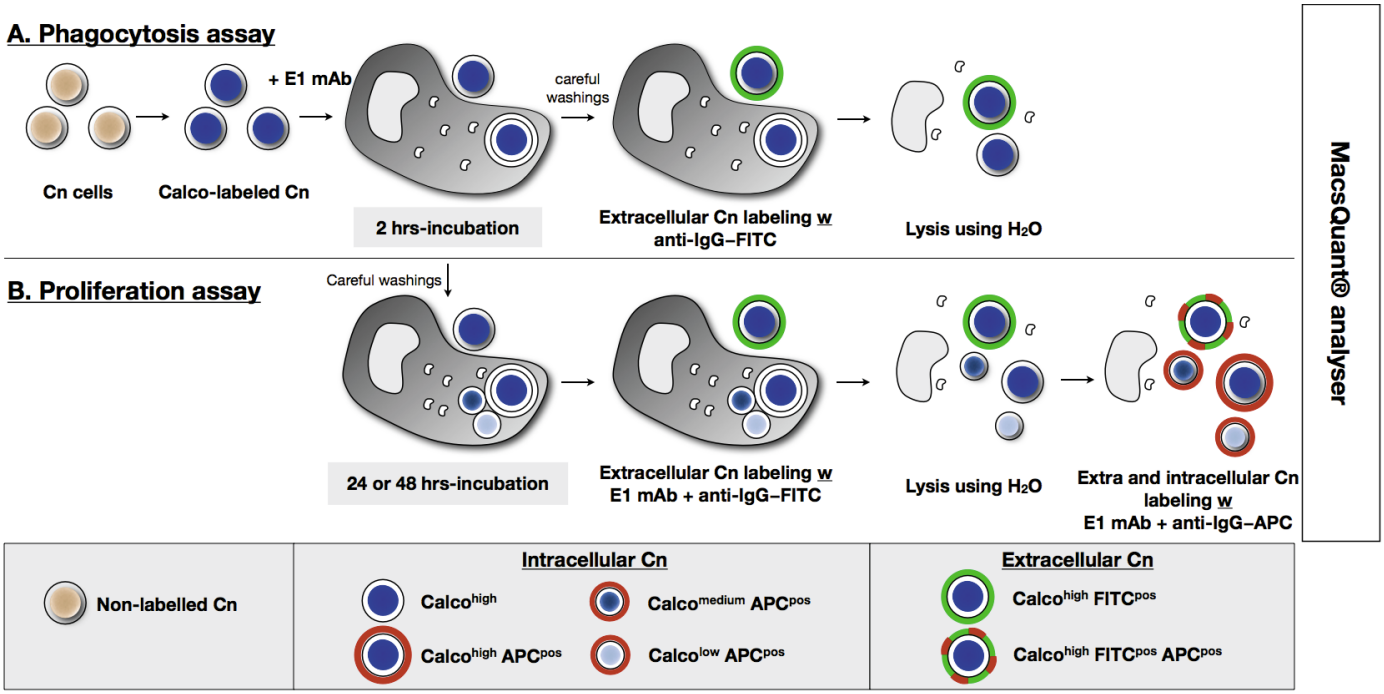

Figure 2: Schematic representation of *C. neoformans* labeling steps for flow cytometry analysis of yeasts/macrophages interaction (FACS-YMI).

Yeasts were first stained with calcofluor and then incubated with J774 cells at 37°C in the presence of E1 mAb (opsonin). After careful PBS washings, the incubation was stopped after 2 hours incubation (phagocytosis assay, **A**) or prolonged up to 48 hours in fresh medium (proliferation assay, **B**). In both assays, remaining extracellular yeasts were then stained with anti-IgG–FITC antibody, washed and J774 cells lysed using H_2O. An additional labeling step was performed in the proliferation assay with E1 mAb and an anti-IgG–APC added to stain daughter yeast cells. Samples were analyzed using the MacsQuant® analyzer.

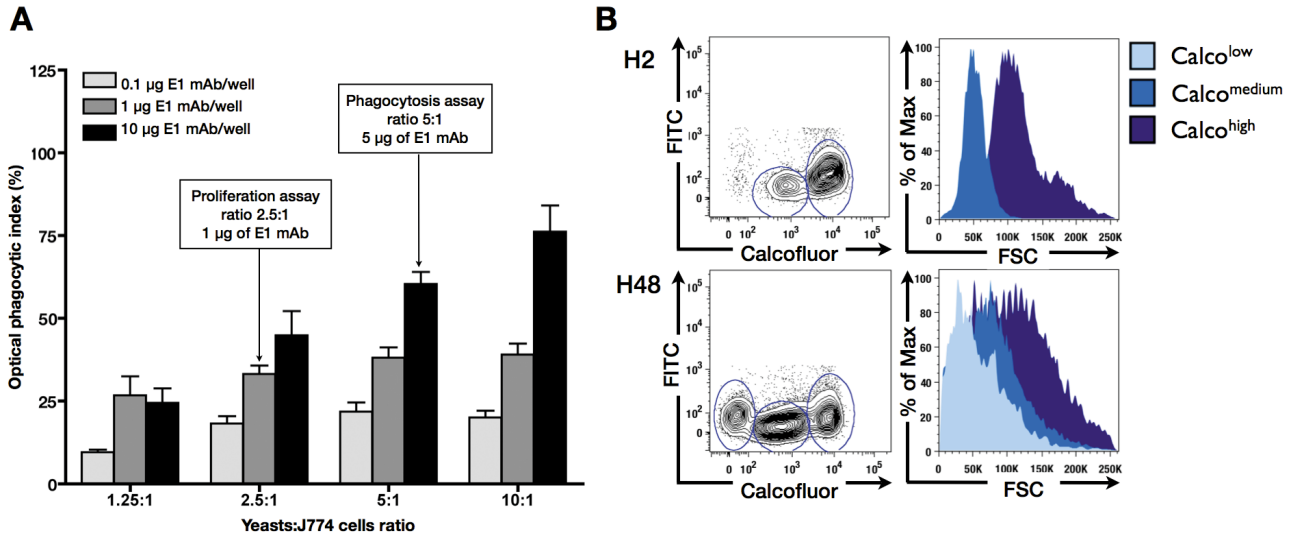

Figure 3: Preliminary experiments.

(A) Influence of the Cn:macrophages ratio and of the E1 mAb quantity on the magnitude of yeast strain H99 phagocytosis by murine macrophage cell line J774. The concentration of macrophages was kept constant while that of H99 varied to provide a ratio ranging from 1:1 to 10:1. The anti-capsular polysaccharide E1 mAb was added at 0.1, 1 or 10 µg/well. The optical phagocytic index (Opt-PI) was calculated as the number of intracellular yeasts /100 macrophages. Each condition was tested in duplicate in 2 independent experiments. Optimal conditions for the phagocytosis and the proliferation assays are shown. The bars represent the mean ± SD of one representative experiment.**(B)** During intracellular proliferation of H99 yeast cells, the size of each yeast cell using forward scatter (FSC) histograms (right panel) is lower in the daughter cell populations ($CALCO^{low}$ and $CALCO^{med}$) compared to mother cells ($CALCO^{high}$) at H2 and H48.

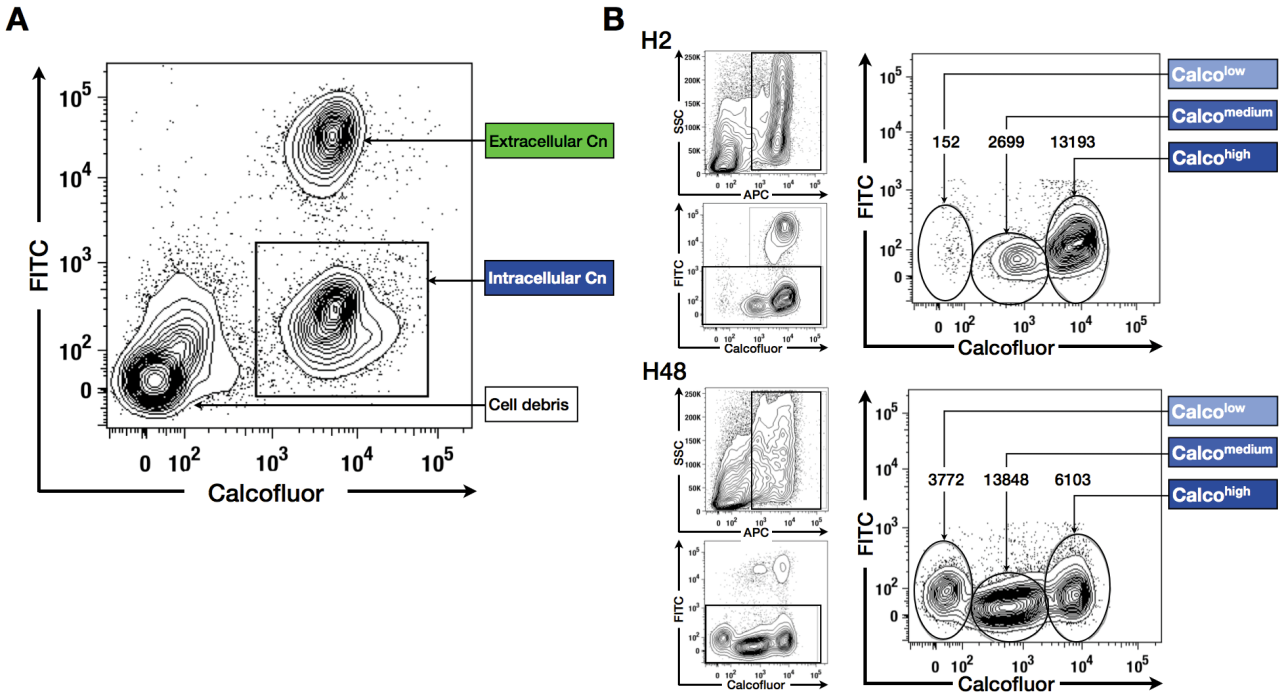

Figure 4: The FACS-YMI allowed assessment of the dynamics of yeasts/ macrophages interactions.

(A) Determination of phagocytosis. Intracellular yeasts ($CALCO^{high}FITC^{neg}$) were easily discriminated from extracellular yeasts ($CALCO^{high}FITC^{pos}$) and macrophage debris ($CALCO^{neg}FITC^{neg}$). **(B)** Determination of yeasts intracellular proliferation. After selection of the APC^{pos} (excluding cell debris, upper left graphs) and $FITC^{neg}$ populations (intracellular Cn, lower left panels), different subsets of intracellular Cn corresponding to mother Cn cells ($CALCO^{high}$), and daughter Cn cells ($CALCO^{med}$ and $CALCO^{low}$) were observed (right panels). A decrease of mother cells in parallel to an increase of daughter cells populations was observed between 2 hours (H2) and 48 hours (H48) of coincubation, asserting intracellular proliferation (number of events reported above each subset).

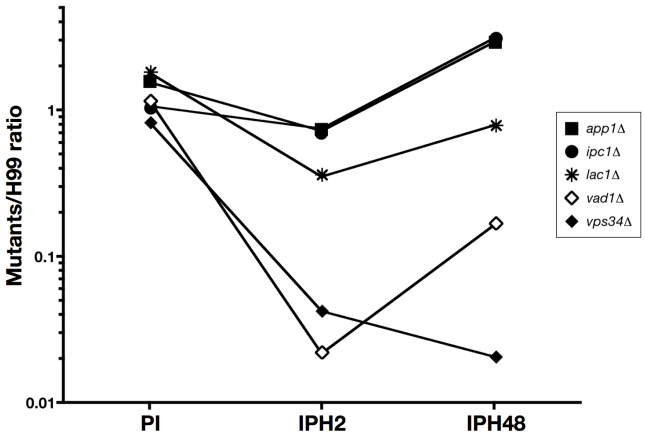

Figure 5: Screening of well-characterized mutant strains compared to H99 using the FACS-YMI.

Dot plots presenting the corresponding phagocytosis (PI), intramacrophagic proliferation at H2 (IPH2), and H48 (IPH48) values for each mutant linked by a solid line (Log_{10} scale). PI were categorized in 2 groups: similar to H99 (*vps34Δ*, *ipc1Δ*, *vad1Δ*), higher (*app1Δ*, *lac1Δ*). Three categories were also delineated for IPH2 (very low for *vad1Δ*, *vps34Δ*; intermediate low for *lac1Δ*, and low for *app1Δ* and *ipc1Δ*), and for IPH48 (very low) for *vps34Δ* and *vad1Δ*; low for *lac1Δ*, and high for *app1Δ* and *ipc1Δ*).

Table 1: Characteristics of the 54 patients corresponding to the 54 clinical isolates of *Cryptococcus neoformans* studied.

Parameter	*n* (%)
Male/female ratio	4.4:1
Born in Africa	12/54 (22.2)
HIV infected	45/54 (83.3)
Non-HIV infected	9/54 (16.7)
Abnormal neurology	24/54 (44.4)
Abnormal brain imaging	18/51 (35.3)
Disseminated infection	35/54 (64.8)
Capsular polysaccharide titer of >512 in CSF	27/49 (55.1)
Nonsterilization of CSF at wk 2	24/45 (53.3)
Death at mo 3	11/53 (20.8)

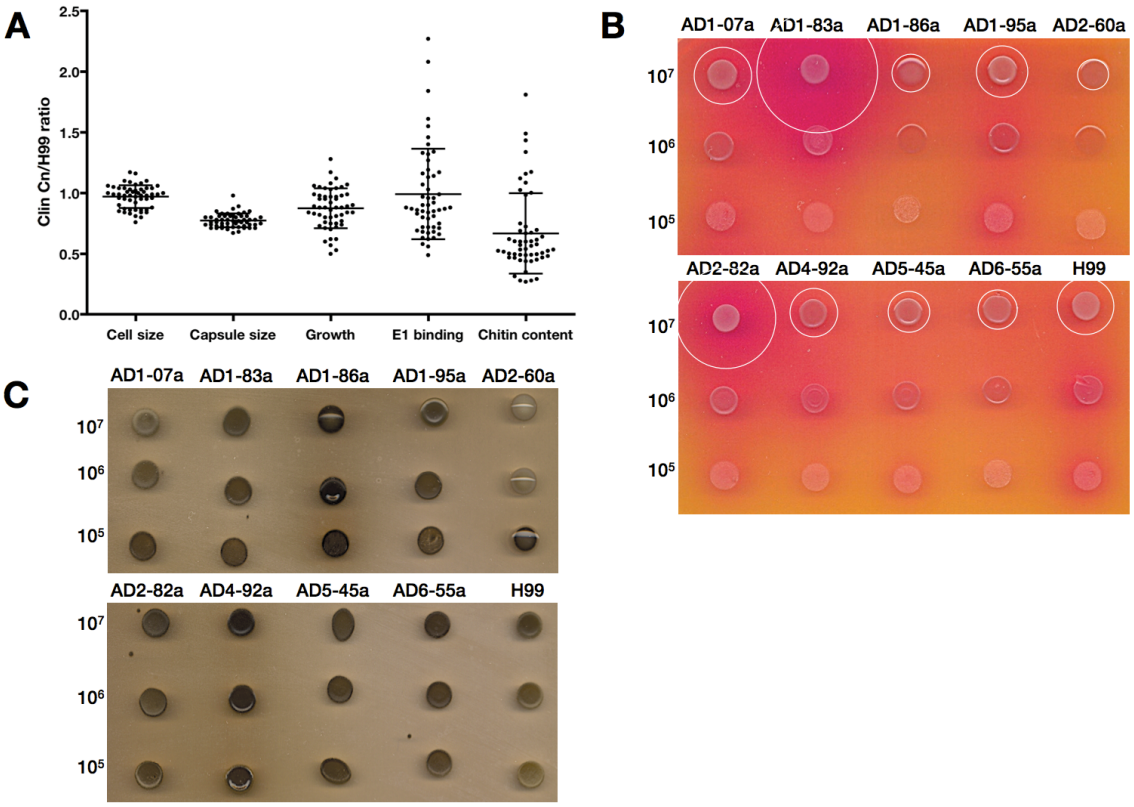

Figure 6: The baseline phenotype of the ClinCn is diverse in terms of enzymatic activity and cell characteristics.

(A) Distribution of cell sizes, capsule sizes, growth rates (slope), E1 mAb binding level and chitin content compared to H99 reference strain (horizontal lines represent mean ± SD). **(B)** Variability of urease activity in the s9-ClinCn (10^5 to 10^7 cells) expressed as the diameter of the red colored circle around the colony (ImageJ software v1.42q). **(C)** Variability of melanin production in the s9-ClinCn (10^5 to 10^7 cells) as shown by the intensity of the brown pigment.

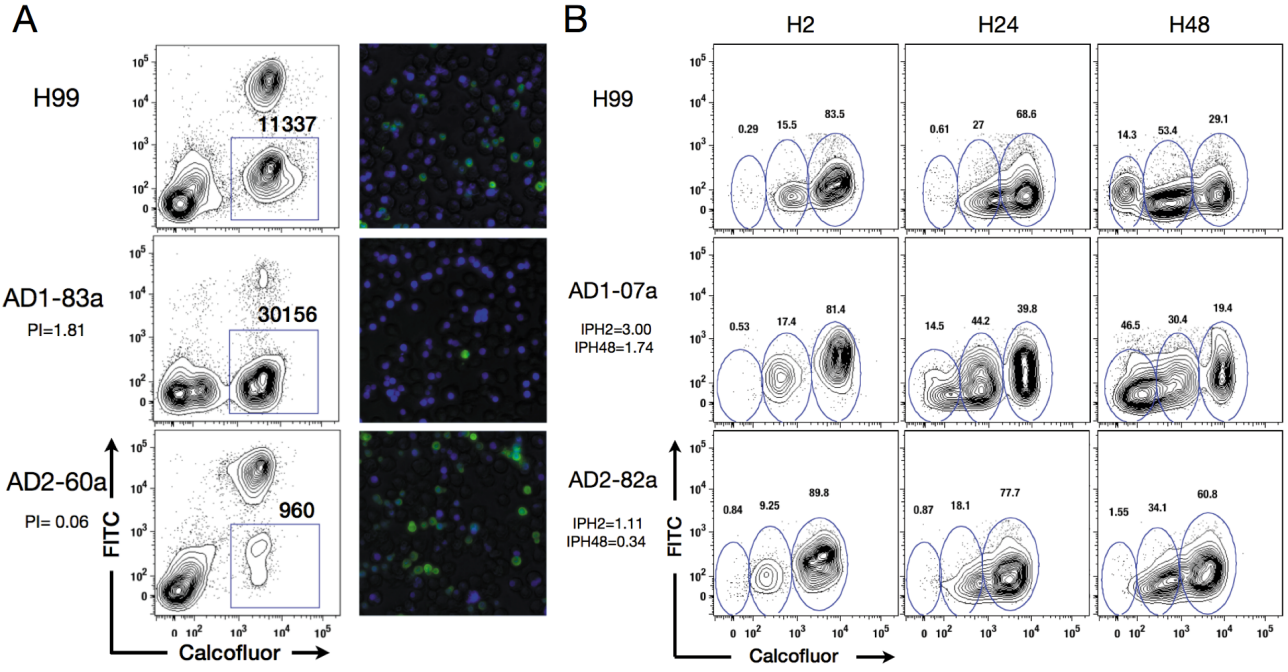

Figure 7: Phagocytosis and proliferation assays.

(A) Contrasted phagocytic indexes for 2 ClinCn compared to H99 assessed using FACS-YMI (left panel) and fluorescence microscopy (right panel). The number of CALCO^{high}FITC^{neg} events (intracellular yeasts) is reported above the gates. Blue-fluorescent Cn cells are intracellular whereas blue- and green-fluorescent Cn cells are extracellular (Right panel). **(B)** Contrasted proliferation indexes (IPH2 and IPH48) for 2 ClinCn compared to H99 assessed using FACS-YMI at 2 hours (H2), 24 hours (H24) and 48 hours (H48) of coincubation. The proportion of CALCO^{high}, CALCO^{med}, CALCO^{low} events in the APC^{pos}, FITC^{neg} gates is reported above each gate.

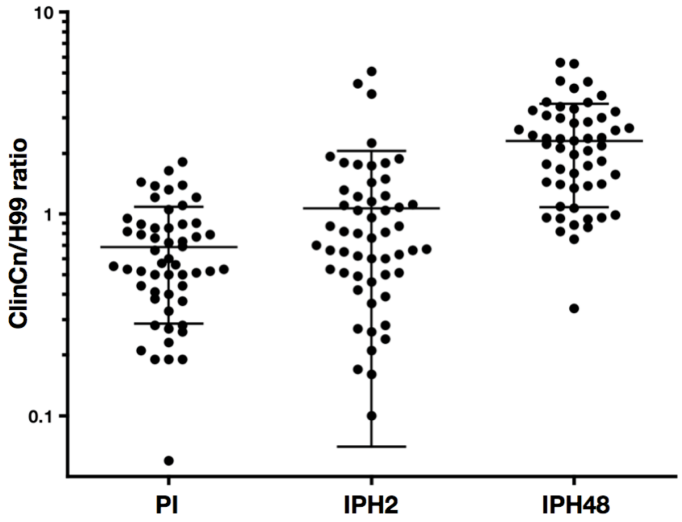

Figure 8: The 54 Cn clinical isolates (ClinCn) harbored variable interactions with macrophages.

Compared to H99, the distribution of phagocytic (PI), 2 hours-proliferation (IPH2), and 48 hours-proliferation (IPH48) indexes showed 30-fold, 50-fold, 16-fold variations, respectively (Log_{10} scale). Each circle represents the mean of duplicates for a given ClinCn obtained from 2 independent experiments. Bars represent mean ± SD for the 54 ClinCn.

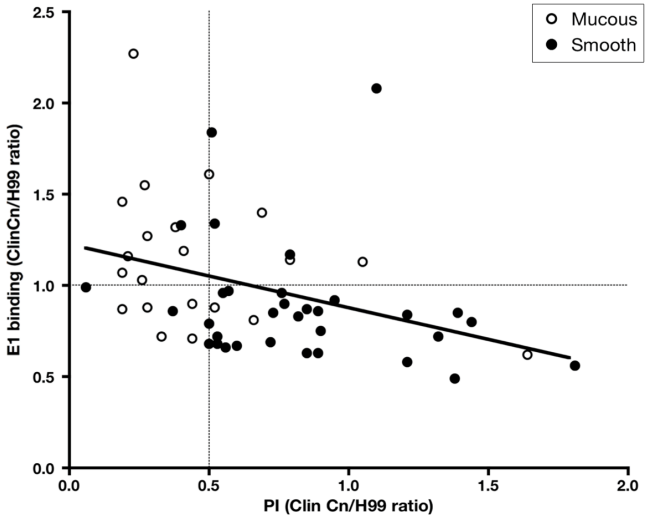

Figure 9: Scatter plots presenting PI *vs.* E1 binding

The E1 mAb binding level is inversely correlated with PI. Scatter plot of PI vs. E1 mAb binding level for the 54 ClinCn compared to H99 according to colony morphology recorded as mucous (open circle) or smooth (black circle). The solid line represents the regression line (*P*=0.006). Dotted lines show the cut-off values for PI and E1 mAb binding delineating a significant association with colony morphology (*P*<0.0001).

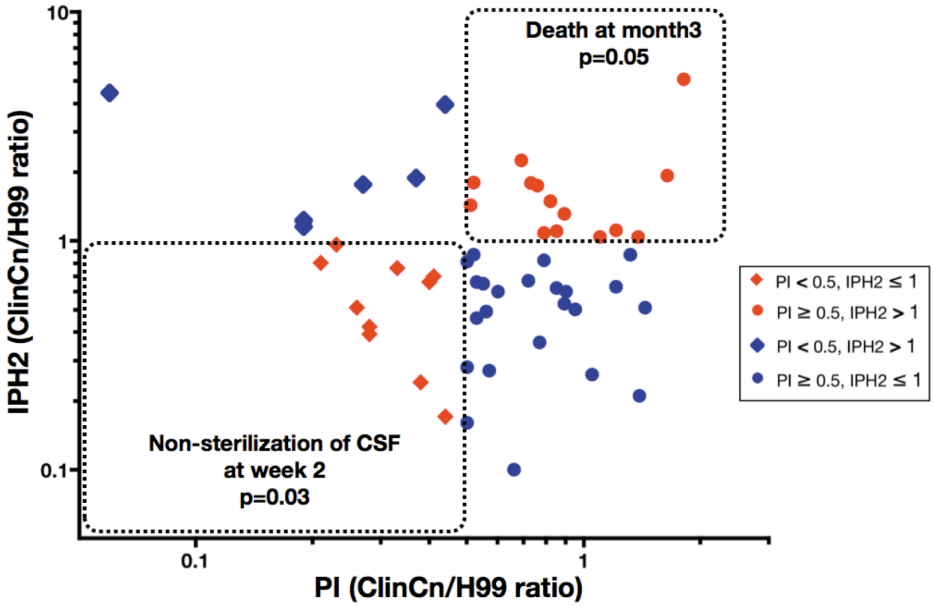

Figure 10: Scatter plots presenting PI *vs.* IPH2

Four categories of isolates were defined according to PI (<0.5 and ≥0.5) and IPH2 (≤1 and >1). Population of isolates harboring PI <0.5 and IPH2 ≤1 was significantly associated to non-sterilization of CSF at week 2 (*P*=0.03) and that harboring PI ≥0.5 and IPH2 >1 was significantly associated to death at months 3 (*P*=0.05).

Table 2 : Analysis of patient's outcome considering the four categories of isolates defined based on PI and IPH2.

Patients' outcomes (non-sterilization of CSF at week 2 and death at month 3) are significantly associated with the phenotypes of interaction with J774 macrophages (phagocytic index (PI) and intracellular proliferation at H2 (IPH2)) of the clinical isolates for which the corresponding outcome was available.

		No. (%) of patients with:		Univariate analysis			Multivariate analysis		
Outcome[a]	Parameter	Failure (n = 24) or death (n = 11)	Success (n = 21) or survival (n = 42)	OR	95% CI	P	OR	95% CI	P
Yeast eradication from CSF at wk 2	PI ≥ 0.5, IPH2 ≤ 1	7 (36.8)	12 (63.2)	Reference					
	PI < 0.5, IPH2 > 1	4 (80.0)	1 (20.0)	6.86	0.63–74.19	0.113	5.79	0.53–63.37	0.150
	PI ≥ 0.5, IPH2 > 1	6 (50.0)	6 (50.0)	1.71	0.40–7.43	0.471	3.48	0.61–19.78	0.159
	PI < 0.5, IPH2 ≤ 1[c]	**7 (77.8)**	**2 (22.2)**	**6.00**	**0.97–37.30**	**0.055**	**15.51**	**1.30–184.43**	**0.030**
	HIV positive[b]	**23 (95.8)**	**14 (66.7)**	**1.64**	**0.85–3.19**	**0.012**	**25.16**	**1.84–348.63**	**0.016**
	HIV negative	1 (4.2)	7 (33.3)	0.14	0.02–1.16				
Death at mo 3	PI ≥ 0.5, IPH2 ≤ 1	3 (13.0)	20 (87.0)	Reference					
	PI < 0.5, IPH2 > 1	1 (16.7)	5 (83.3)	1.34	0.11–15.70	0.819			
	PI ≥ 0.5, IPH2 > 1	**6 (42.9)**	**8 (57.1)**	**5**	**1.00–25.02**	**0.050**			
	PI < 0.5, IPH2 ≤ 1	1 (10.0)	9 (90.0)	0.74	0.07–8.13	0.806			

[a] Patients' outcomes are represented by nonsterilization of CSF at week 2 (i.e., failure or success at yeast eradication from CSF) and death at month 3 (i.e., death or survival).
[b] Only two variables were added to the model due to the small number of events recorded (n = 24).
[c] Parameters appearing in bold are statistically significant.

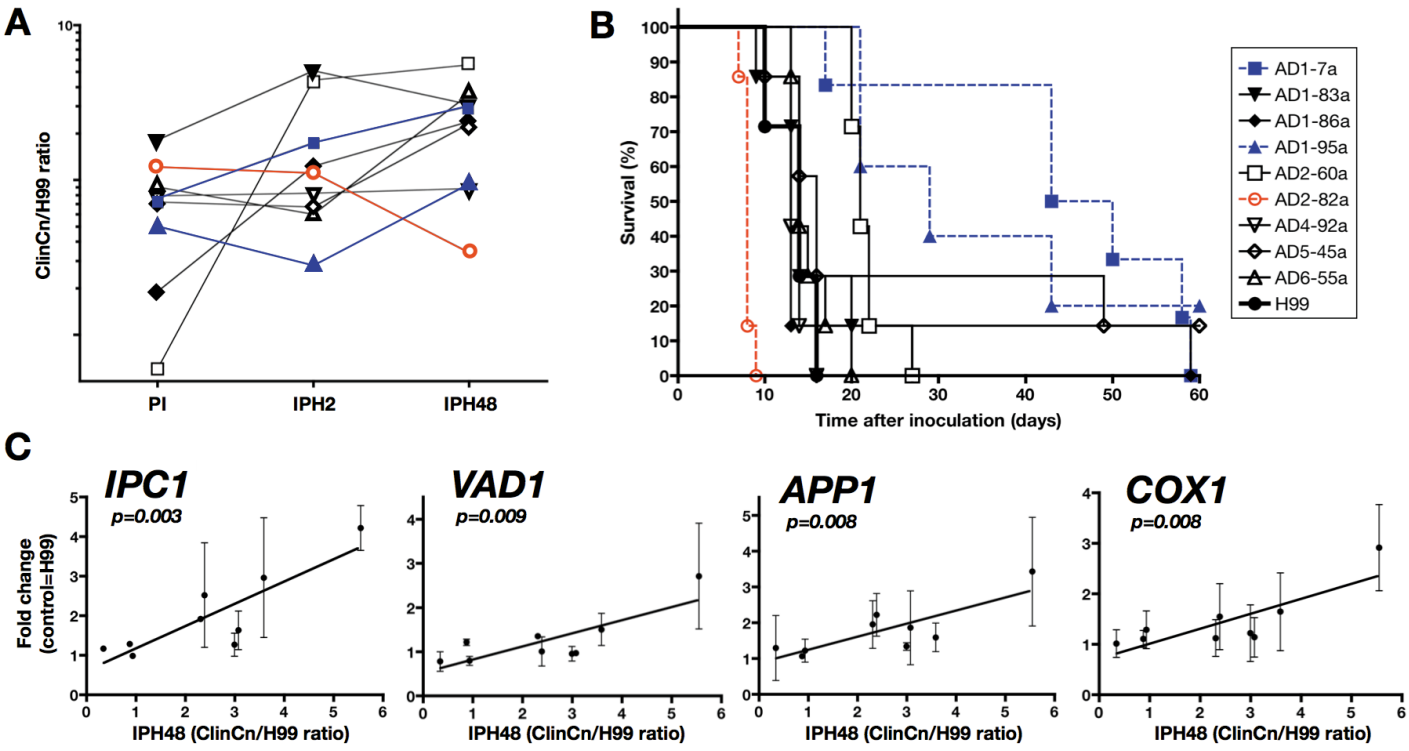

Figure 11: The *in vivo* behavior (virulence in mice) of the s9-ClinCn is heterogeneous and the intracellular (J774 cells) expressions of known virulence factors correlate with the 48 hours-proliferation index.

(A) Dot plots presenting the corresponding PI, IPH2, and IPH48 values for each s9-ClinCn. The values corresponding to a given isolate are linked by a solid line (Log_{10} scale). (B) Outbred male mice were intravenously inoculated with 10^5 yeasts, and death recorded over 60 days. Compared to H99 (Black circle, thick line), AD2-82a (opened circles, dotted line) is more virulent (median survival ratio = 0.57), whereas AD1-95a (black triangle, dotted line) and AD1-7a (black square, dotted line) are less virulent (median survival ratio = 2.1 and 3.3, respectively). (C) Compared to H99, IPH48 of the s9-ClinCn correlated with the intracellular expression of *IPC1*, *VAD1*, *APP1*, *COX1* genes. Bars represent mean ± SD of duplicates from 2 independent experiments for each s9-ClinCn. The linear regression curve is shown.

Implementation of a new flow cytometry assay to analyze simultaneously multiplication and stress response in *C. neoformans*

To study yeast adaptation to different environments, we developed an assay that combined analysis of multiplication and stress response. Multiplication was quantified as described above (**Figure 1A**). Stress response was evaluated using 5-chloromethylfluorescein diacetate (CMFDA) (**Figure 12A-C**) that measured a glutathione-dependent phenomenon as shown by preliminary experiment using diethyl maleate, a glutathione-depleting agent (DiEM, **Figure 12A**). The yeast cells in stationary phase (Baseline, H0) harbored basal fluorescence that increased over time with various stresses (water, hydrogen peroxide, fresh medium and heat (**Figure 12B**). Of note, after 24 hours of incubation in hydrogen peroxide, the CMFDA fluorescence level was comparable to the unstained condition (**Figure 12B**, right upper panel) with CFU analysis revealing that all yeasts were dead (data not shown). The level of CMFDA fluorescence depended on the stimulus (2 hours) with YNB medium inducing the lowest and hydrogen peroxide the highest stress response (**Figure 12C**).

Viability of the yeasts was assessed based on Topro-3 iodide (TOPRO) fluorescence (**Figure 13**), allowing exclusion of dead cells in all subsequent experiments.

Dynamics of *C. neoformans* adaptation to host

We used two models to study the yeasts adaptation to the hosts in terms of multiplication and stress response, looking for changes over time in vitro (J774 macrophages) and in vivo (mice) (**Figure 14**).

A population of daughter yeast cells was observed as soon as 2 hours after interaction with J774 cells and 15 hours in lungs (**Figure 14A, 14C**) and increased overtime (**Figure 14B, 14D**). CMFDA fluorescence of yeast cells rapidly increased 2 hours after J774 cells interaction and 7 hours in lungs compared to the control with the majority of the population remaining $CMFDA^{high}$ over time. However, a sub-population harboring a lower CMFDA fluorescence (called '$CMFDA^{low}$', black arrows) at H24 in J774 cells and at H30 in lungs appeared and increased overtime. This phenomenon affected first mother cells (H24) and then daughter cells (H48) in J774 cells and both populations at H30 in lungs.

Subsequent experiments were done with mice inoculated 7 days before, based on the assumption that dormant cells could already be present and in sufficient number for further analysis.

Multiplication and stress response of yeast cells were then assessed in brain, lungs and spleen of 6 individual OF1 mice (**Figure 15**) and analyzed using classical flow cytometry (Macsquant analyzer, Miltenyi). Mother cells were not observed in brain, rare in spleen, and present in the lung of 3/6 OF1 mice. The mother cell population was never detected in any organ of BALB/c mice (data not shown). The pattern of stress response differed between organs but was specific with several circumscribed populations in lungs from 5/6 mice.

We thus decided to explore morphological features and fluorescence characteristics of the resident viable yeasts in pooled lungs homogenates using multispectral imaging flow cytometry ($Imagestream^{X}$) (**Figures 16-18**). After determination of the optimal analysis strategy (**Figure 16**), we defined 9 populations based on CMFDA/CALCO dot plot and optical control (**Figure 17A; Figure 16G**) and quantified the proportion of each population (**Figure 17B-D)**. Daughter cells always represented less than 20% of the three CMFDA populations. Mother cells represented more than half of the $CMFDA^{high}$ population and less than 40% of the others (**Figure 17D**). The largest cells were mostly composed of

mother cells, but a sub-population of mother cells was small-sized cells. Daughter cells were mostly small cells (**Figure 17E-F**). The global analysis of morphological features (54 algorithms) revealed several clusters with 3 well-defined populations containing daughter cells, mother cells and CMFDA^{low} (**Figure 17G**).

Analysis of specific *C. neoformans* populations

To go further into the analysis of the different populations, we focused first on the CMFDA^{high}/mother cells population (**Figure 18**). Two patterns of CMFDA fluorescence were observed, some cells harboring peripheral extracellular fluorescence (designated 'surrounded', CMFDA^{sur}) and others intracellular fluorescence (CMFDA^{intra}) visualized by Imagestream^{X} (**Figure 18A**) and fluorescence microscopy (**Figure 18B**). These two populations were discriminated based on the modulation (texture analysis) and the area (size analysis) algorithms dot plot (**Figure 18C**). The majority of mother cells were found in the CMFDA^{intra} while CMFDA^{sur} contained the same proportion of mother and daughter cells (**Figure 18D**). In the CMFDA^{sur} population, some yeasts harbored a typical morphology as observed using Imagestream^{X} (**Figure 18A-C**) and interferential contrast microscopy (**Figure 19A**). These cells (thereafter called 'Drop Cn') were small (5.80µm ± 0.80) with an enlarged cell wall and a well-defined round refringent vesicle. This population was composed of a higher proportion of mother cells compared to yeast cells harboring a regular morphology ('Reg Cn') (**Figure 18E**). Drop Cn represented less than 25% of each CMFDA population (**Figure 18C**). Compared to Reg Cn, Drop Cn did not harbor a well-organized nucleus (DAPI staining), had a low RNA content (SYTO 85) and mitochondrial activity (Mitotracker) and exhibited a complete retraction of the cytoplasm around the central vesicle (MDY64, **Figure 19B-C**). These observations suggested that Drop Cn were dead yeasts with low transcriptional and mitochondrial activity, and disorganized cytoplasm and nucleus architectures, despite having been initially selected in the TOPRO^{low} (viable) population. This was confirmed by dynamic imaging after observation that Drop Cn cells were unable to bud over 48 hours in YPD + 10% penicillin streptomycin (YPDps) (data not shown)**.** Additional experiments showed that the relative proportion of the different yeasts populations in terms of multiplication and stress response varied with yeast strains (**Figure 20A-C)**, comparing H99 and two previously characterized clinical isolates (AD1-07a and AD1-83a) [23]. In addition, the proportion of the repartition of the Drop Cn population (**Figure 20D-E)**, the proportion of dead yeasts (**Figure 20F)**, and CMFDA^{sur} (**Figure 20G)** varied also among isolates.

Specific phenotype of the CMFDA^{low} population

Cell sorting was implemented to focus on CMFDA^{low} population compared to others recovered from both models of interaction with host [24 hours incubation with macrophages (MP) or infected lungs from OF1 mice (MO)] and to control yeasts in stationary phase stained in the same conditions (sSTAT) (**Figure 21A, 21C**). The sorted populations were controlled visually using fluorescence microscopy (**Figure 21E**). We wondered whether they harbored specific phenotypes in terms of growth capacity and specific transcriptional activity.

Growth curves analysis revealed important differences among the various populations with the CMFDA^{low} population unable to grow (MO) or exhibiting delayed growth (MP) in YPD compared to the other populations and sSTAT (**Figure 21B, 21D**).

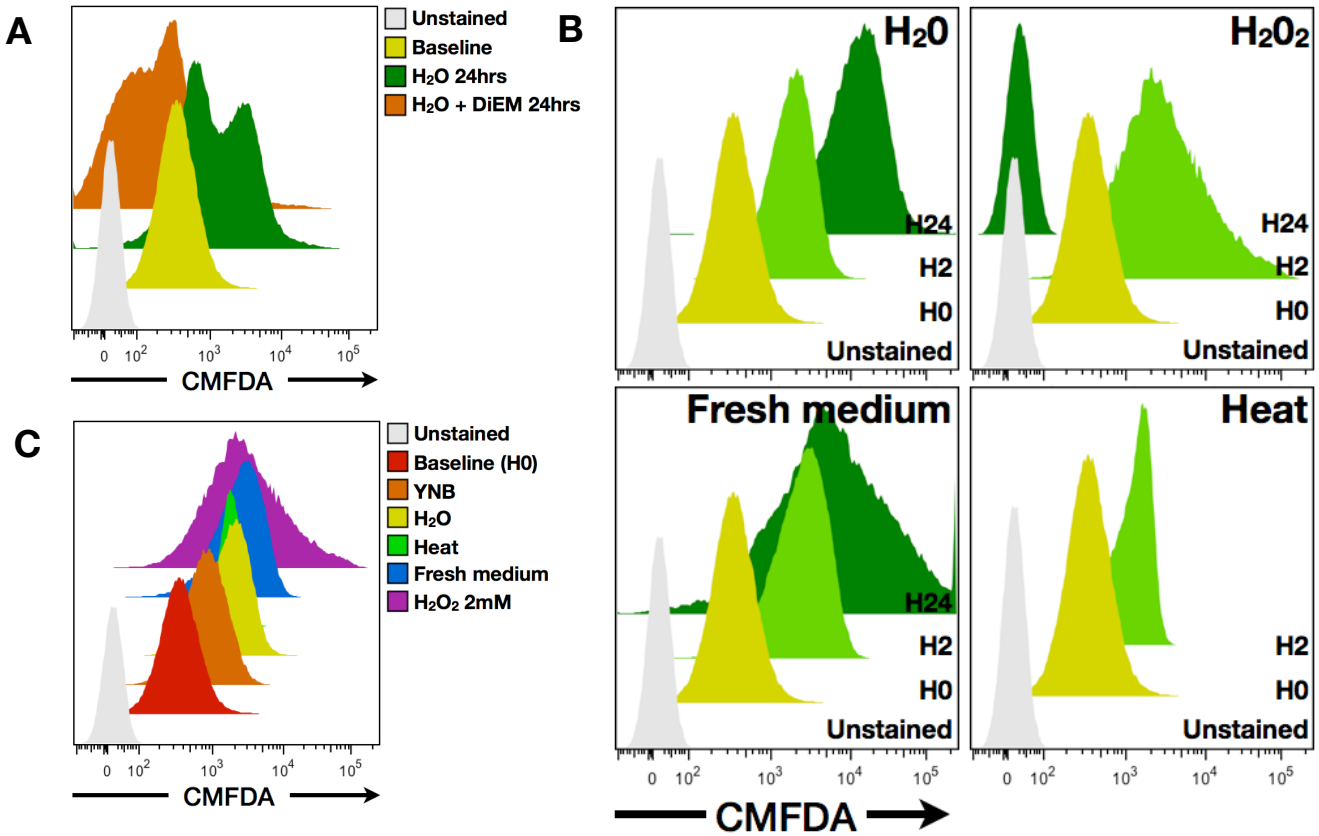

Figure 12: Quantification of *C. neoformans* stress response using CMFDA and flow cytometry

C. neoformans (H99) stress response was evaluated based on 5-chloromethylfluorescein diacetate (CMFDA) staining. (**A**) Stress response as determined by CMFDA staining measured a glutathione-dependent phenomenon. An inhibition of the increased CMFDA fluorescence after addition of diethyl maleate [glutathione-depleting agent (DiEM)] was observed in comparison with water alone after 24 hours of incubation. (**B**) Various stresses [H2O, H2O2, DMEM+10%FCS (fresh medium) and heat killing (Heat)] were applied to stationary phase (H0) yeasts for 2 hours and 24 hours. CMFDA fluorescence increased over time except at H24 after H_2O_2 incubation where it became negative. (**C**) Stress responses increased depending on the medium of incubation [Yeast base nitrogen (YNB), H_2O, H_2O_2, fresh medium and Heat] were compared to baseline (H0) after 2 hours of incubation.

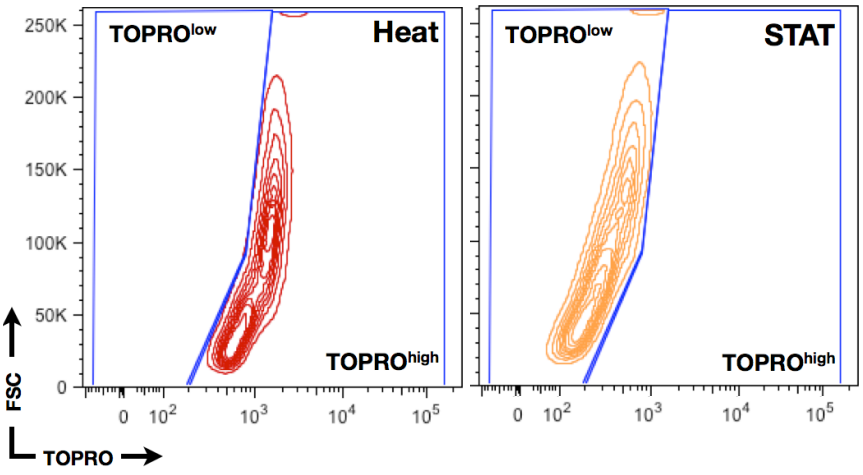

Figure 13: Quantification of viability using TOPRO and flow cytometry

C. neoformans viability was evaluated based on the level of fluorescence after TOPRO staining. Membrane disrupted cells after heat killing (Heat) were highly stained ($TOPRO^{high}$) compared to living yeasts cells (STAT, $TOPRO^{low}$).

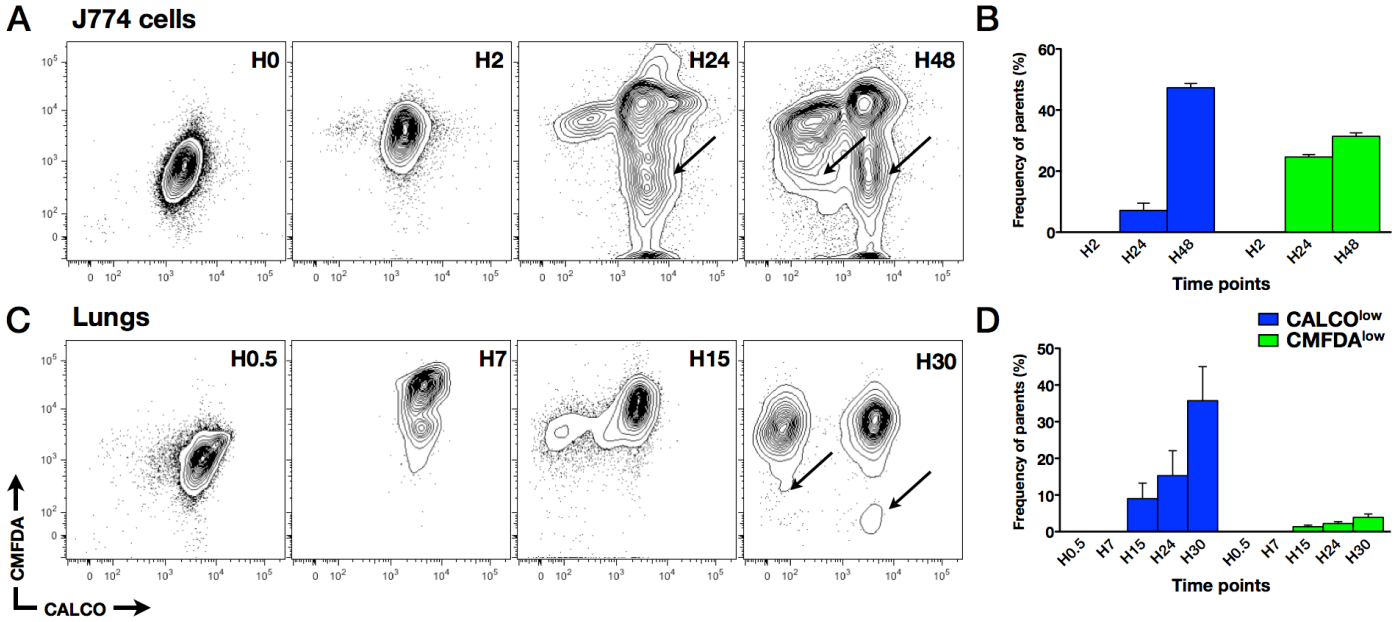

Figure 14: Evolution of *C. neoformans* multiplication and stress response in two host environments.

The CALCO and the CMFDA fluorescence were analyzed after interaction with macrophages **(A, B)**, and in lungs of infected mice **(C, D)**. After macrophage lysis and organ grinding, the pellet of H99 yeasts was stained using CMFDA (10µM) and TOPRO (10µM) 30 min at 37 °C (CMFDA/TOPRO assay). The analysis of the fluorescence was performed using flow cytometry after exclusion of $TOPRO^{high}$ population (dead yeasts). The generation of daughter cells ($CALCO^{low}$) was observed as soon as 2 hours of incubation after macrophage interaction **(A)** and 15 hours after mice inoculation **(C)** and increased over time **(B, D)**. The yeast's stress response (CMFDA fluorescence) rapidly increased as soon as H2 in macrophages **(A)** and H7 in the lungs **(B)**. A population harboring a lower CMFDA fluorescence (black arrows) was observed at H24 in macrophage **(A, B)** and at H30 in lungs **(C, D)**, that affected first mother cells (H24) and then daughter cells (H48) in macrophages.

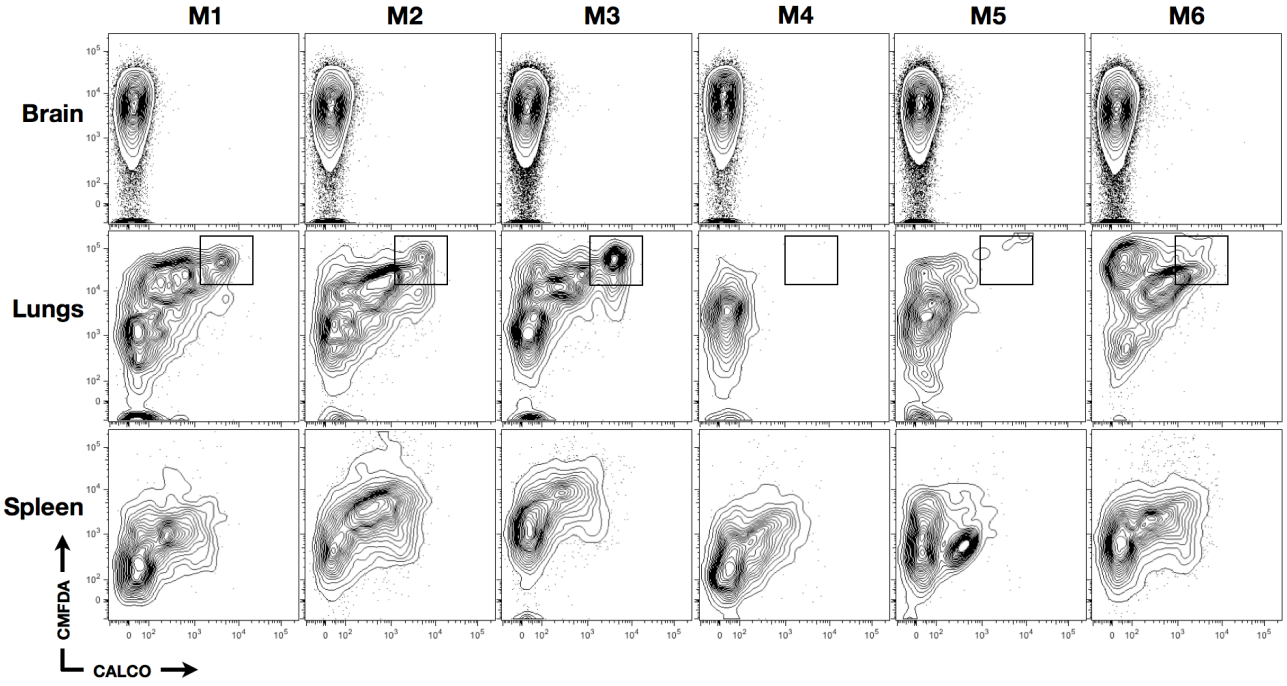

Figure 15: Yeasts stress response and multiplication depends on individuals (OF1 outbred mice) and tissues.

Seven days after inoculation with 10^5 CALCO stained H99, mice were sacrificed and their organs (brain, lungs, spleen) ground. Yeasts were stained for stress response and viability using CMFDA/TOPRO assay. The analysis was performed using flow cytometry after exclusion of $TOPRO^{high}$ population (dead yeasts) (MacsQuant analyzer, Miltenyi). The profile of brain and spleen Cn was homogenous in terms of multiplication and stress response, whereas two profiles were observed in lungs. A well-defined $CALCO^{high}$/$CMFDA^{high}$ population (black gate) was observed for some mice (M1, M2, M3), and not for others (M4, M5, M6).

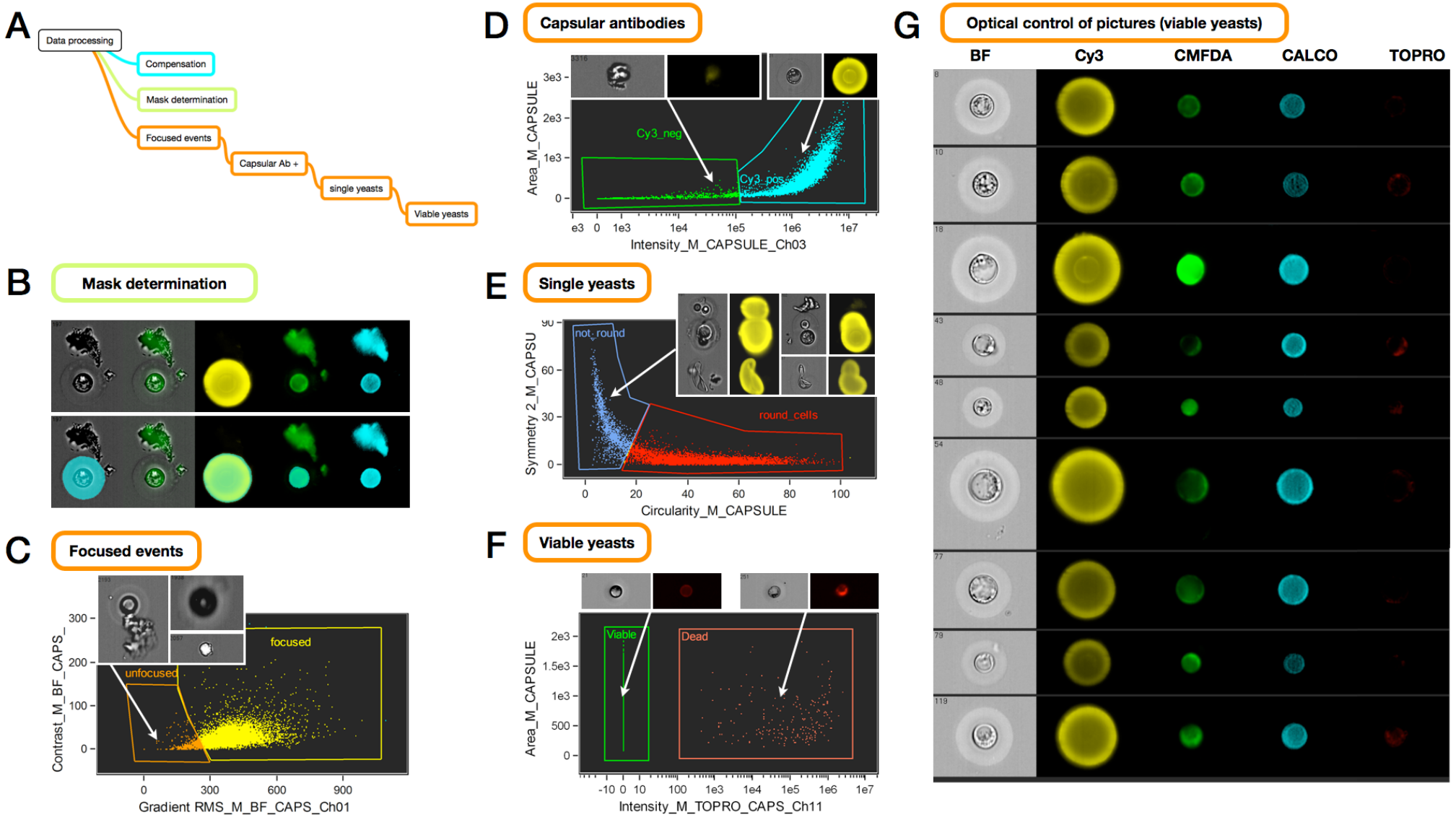

Figure 16: Multispectral imaging flow cytometry analysis workflow.

C. neoformans obtained from pooled mouse lungs were analyzed using Multispectral imaging flow cytometry (Imagestream^X) after CMFDA/TOPRO and Cy3 anti-capsular antibody stainings. After fluorescence compensation, the complete workflow (**A**) consisted in mask determination to delineate the interesting part of each picture (**B**), exclusion of unfocused events (**C**), of tissue debris (**D**), aggregates (**E**) and dead yeasts (**F**), to obtain relevant pictures that are ready to be further analyzed for specific questions.

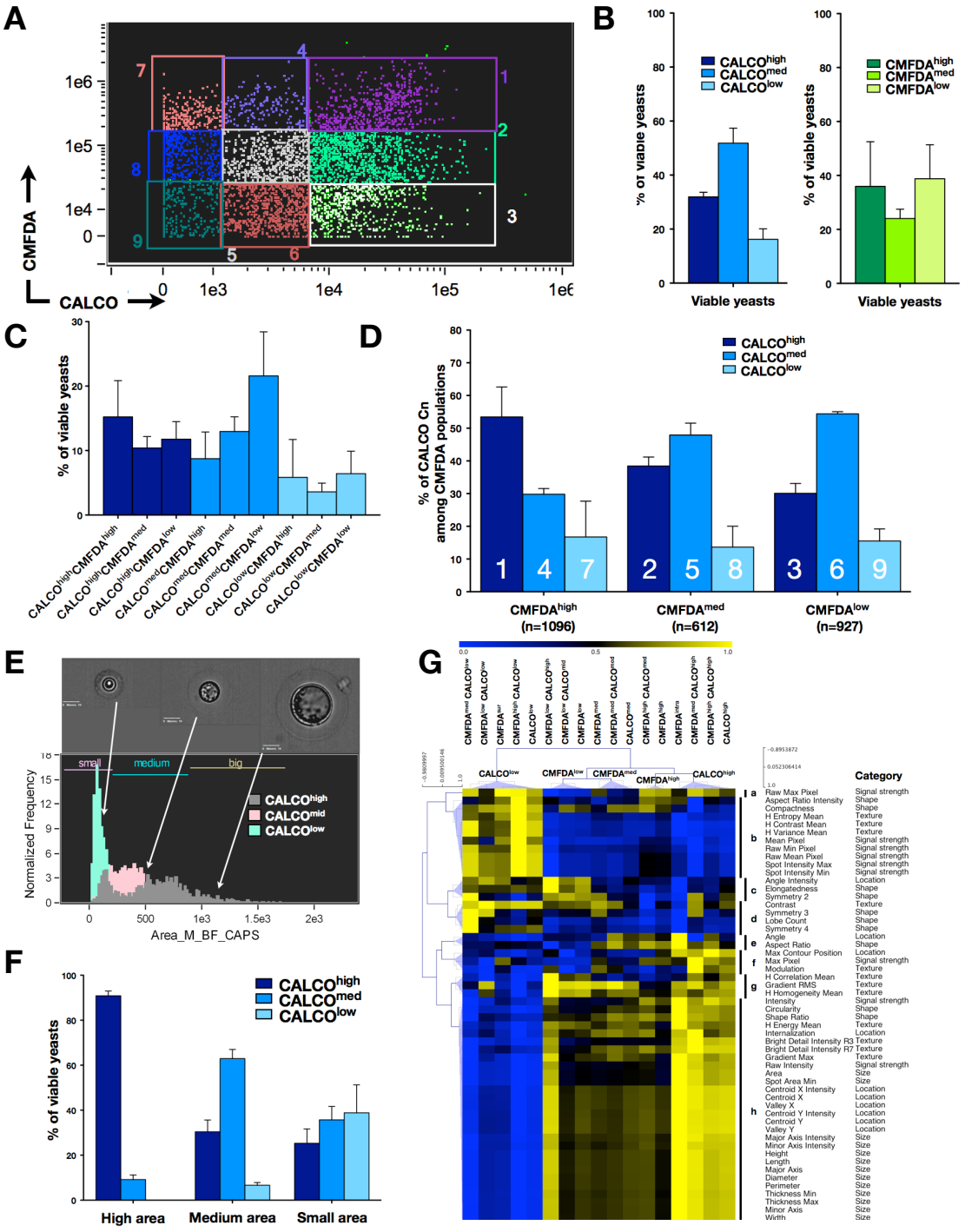

Figure 17: Multispectral imaging flow cytometry confirms heterogeneity of the yeast populations in the lungs of OF1 outbred mice

Yeasts from pooled lungs of 14 mice (2635 total yeast cells) were analyzed for multiplication, stress response and viability. (**A**) Nine H99 populations (1 to 9) were delineated using multispectral imaging flow cytometry (Imagestream^{X}). The nine gates were adjusted based on optical control of the fluorescence intensity of the corresponding pictured events. One representative of two independent experiments is shown. (**B-C**) The distribution of the different populations. The distribution of the CALCO populations (high, med, low) in the different CMFDA population is shown (**D**). Bars represent means ± SD for each of the 9 populations numbered in panel 4A. The CALCO^{low} population represented always less than 20%. In the CMFDA^{high} population, the CALCO^{high} population was predominant whereas the CALCO^{med} population was predominant in the CMFDA^{med} and CMFDA^{low} populations. (**E-F**) The analysis of the size of the 3 CALCO populations based on the area algorithm revealed that mother yeasts cells are composed of small and medium to high yeasts and daughter cells mainly of small cells. (**G**) Heat map was generated from the bright field channel pictures based on the geometric mean of 54 different algorithms. Five populations of yeasts (CALCO^{low}, CALCO^{high} and CMFDA^{high}, CMFDA^{med}, CMFDA^{low}) and 8 groups (a to h) of algorithms clustered. Cluster h that includes all size and most location algorithms allowed discrimination between CALCO^{high}, CALCO^{low} and the 3 other populations. Cluster b distinguished CALCO^{low} from the 4 other populations based on some signal strength and texture algorithms. Cluster c highlighted CMFDA^{low} compared to the 4 other populations based on some shape and location algorithms.

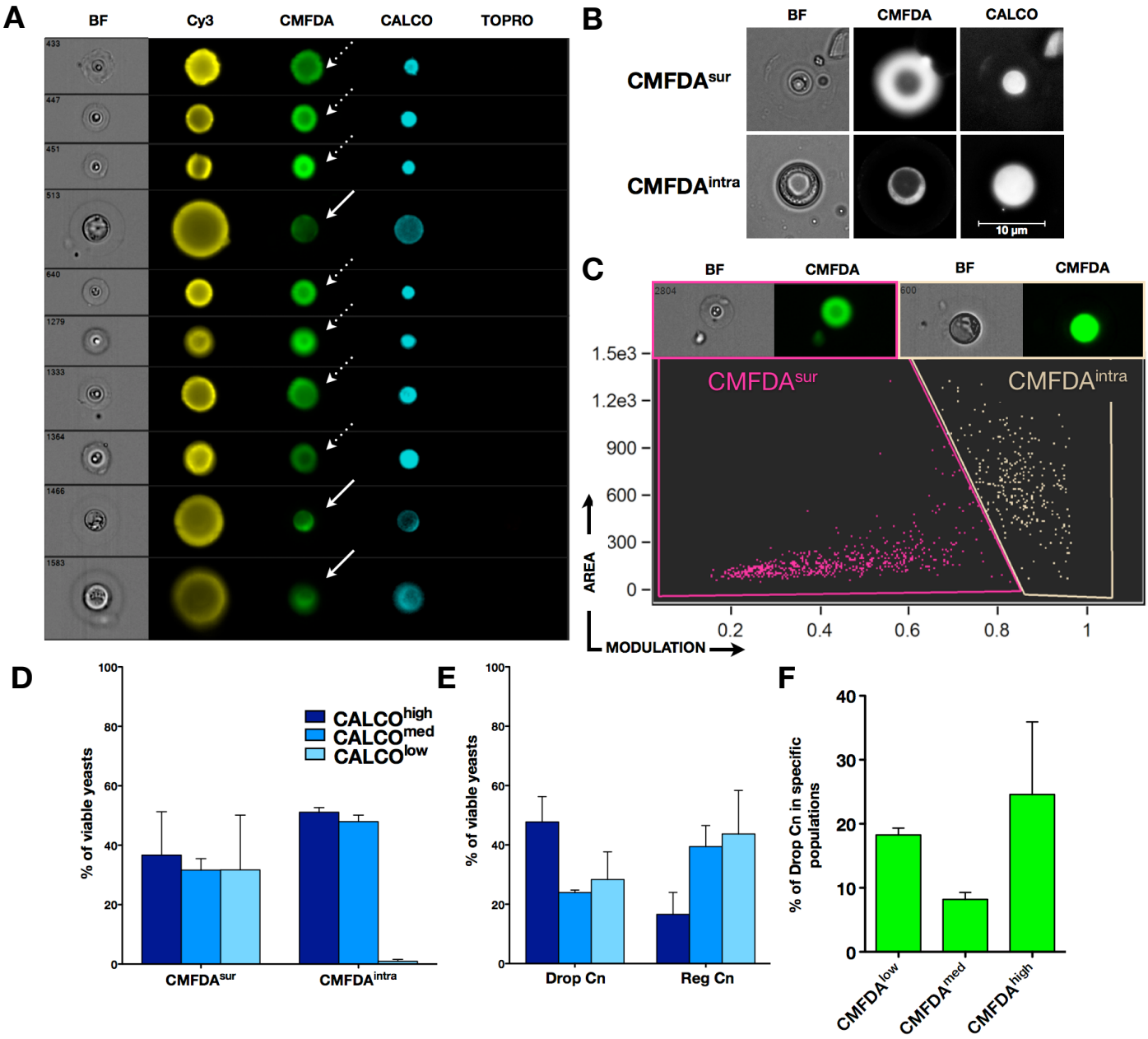

Figure 18: Morphological and fluorescence features of the CALCO^{high}/CMFDA^{high} H99 population in lungs of OF1 outbred mice.

A) Multispectral imaging flow cytometer (ImageStream^X, Amnis) was used to picture each event of the CALCO^{high}/CMFDA^{high} population in 5 channels: bright field (BF, transmitted light), yellow (Cy3, capsule), green (CMFDA, stress response), blue (CALCO, multiplication), red (TOPRO, viability). Different patterns of morphology and CMFDA fluorescence were observed. **B)** The CALCO^{high}/CMFDA^{high} population of yeasts from lung homogenates was also observed using classical fluorescence microscopy. CMFDA fluorescence was observed surrounding the cell wall CMFDA^{sur} (white dotted arrows in panel A), or within the cytoplasm of the yeast (CMFDA^{intra}, white arrows in panel A). **C)** Based on the modulation algorithm (texture) and the area (size) of the yeasts, CMFDA^{intra} and CMFDA^{sur} were easily discriminated. The CMFDA^{sur} yeasts were composed of regular Cn cells and 'Drop Cn' cells. Distribution of the CMFDA^{sur} and CMFDA^{intra} yeasts (**D**) and Drop and Reg Cn (**E**) in the 3 CALCO populations. (**F**) Proportion of Drop Cn in the 3 CMFDA populations.

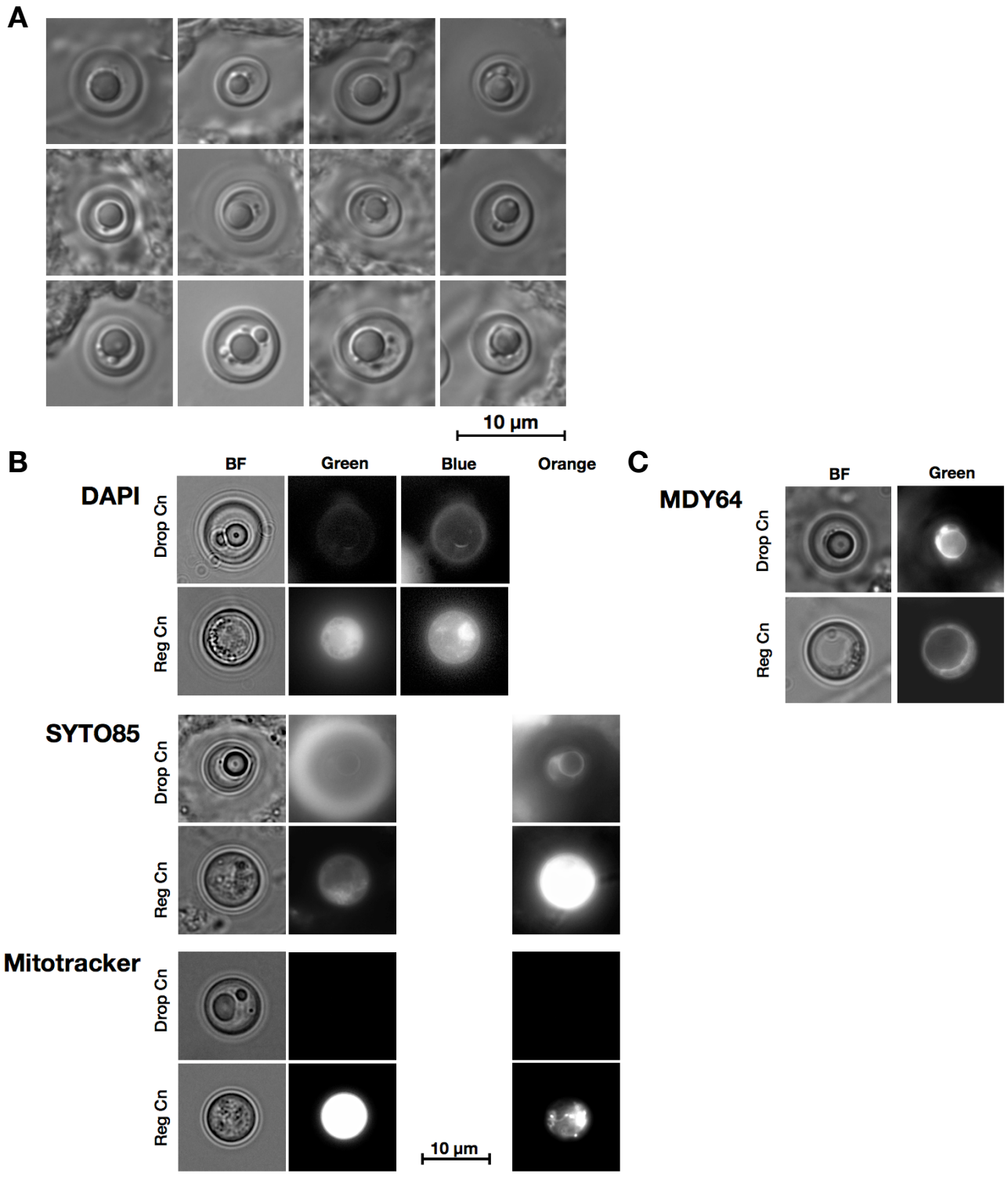

Figure 19: Morphological features and metabolic activity of the 'Drop Cn' population in the lungs of OF1 outbred mice.

Yeasts from lung homogenates were observed using interferential contrast microscopy. **A)** A subpopulation of yeasts was observed with a typical morphology: small size (5.80µm ± 0.80, n=12), thick cell wall, and one well-defined round refringent vesicle. **B)** Nucleus morphology (DAPI, Blue), RNA content (SYTO85, Orange) and mitochondrial activity (Mitotracker, Orange) were assessed in yeasts previously stained with CMFDA (green). 'Drop Cn' were devoid of nucleus (regular shape and regular DAPI fluorescence), RNA and mitochondrial activity in comparison with regular yeasts (Reg Cn). **C)** Lipid membrane layers (MDY64, green) was assessed in unstained yeasts. 'Drop Cn' harbored a complete retraction of the cytoplasm around the central refringent vesicle.

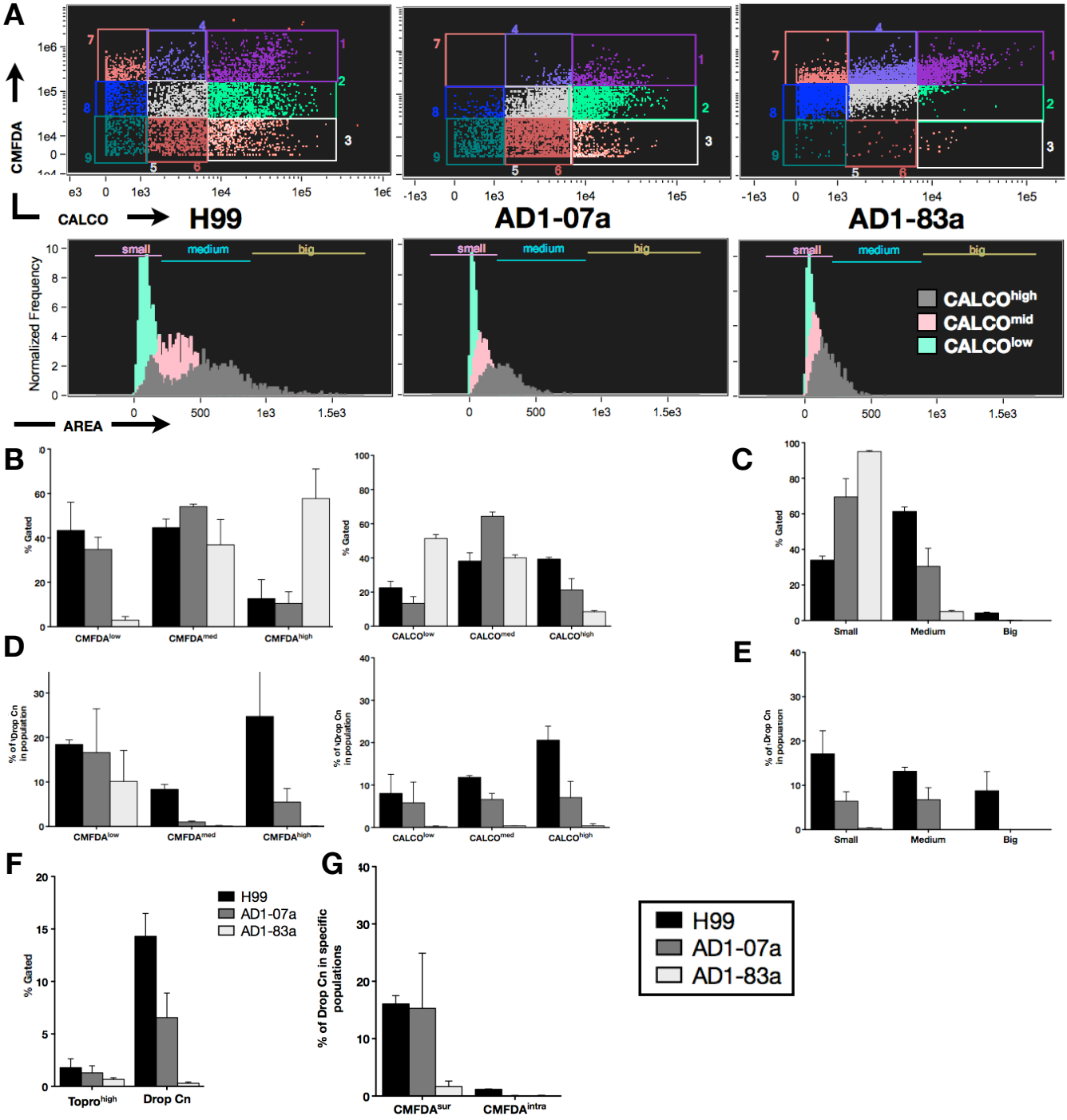

Figure 20: Diversity of phenotype of 2 clinical isolates compared to H99

Contrasted distribution of CALCO/CMFDA (**A higher panel, B**) and sizes (**A lower panel, C**) for AD1-07a and AD1-83a compared to H99 assessed using Imagestream^{X}. **(D-F)** Contrasted proportion of Drop Cn considering specific populations for AD1-07a and AD1-83a compared to H99. (**F**) Similar proportion of dead yeasts as assessed by TOPRO fluorescence cells for clinical isolates and H99. (**G**) Contrasted proportion of CMFDA^{sur} and CMFDA^{intra} populations for AD1-07a and AD1-83a compared to H99 with a lower proportion of Drop Cn being CMFDA^{sur} in AD1-83a.

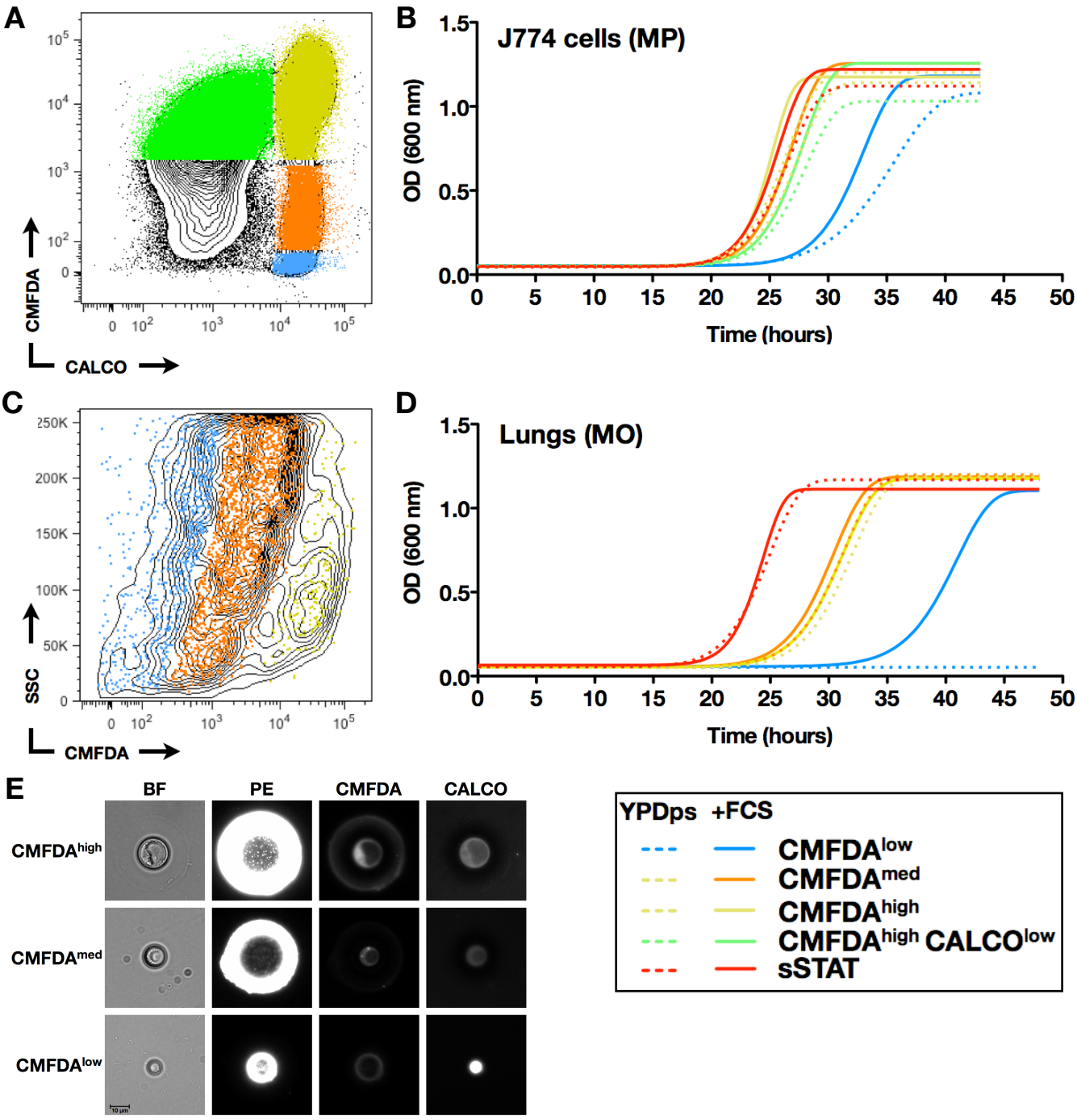

Figure 21: Growth curves analysis of different CMFDA populations after sorting.

The yeasts recovered from macrophage lysis (MP) after 24 hours of interaction **(A, B)** or lung homogenates (MO) from infected outbred mice **(C, D)** were stained and then sorted (FACSAria II, BD) and optically controlled (**E**). Stationary yeasts stained at the same time (sSTAT, red) were used as control. For each population, yeasts (10^4/ml) were allowed to grow in YPDps (dashed lines) or YPDps+10% fetal calf serum (+FCS, solid lines) in 96 well-plate at 30°C with agitation (800 rpm). The optical density (OD) at 600 nm was recorded over time. **A)** Four CMFDA populations (CMFDA/CALCO dot plot) were studied: $CMFDA^{high}CALCO^{high}$ (yellow), $CMFDA^{med}CALCO^{high}$ (orange) $CMFDA^{low}CALCO^{high}$ (blue) and $CMFDA^{high}CALCO^{low}$ (green). **B)** The exponential growth phase of the $CMFDA^{low}$ population (blue) was delayed compared to that of the 3 other populations and sSTAT. Onset of the exponential phase occurred earlier with addition of FCS. **C)** Three CMFDA populations (CMFDA/SSC dot plot) of yeasts recovered from pooled lungs homogenates were analyzed: $CMFDA^{high}$ (yellow), $CMFDA^{med}$ (orange) $CMFDA^{low}$ (blue). **D)** The $CMFDA^{low}$ population (blue) failed to grow in YPD even after 48 hours of incubation. Addition of FCS restored growth capacities even though onset was delayed by ≥10hours compared to the other populations and sSTAT. In addition, growth of $CMFDA^{high}$ and $CMFDA^{med}$ populations was delayed compared to sSTAT.

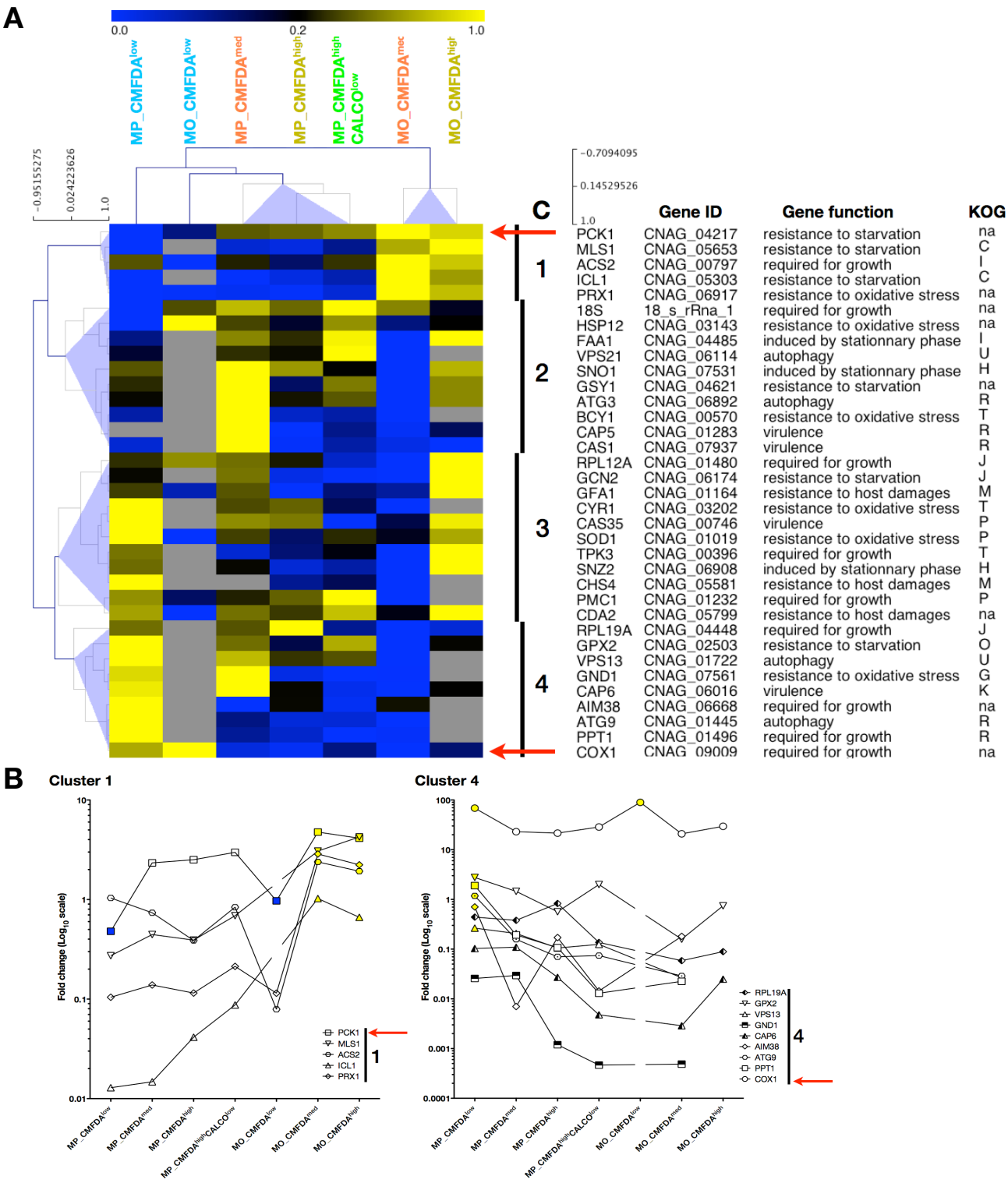

Figure 22: Heat map of genes expression analysis (n=37) for different CMFDA populations using real-time quantitative PCR.

CMFDA populations of yeasts recovered from macrophages (MP) or murine lungs (MO) were studied. After lyophilization, yeasts were lysed and primer specific reverse transcription and quantitative PCR were performed. The target selected (n=37) were genes involved in growth, stationary phase, resistance to oxidative stress, autophagy, adaptation to lung environment, and capsule and chitin formation. For each gene, the fold change compared to *ACT1* and *GAPDH* genes was normalized between 0 and 1 (**A**). The genes for which amplification failed are depicted in grey. MO_CMFDA^{med} and MO_CMFDA^{high} from mice clustered together apart from the other populations. All macrophage populations except MP_CMFDA^{low} clustered together. The pattern of expression for MP_CMFDA^{low} and MO_CMFDA^{low} was different from the other populations and between them except for *PCK1* and *COX1* (red arrows). Four clusters of genes can be differentiated with C1 specifically clusters genes involved in lung adaptation during infection [26] and C4 composed of genes more expressed in the MP_CMFDA^{low} population (**A, B**).

Addition of FCS restored growth for the MO_CMFDA^{low} population and markedly accelerated growth for all populations including sSTAT in MP. Of note, for CMFDA^{med} and CMFDA^{high}, growth curves in MO but not in MP were delayed compared to sSTAT and close to each other (**Figure 21B, 21D**).
Gene expression analysis based on 37-selected genes was performed for the above populations using real-time quantitative PCR (**Figure 22A-B**). Hierarchical clustering of yeasts populations revealed that for both MP and MO conditions CMFDA^{med} and CMFDA^{high} populations were close to each other. Overall, four groups were delineated: the MO_CMFDA^{high}, the MP_CMFDA^{high} population, and the CMFDA^{low} populations of MO and that of MP. Of note, the CMFDA^{high} population clustered with sSTAT (data not shown). Hierarchical clustering of genes revealed 4 clusters with 2 clusters of particular interest, clusters 1 (C1) and 4 (C4) (**Figure 22A-B**). C1 was composed of genes known to be up-regulated in lung during early infection [26]. C4 included genes that were more expressed in the MP_CMFDA^{low} population. Finally, *PCK1* down-regulation and *COX1* up-regulation were observed only in the MO_ and MP_CMFDA^{low} populations.

Table 3: Distribution of the various CMFDA populations studied after 24 hours of macrophage interaction (MP) and in lungs of infected outbred mice (MO)

	No. of yeasts x10^5 (mean±SD[a]) for analysis of			
	Growth curves		Gene expression	
	MP	MO	MP	MO
CMFDA^{low}	5.8 ± 0.1	0.7 ± 0.2	8 ± 1.6	1.1 ± 0.6
CMFDA^{med}	12.8 ± 2.5	2.5 ± 1.5	17.4 ± 2.1	4.6 ± 0.3
CMFDA^{high}	38.8 ± 3.9	0.6 ± 0.2	26.5 ± 0.7	0.9 ± 0.1
CMFDA^{high}CALCO^{low}	27.0 ± 7.1	ND	27.5 ± 3.5	ND

ND: not done; [a] Two independent experiments for MP and for MO (21 and 42 pooled lungs recovered 7 days after inoculation)

Discussion and Perspectives

Rapid overview of the literature on *C. neoformans* and cryptococcosis clearly shows the complexity and the diversity of the host/yeast interplay. This includes on the host side multiplicity of organisms potentially exposed to *C. neoformans* [29,175], diversity in human susceptibility to infection [109] and clinical presentation [11] and well-established differences in the interaction between yeasts and immune cells [5,153,176]. On the fungal side, the diversity is also noticeable at several levels: genome [177], genotypes [38], capsule structure [178,179], production of other virulence factors [40,41], interaction with hosts cells [22,23,151], virulence in mice [22,23], microevolution during infection [5,30,180].

1. How new standardized assays and new tools are needed to study *C. neoformans* adaptation

To study the dynamics of the *C. neoformans* adaptation to host and to analyze microbiological phenotypes according to clinical parameters, we implemented new tools and standardized assays that bypass pitfalls of classical methodologies. A careful reading of common methods in immunology as well as eukaryote cellular biology lead us to hijack tools that have rarely or never been used with fungi.

The quantification of *C. neoformans* multiplication was based on calcofluor staining and its ability to be sparsely transmitted to daughter cells during budding. Indeed, bud formation in basidiomycetous yeasts is enteroblastic [181]. The inner layer of the parental multilamellar cell wall is in direct continuation with the outer layer of the bud [182]. Given that chitin (~9% of the cell wall) is distributed throughout the cell wall [183], the calcofluor-labeled chitin of the mother cell wall could contribute to the fluorescence of the daughter cells. This assay represents a promising alternative to current studies dealing with microscopic or colony forming units enumeration and have potential wide applications. It could become, as CFSE assay in immunology [184], an easy/reliable test to study dynamics of fungal cell proliferation. Such assay could be easily used for drug discovery [185] or to study the basics of cellular biology of *Cryptococcus* infection (phagocytosis, trafficking, antimicrobial properties) using either *C. neoformans* mutant libraries or RNAi library for macrophage modifications [47,186].

Glutathione is a non-enzymatic defense system against oxidative stress. CMFDA has previously been used in mammalian and fungi to quantify glutathione [161,162,187] or as a long-term cell tracker since it leaves the yeasts viable [86]. Our experiments in *C. neoformans* demonstrated that yeasts responded to various stresses by increasing glutathione. In case of protracted or violent stress exposition (hydrogen peroxide), the pool of glutathione is emptied in *C. neoformans* as also shown in *Saccharomyces cerevisiae* [188,189]. The combined use of CALCO staining allowed us to compare stress response in mother and daughter cells.

To detect and exclude dead cells from the analysis, we used Topro-3 iodide that follows the same principle than propidium iodide staining only yeasts with altered cellular membrane [190]. Since propidium iodide fluorescence can be detected in the FITC channel, already used for CMFDA detection, it was necessary to use a marker that emits fluorescence in other wavelength and Topro-3 iodide emitting in the APC channel was the ideal one.

The use of quantitative flow cytometry (Macsquant® analyzer, Miltenyi) allowed absolute quantification of large samples when dealing with yeasts/macrophages interactions (more than 10^6 yeasts and 10^5 macrophages) and accurate intra vs. extracellular, and mother vs. daughter yeast cells' discriminations. A combination of a panel of dyes (4 fluorescence

channels of detection) and the three assays described above (multiplication, stress response and viability) allowed quantification in a unique step.
Flow cytometry is a powerful tool especially when dealing with planktonic mammalian cells. However, for yeasts that can harbor various morphological features and be associated with tissue debris when recovered from in vivo experiments, fluorescence quantification alone is insufficient to obtain accurate data. Consequently, to detect artifacts and analyze morphological features of *C. neoformans* cells obtained from mice, we used imaging multispectral flow cytometry (Imagestream^{X}®, Amnis corp.) that put together pictures and fluorescence intensity data for about 10,000 events. We were able to detect artifacts of the CMFDA staining as the location of the staining was high and extracellular for some yeasts cells (**Figure 18**), allowing us to re-classified these cells as CMFDA^{low} population since intracellular staining was low. In addition, numerous algorithms generated from pictures in the bright field channel provided deeper analysis of the morphology and allowed delineation of homogenous yeast populations. Based on the 13 size algorithms, the biggest cells corresponding to titan cells clustered together and were almost exclusively composed of mother cells in the lungs (**Figure 20D**) confirming data obtained from in vitro culture [67]. Furthermore, the CMFDA^{low} population also clustered separately based on 3 algorithms (angle intensity, elongatedness, symmetry2). This specific population would not have been detected by classical tools, highlighting the power of multispectral flow cytometry.
However, we were confronted with the low number of yeasts cells recovered from in vivo experiments. This forced us to develop tools using relative quantitative real-time PCR adapted for reduced size samples (**Table 3**). RNA extraction from low number of cells especially yeasts cells is tricky. Previous study reporting on relative quantitative PCR without RNA extraction [191] lead us to implement a direct one step real-time PCR. Lysis steps with buffer inhibiting PCR inhibitors provides stabilization of mRNA for primer specific reverse transcription and subsequent quantitative amplification based on the detection of specific fluorescent probes. Since a library of 90 octamer fluorescent probes was commercially available, we designed quantification assays for 54 genes that were validated for 37 genes. However, amplification sometimes failed for the samples containing the lowest quantity of yeasts (Mo_CMFDA^{low} or Mo CMFDA^{high} samples). Another explanation could be a profound down-regulation of these genes.

2. How to study the complexity *C. neoformans*/macrophage interaction from a fungal point of view.

Cryptococcus neoformans interacts closely with various host cells (murine and human macrophages or amoeba [2,5,141]) with the hypothesis that interaction with unicellular predators in nature shaped *C. neoformans* behavior in metazoan organisms [1].
With the aim to compare the phenotype of clinical isolates upon macrophage interaction, we chose J774 cells for the assays. Although results from this model could not be generalized to other systems and in particular to what happens in vivo in humans, it has the advantage of reproducibility, standardization, and wide use in the literature and allows the use of a murine IgG monoclonal antibody as opsonin.
The fate of *C. neoformans* in contact with host cells is dependent of multiple and yet partially unknown factors. The first one is phagocytosis. Phagocytosis of *C. neoformans* is known to be inhibited by capsule components so that an opsonin (complement or immunoglobulin) is required to study this process. Unexpectedly, we found that E1 (anti-capsular monoclonal antibody) binding level inversely correlated with the phagocytic

index (**Figure 9**). This suggests that, in addition to Fc and complement-receptors [192], other receptors involved in innate immunity, such as mannose receptors, CD14, TLR-4 [193], or factors modulating phagocytosis, such as the secreted protein App1p [63], the pleiotropic transcription factor Gat201p or the Gat201-bound gene Gat204p [66], play a role in the phagocytosis process.
After phagocytosis, *C. neoformans* intracellular persistence and proliferation are key steps in the pathogenesis process. We found a relationship between the intracellular proliferation of clinical isolates and intra-macrophagic expression of *COX1, IPC1*, *VAD1*, *APP1*, and *PLB1*. Specific mitochondrial morphology and metabolism were associated with *C. gattii* isolates recovered from the Vancouver Island outbreak [22]. This validates the FACS-YMI assays as an innovative mean to study virulence factors and potentially decipher the mechanisms by which *C. neoformans* escape or survive phagocytosis. Dissociation between early (IPH2) and late (IPH48) intracellular proliferation indexes was observed for some clinical isolates as well as for *lac1Δ* mutant. We also found that a variable proportion of the intracellular yeasts were still $CALCO^{high}$ after 48 hours of incubation, suggesting that they could either be viable mother cells that did not lose their fluorescence or mother cells in a low-replicative stage. There is no clue to favor one hypothesis since observation of replication of mother cells during its life course is technically difficult. The use of microfluidic device that block the mother cell and eliminate daughter yeasts cells as soon as they are generated though a flow could be an option but this kind of tool is rare. Nevertheless, these data suggest that adaptation inside macrophage occurs.
Using dynamic imaging of *C. neoformans*/macrophage interaction, we observed macrophage division after yeast uptake, as previously described [85]. This suggests that *C. neoformans* is not toxic for the phagocytic cell and reinforce some steps of cryptococcosis' pathophysiology such as the phagocytic cell as a potential niche for *C. neoformans* latency and as a vehicle (Trojan horse) for dissemination [7] and bypass of the immune response. Interestingly, we did not observed vomocytosis during our experiments. The lack of macrophage activation with interferon gamma or LPS could be an explanation.

3. How diverse are *C. neoformans* clinical isolates

Using a large collection of clinical isolates, we uncovered highly variable phenotypes of *C. neoformans*/macrophage interaction without correlation with genotypes in contrast with what was demonstrated for the clonal hypervirulent VGII *C. gattii* isolates [22]. This could be explained by differences in the pathophysiology of infections due to *C. gattii* and *C. neoformans*, the first being more frequently responsible for primary infection rather than reactivation in contrast with *C. neoformans*-related diseases [15,147]. As a consequence, virulence of these two pathogenic fungi in humans could be different in terms of host adaptation and immunological escape mechanisms. One may also wonder if the phenotypic intra-species diversity reported for eukaryotes, as opposed to prokaryotes, could be explained by their complex genome, and potential recombination events during mating. This is especially true for *C. neoformans*, knowing its complex sexual reproduction [28]. Some strains may have "ready made" virulence [1] (high IPH2, high IPH48) whereas, for others (low IPH2, high IPH48), a longer period of metabolic adaptation to hypoxia or starvation inside macrophages could be needed to multiply and express virulence factors as described in vivo [26]. Overall, these various phenotypes could reflect different patterns of pathogenicity. Given the complex biological processes that lead to survival or multiplication inside the phagolysosome, other studies are needed

to decipher the precise mechanisms and molecular events involved. At the end, one can wonder if the use of one strain (a reference strain) is sufficient to draw general conclusion on the global knowledge of *C. neoformans* phenotype in various contexts. Variations of 30-, 50-, and 16-fold were observed among clinical isolates in terms of phagocytic, 2-hours or 48-hours proliferation indexes respectively (**Figure 8**). These variations must impact *C. neoformans* interactions with hosts in vivo, especially when innate immunity is known to be important during infection. These variations have also been observed in 6 isolates of the same reference strain (NIH52D) originating from 6 research laboratory, for which a local evolution through iterative in vitro experiments or inappropriate storage conditions were suspected [194]. To circumvent partially this issue, some authors systematically screened different reference strains.

4. How the diversity of *C. neoformans* clinical isolates impacts clinical outcome

Up to now, *C. neoformans*/host cells interactions have mostly been studied using reference or mutant strains. Few reports discuss the variability inferred by clinical isolates for *C. neoformans* [151], other fungal species [22,195], or parasites [196-199], and none analyzed correlation with clinical outcome. Since yeast/macrophages interactions are involved in pathogenesis, we assessed whether the phenotypes determined in vitro were associated with specific outcome in humans. We found that isolates harboring low PI and low IPH2 were significantly associated with non-sterilization of CSF at week 2, whereas those harboring high PI and high IPH2 were associated with death at month 3. Our results suggest that fungal determinants are involved, as are host factors (genetic background, type of immunosuppression) in the outcome of cryptococcal meningoencephalitis. These results highlight the monocyte/macrophage lineage as a major key player in the pathophysiology of the infection in humans, as already suggested by studies on blood-brain barrier crossing and dissemination in mice [7,200,201]. Additional experiments are needed to assess the relevance of these data in different clinical settings, such as infections with other serotypes, mixed infections, and extrameningeal cryptococcosis. Unpublished data from another group corroborate our hypothesis since they found that highly phagocytosed strains are associated with high CSF burden which is known to be associated with poor outcome [202]. In addition, a recent report found a relationship between capsular size in CSF at baseline ex vivo (and not in vitro) and slower rate of fungal clearance and high intracranial pressure in patients [203]. Both parameters are known to be associated with a poor outcome, reinforcing the hypothesis that fungal determinant and/or fungal adaptation to hosts are involved in clinical features of the disease [204,205].

While many studies established that host susceptibility to infection is crucial and that virulence factors of the pathogens can be differentially expressed as a function of environmental conditions (medium, intracellular vs. free yeasts, etc.), we demonstrate that, in the same experimental conditions, clinical isolates of *C. neoformans* behaved differently, a diversity that could participate in the variable outcome of meningoencephalitis in humans. As a consequence, our assays developed to quantify phagocytic and proliferation indexes can be used as a prognostic tool that could in the future be used to intensify antifungal therapy if the isolate harbor a phenotype associated with mortality (high PI, high IPH2).

To go further and to understand which are the fungal determinants that play a role in some specific intrinsic phenotypes of the clinical isolates, we are currently performing (i)

whole genome sequencing, and (ii) transcriptome analysis using RNAseq methodology at baseline and upon 2 hours uptake by macrophages. We already identified several factors associated with resistance to phagocytosis by analyzing gene expression of 13 clinical isolates at baseline. Since KO mutants impact drastically the metabolism of the yeast by abolishing the expression of one protein but also down stream and/or upstream pathways, analyzing precisely well-selected clinical isolates could be a way to understand phenotypes more physiologically. However, this kind of study will generate complex data and could be therefore difficult to interpret.

5. How heterogeneous is *C. neoformans* population upon interaction with host

Fungal adaptation to specific host environments has been demonstrated [26,27,206,207] without focus on specific subpopulations of yeasts, except for the titan cells that have been recently reported in the lungs of infected mice [67,68]. We hypothesized that metabolically-different subpopulations of yeasts coexist in organs upon infection with the ambition to identify a population of dormant cells thanks to the combination of complementary tools (discussed above).
An intriguing observation was the extracellular ($CMFDA^{sur}$) and not cytoplasmic ($CMFDA^{intra}$) pattern associated with yeasts harboring specific morphology (Drop Cn) in lungs. The peripheral extracellular staining could be related to either excretion of glutathione or diffusion of host's glutathione during infection or processing of the samples. Various stainings for metabolic activity (stress response, mitochondria, RNA content) and cell architecture (nucleus, plasma membrane, cell wall, capsule) as well as dynamic imaging strongly suggested that Drop Cn cells are mostly mother cells but dead cells. The negative TOPRO staining can be explained by the loss of nucleic acids evidenced by DAPI and SYTO 85 stainings. It is noteworthy that yeasts cells looking like Drop Cn are brought out in many publications without discussion of their viability. It is noticeable that these dead yeasts are not completely cleared. Their intact cell wall and capsule could prevent clearance and inhibit phagocytosis.
Analysis of multiplication and stress response revealed the coexistence of several subpopulations of yeasts that evolved over time in the host. The proportion of the various populations also varied upon hosts (OF1 *vs.* BALB/c), tissues (lungs *vs.* brain), models (in vitro *vs.* in vivo) and *C. neoformans* strains (H99 *vs.* well-characterized clinical isolates). This clearly underlines that results on global *C. neoformans* adaptation to various environments should be interpreted with caution. Sorting of the various populations of yeasts may thus help understanding *C. neoformans* biology in the host.

6. Biological evidence of dormancy

The commonly accepted pathophysiology is that most cases of *C. neoformans* infection result from the reactivation of dormant yeasts cells without precise knowledge on their site of residence. We focused here on the lungs of infected mice because it was the only body site in which well-delineated populations with sufficient number of cells for specific analysis were observed. Zaragoza and Nielsen evoked the possible role of titan cells in dormancy [208]. However, our experiments showed that CMFDA phenotype is not correlated to the size of the cell suggesting that titan cells may not be dormant cells knowing also from previous reports that they are prone to spontaneous multiplication upon standard culture conditions (Sabouraud agar plates) [67].
Dormancy has already been described in various environments in a wide range of

organisms including bacteria [209] (*Bacillus* spp., *Clostridium difficile*, *Chlamydia* spp., *Vibrio* spp, *Pseudomonas* spp.), mycobacteria (*Mycobacterium tuberculosis* [210-212]), Apicomplexan parasites (in particular Plasmodium spp. [213]) and yeasts (*Saccharomyces cerevisiae* [214], *Schizosaccharomyces pombe* [215]), and potentially spores of filamentous fungi (*Aspergillus fumigatus* [216] and *Neurospora crassa* [217]). In *C. neoformans*, dormancy has only been identified epidemiologically [16] and evoked for basidiospores [218]. From a biological point of view, we assumed that dormant cells would be metabolically poorly active. The population that met this criterion was the $CMFDA^{low}$ that included less than 20% of Drop Cn. The delayed or nil growth of $CMFDA^{low}$ population in YPD was partially rescued after addition of fetal calf serum, a phenotype described for dormant cells of various origins (mammalian fibroblasts, mammalian cancer cells, stem cells, bacteria and *S. cerevisiae*) [219]. This suggested that $CMFDA^{low}$ population could be composed predominantly of dormant cells.

The limited number of cells after sorting (**Table 3**) led us implement transcriptional gene analysis based on adaptation of single-PCR assays. The finding that a cluster of genes (C1, **Figure 26**), known to be overexpressed during lung infection [26], was up-regulated only in yeasts recovered from lungs (MO_CMFDA^{med}, MO_CMFDA^{high}), was a means to validate the technical and biological approach.

The major difference between the $CMFDA^{low}$ population and the others whatever the condition, was the modulated expression of *PCK1* (decrease) and *COX1* (increase) genes.

The phosphoenolpyruvate carboxykinase 1 (Pck1) protein plays a major role in gluconeogenesis, known to impact yeasts survival and to be required for virulence [158]. It is dependent on the DEAD-box Rna helicase, Vad1. *PCK1* in *S. cerevisiae* is shown to be up-regulated under elevated CO_2 concentration during carbon limitation [220]. The decreased *PCK1* expression in $CMFDA^{low}$ populations suggests active glycolysis metabolism in contrast with $CMFDA^{med}$ and $CMFDA^{high}$ populations where glyoxylate cycle and gluconeogenesis is activated (**Figure 22**, Cluster1). As reported recently, glucose utilization is critical for virulence and persistence of the yeasts in CSF of rabbits [221].

COX1 (encoding the mitochondrial cytochrome c oxidase subunit 1) is up-regulated during stress response induced by high temperature (39°C) [174] and differentially expressed in well-characterized clinical isolates in correlation with intra-macrophagic proliferation [23]. *COX1* and respiratory proteins in general are up-regulated in response to hypoxia as opposed to what is observed in *S. cerevisiae*, *S. pombe*, *C. albicans* where they are down regulated [222,223]. In *C. neoformans*, mutations in various mitochondrial genes affect respiration rate, response to oxidative stresses and ability to survive in low oxygen conditions [224,225], and this, independently of glutathione activity. In *C. gattii*, enhanced mitochondrial activity and modifications of mitochondrial morphology was found to be related to increased proliferation rate and virulence [22].

The increased *ATG9* and *VPS13* expressions (MP_CMFDA^{low}) give additional evidence that $CMFDA^{low}$ population could use autophagy to survive.

Taken together, these data suggest that the $CMFDA^{low}$ population is dormant in response to hypoxic conditions that could take place in some niches of the lung (for example in granuloma) during infection [222]. Further experiments are needed to find a way to generate dormant *C. neoformans* cells to go deeper in the biology of dormancy in this organism.

References

1. Casadevall A, Steenbergen JN, Nosanchuk JD (2003) 'Ready made' virulence and “dual use” virulence factors in pathogenic environmental fungi--the *Cryptococcus neoformans* paradigm. Curr Opin Microbiol 6: 332–337.
2. Steenbergen JN, Shuman HA, Casadevall A (2001) *Cryptococcus neoformans* interactions with amoebae suggest an explanation for its virulence and intracellular pathogenic strategy in macrophages. Proc Natl Acad Sci USA 98: 15245–15250. doi:10.1073/pnas.261418798.
3. Derengowski LDS, Paes HC, Albuquerque P, Tavares AHFP, Fernandes L, et al. (2013) The transcriptional response of *Cryptococcus neoformans* to ingestion by Acanthamoeba castellanii and macrophages provides insights into the evolutionary adaptation to the mammalian host. Eukaryotic Cell 12: 761–774. doi:10.1128/EC.00073-13.
4. Frager SZ, Chrisman CJ, Shakked R, Casadevall A (2010) Paramecium species ingest and kill the cells of the human pathogenic fungus *Cryptococcus neoformans*. Med Mycol 48: 775–779. doi:10.3109/13693780903451810.
5. Fries BC, Taborda CP, Serfass E, Casadevall A (2001) Phenotypic switching of *Cryptococcus neoformans* occurs in vivo and influences the outcome of infection. J Clin Invest 108: 1639–1648. doi:10.1172/JCI13407.
6. García-Rodas R, Zaragoza O (2012) Catch me if you can: phagocytosis and killing avoidance by *Cryptococcus neoformans*. FEMS Immunol Med Microbiol 64: 147-161. doi:10.1111/j.1574-695X.2011.00871.x.
7. Charlier C, Nielsen K, Daou S, Brigitte M, Chretien F, et al. (2009) Evidence of a role for monocytes in dissemination and brain invasion by *Cryptococcus neoformans*. Infect Immun 77: 120–127. doi:10.1128/IAI.01065-08.
8. Santangelo R, Zoellner H, Sorrell T, Wilson C, Donald C, et al. (2004) Role of extracellular phospholipases and mononuclear phagocytes in dissemination of cryptococcosis in a murine model. Infect Immun 72: 2229–2239.
9. Park BJ, Wannemuehler KA, Marston BJ, Govender N, Pappas PG, et al. (2009) Estimation of the current global burden of cryptococcal meningitis among persons living with HIV/AIDS. AIDS 23: 525–530. doi:10.1097/QAD.0b013e328322ffac.
10. Casadevall A, Perfect JR (1998) *Cryptococcus neoformans*. Washington, DC: ASM Press.
11. Dromer F, Mathoulin-Pélissier S, Launay O, Lortholary O, Group F (2007) Determinants of disease presentation and outcome during cryptococcosis: the CryptoA/D study. Plos Med 4: e21. doi:10.1371/journal.pmed.0040021.
12. Kronstad JW, Attarian R, Cadieux B, Choi J, D'Souza CA, et al. (2011) Expanding fungal pathogenesis: *Cryptococcus* breaks out of the opportunistic box. Nat Rev Micro 9: 193–203. doi:10.1038/nrmicro2522.
13. Goldman DL, Khine H, Abadi J, Lindenberg DJ, Pirofski La, et al. (2001) Serologic evidence for *Cryptococcus neoformans* infection in early childhood. Pediatrics 107: E66.
14. Baker RD (1976) The primary pulmonary lymph node complex of crytptococcosis. Am J Clin Pathol 65: 83–92.
15. Dromer F, Casadevall A, Perfect J, Sorrell T (2010) *Cryptococcus neoformans*: Latency and Disease. *Cryptococcus*: From Human Pathogen to Model Yeast. ASM Press. p. p.429.
16. Garcia-Hermoso D, Janbon G, Dromer F (1999) Epidemiological evidence for dormant *Cryptococcus neoformans* infection. J Clin Microbiol 37: 3204–3209.
17. Dromer F, Ronin O, Dupont B (1992) Isolation of *Cryptococcus neoformans* var. *gattii*

from an Asian patient in France: evidence for dormant infection in healthy subjects. J Med Vet Mycol 30: 395–397.
18. Eisenman HC, Casadevall A, McClelland EE (2007) New insights on the pathogenesis of invasive *Cryptococcus neoformans* infection. Curr Infect Dis Rep 9: 457–464.
19. Chrétien F, Lortholary O, Kansau I, Neuville S, Gray F, et al. (2002) Pathogenesis of cerebral *Cryptococcus neoformans* infection after fungemia. J Infect Dis 186: 522–530. doi:10.1086/341564.
20. French N, Gray K, Watera C, Nakiyingi J, Lugada E, et al. (2002) Cryptococcal infection in a cohort of HIV-1-infected Ugandan adults. AIDS 16: 1031–1038.
21. Olszewski MA, Zhang Y, Huffnagle GB (2010) Mechanisms of cryptococcal virulence and persistence. Future Microbiol 5: 1269–1288. doi:10.2217/fmb.10.93.
22. Ma H, Hagen F, Stekel DJ, Johnston SA, Sionov E, et al. (2009) The fatal fungal outbreak on Vancouver Island is characterized by enhanced intracellular parasitism driven by mitochondrial regulation. Proc Natl Acad Sci USA 106: 12980–12985. doi: 10.1073/pnas.0902963106.
23. Alanio A, Desnos-Ollivier M, Dromer F (2011) Dynamics of *Cryptococcus neoformans*-Macrophage Interactions Reveal that Fungal Background Influences Outcome during Cryptococcal Meningoencephalitis in Humans. mBio 2: e00158–11–e00158–11. doi:10.1128/mBio.00158-11.
24. Feldmesser M, Kress Y, Novikoff P, Casadevall A (2000) *Cryptococcus neoformans* is a facultative intracellular pathogen in murine pulmonary infection. Infect Immun 68: 4225–4237.
25. Fan W, Kraus PR, Boily M-J, Heitman J (2005) *Cryptococcus neoformans* gene expression during murine macrophage infection. Eukaryotic Cell 4: 1420–1433. doi: 10.1128/EC.4.8.1420-1433.2005.
26. Hu G, Cheng P-Y, Sham A, Perfect JR, Kronstad JW (2008) Metabolic adaptation in *Cryptococcus neoformans* during early murine pulmonary infection. Mol Microbiol 69: 1456–1475. doi:10.1111/j.1365-2958.2008.06374.x.
27. Steen BR, Zuyderduyn S, Toffaletti DL, Marra M, Jones SJM, et al. (2003) *Cryptococcus neoformans* gene expression during experimental cryptococcal meningitis. Eukaryotic Cell 2: 1336–1349.
28. Hsueh Y, Lin X, Kwon-chung K, Heitman J (2010) Sexual Reproduction of *Cryptococcus*. *Cryptococcus*: From Human Pathogen to Model Yeast. ASM Press. p. p.81.
29. Lin X, Heitman J (2006) The biology of the *Cryptococcus neoformans* species complex. Annu Rev Microbiol 60: 69–105. doi:10.1146/annurev.micro.60.080805.142102.
30. Desnos-Ollivier M, Patel S, Spaulding AR, Charlier C, Garcia-Hermoso D, et al. (2010) Mixed Infections and In Vivo Evolution in the Human Fungal Pathogen *Cryptococcus neoformans*. mBio 1. doi:10.1128/mBio.00091-10.
31. Emmons CW (1951) Isolation of *Cryptococcus neoformans* from soil. J Bacteriol 62: 685–690.
32. Littman ML, Schneierson SS (1959) *Cryptococcus neoformans* in pigeon excreta in New York City. Am J Hyg 69: 49–59.
33. Walter JE, Atchison RW (1966) Epidemiological and immunological studies of *Cryptococcus neoformans*. J Bacteriol 92: 82–87.
34. Fink JN, Barboriak JJ, Kaufman L (1968) Cryptococcal antibodies in pigeon breeders' disease. J Allergy 41: 297–301.
35. Currie BP, Freundlich LF, Casadevall A (1994) Restriction fragment length polymorphism analysis of *Cryptococcus neoformans* isolates from environmental

(pigeon excreta) and clinical sources in New York City. J Clin Microbiol 32: 1188–1192.
36. Garcia-Hermoso D, Mathoulin-Pélissier S, Couprie B, Ronin O, Dupont B, et al. (1997) DNA typing suggests pigeon droppings as a source of pathogenic *Cryptococcus neoformans* serotype D. J Clin Microbiol 35: 2683–2685.
37. Litvintseva AP, Kestenbaum L, Vilgalys R, Mitchell TG (2005) Comparative analysis of environmental and clinical populations of *Cryptococcus neoformans*. J Clin Microbiol 43: 556–564. doi:10.1128/JCM.43.2.556-564.2005.
38. Litvintseva AP, Mitchell TG (2012) Population Genetic Analyses Reveal the African Origin and Strain Variation of *Cryptococcus neoformans* var. grubii. PLoS Pathog 8: e1002495. doi:10.1371/journal.ppat.1002495.g002.
39. Simwami SP, Khayhan K, Henk DA, Aanensen DM, Boekhout T, et al. (2011) Low diversity *Cryptococcus neoformans* variety grubii multilocus sequence types from Thailand are consistent with an ancestral African origin. PLoS Pathog 7: e1001343. doi:10.1371/journal.ppat.1001343.
40. Clancy CJ, Nguyen MH, Alandoerffer R, Cheng S, Iczkowski K, et al. (2006) *Cryptococcus neoformans* var. grubii isolates recovered from persons with AIDS demonstrate a wide range of virulence during murine meningoencephalitis that correlates with the expression of certain virulence factors. Microbiology (Reading, Engl) 152: 2247–2255. doi:10.1099/mic.0.28798-0.
41. Liaw S-J, Wu H-C, Hsueh PR (2010) Microbiological characteristics of clinical isolates of *Cryptococcus neoformans* in Taiwan: serotypes, mating types, molecular types, virulence factors, and antifungal susceptibility. Clin Microbiol Infect 16: 696–703. doi: 10.1111/j.1469-0691.2009.02930.x.
42. Bliska JB, Casadevall A (2009) Intracellular pathogenic bacteria and fungi--a case of convergent evolution? Nat Rev Micro 7: 165–171. doi:10.1038/nrmicro2049.
43. Wang CJ, Schwarz J (1959) Phagocytosis of yeast cells in vitro. Am J Pathol 35: 901–907.
44. Bulmer GS, Sans MD (1967) *Cryptococcus neoformans*. II. Phagocytosis by human leukocytes. J Bacteriol 94: 1480–1483.
45. Diamond RD, Bennett JE (1973) Growth of *Cryptococcus neoformans* within human macrophages in vitro. Infect Immun 7: 231–236.
46. Syme RM, Spurrell JCL, Amankwah EK, Green FHY, Mody CH (2002) Primary dendritic cells phagocytose *Cryptococcus neoformans* via mannose receptors and Fcgamma receptor II for presentation to T lymphocytes. Infect Immun 70: 5972–5981.
47. Qin Q-M, Luo J, Lin X, Pei J, Li L, et al. (2011) Functional analysis of host factors that mediate the intracellular lifestyle of *Cryptococcus neoformans*. PLoS Pathog 7: e1002078. doi:10.1371/journal.ppat.1002078.
48. Gjomarkaj M, Pace E, Melis M, Spatafora M, Profita M, et al. (1999) Phenotypic and functional characterization of normal rat pleural macrophages in comparison with autologous peritoneal and alveolar macrophages. Am J Respir Cell Mol Biol 20: 135–142. doi:10.1165/ajrcmb.20.1.3221.
49. Mukherjee S, Feldmesser M, Casadevall A (1996) J774 murine macrophage-like cell interactions with *Cryptococcus neoformans* in the presence and absence of opsonins. J Infect Dis 173: 1222–1231.
50. Levitz SM, Tabuni A (1991) Binding of *Cryptococcus neoformans* by human cultured macrophages. Requirements for multiple complement receptors and actin. J Clin Invest 87: 528–535. doi:10.1172/JCI115027.
51. Geunes-Boyer S, Oliver TN, Janbon G, Lodge JK, Heitman J, et al. (2009) Surfactant protein D increases phagocytosis of hypocapsular *Cryptococcus neoformans* by

murine macrophages and enhances fungal survival. Infect Immun 77: 2783–2794. doi:10.1128/IAI.00088-09.
52. Giles SS, Zaas AK, Reidy MF, Perfect JR, Wright JR (2007) *Cryptococcus neoformans* is resistant to surfactant protein A mediated host defense mechanisms. PLoS One 2: e1370. doi:10.1371/journal.pone.0001370.
53. van de Wetering JK, Coenjaerts FEJ, Vaandrager AB, van Golde LMG, Batenburg JJ (2004) Aggregation of *Cryptococcus neoformans* by surfactant protein D is inhibited by its capsular component glucuronoxylomannan. Infect Immun 72: 145–153.
54. Walenkamp AM, Verheul AF, Scharringa J, Hoepelman IM (1999) Pulmonary surfactant protein A binds to *Cryptococcus neoformans* without promoting phagocytosis. Eur J Clin Invest 29: 83–92.
55. Geunes-Boyer S, Beers MF, Perfect JR, Heitman J, Wright JR (2012) Surfactant protein D facilitates *Cryptococcus neoformans* infection. Infect Immun 80: 2444–2453. doi:10.1128/IAI.05613-11.
56. Giles SS, Dagenais TRT, Botts MR, Keller NP, Hull CM (2009) Elucidating the pathogenesis of spores from the human fungal pathogen *Cryptococcus neoformans*. Infect Immun 77: 3491–3500. doi:10.1128/IAI.00334-09.
57. Nakamura K, Kinjo T, Saijo S, Miyazato A, Adachi Y, et al. (2007) Dectin-1 is not required for the host defense to *Cryptococcus neoformans*. Microbiol Immunol 51: 1115–1119.
58. Dan JM, Kelly RM, Lee CK, Levitz SM (2008) Role of the mannose receptor in a murine model of *Cryptococcus neoformans* infection. Infect Immun 76: 2362–2367. doi: 10.1128/IAI.00095-08.
59. Kozel TR, Mastroianni RP (1976) Inhibition of phagocytosis by cryptococcal polysaccharide: dissociation of the attachment and ingestion phases of phagocytosis. Infect Immun 14: 62–67.
60. Bulmer GS, Sans MD (1968) *Cryptococcus neoformans*. 3. Inhibition of phagocytosis. J Bacteriol 95: 5–8.
61. Kozel TR, Gotschlich EC (1982) The capsule of *Cryptococcus neoformans* passively inhibits phagocytosis of the yeast by macrophages. J Immunol 129: 1675–1680.
62. Cross CE, Bancroft GJ (1995) Ingestion of acapsular *Cryptococcus neoformans* occurs via mannose and beta-glucan receptors, resulting in cytokine production and increased phagocytosis of the encapsulated form. Infect Immun 63: 2604–2611.
63. Luberto C, Martinez-Mariño B, Taraskiewicz D, Bolaños B, Chitano P, et al. (2003) Identification of App1 as a regulator of phagocytosis and virulence of *Cryptococcus neoformans*. J Clin Invest 112: 1080–1094. doi:10.1172/JCI18309.
64. Stano P, Williams V, Villani M, Cymbalyuk ES, Qureshi A, et al. (2009) App1: an antiphagocytic protein that binds to complement receptors 3 and 2. J Immunol 182: 84–91.
65. Liu OW, Chun CD, Chow ED, Chen C, Madhani HD, et al. (2008) Systematic genetic analysis of virulence in the human fungal pathogen *Cryptococcus neoformans*. Cell 135: 174–188. doi:10.1016/j.cell.2008.07.046.
66. Chun CD, Brown JCS, Madhani HD (2011) A Major Role for Capsule-Independent Phagocytosis-Inhibitory Mechanisms in Mammalian Infection by *Cryptococcus neoformans*. Cell Host Microbe 9: 243–251. doi:10.1016/j.chom.2011.02.003.
67. Zaragoza O, García-Rodas R, Nosanchuk JD, Cuenca-Estrella M, Rodriguez-Tudela JL, et al. (2010) Fungal cell gigantism during mammalian infection. PLoS Pathog 6: e1000945. doi:10.1371/journal.ppat.1000945.
68. Okagaki LH, Strain AK, Nielsen JN, Charlier C, Baltes NJ, et al. (2010) Cryptococcal cell morphology affects host cell interactions and pathogenicity. PLoS Pathog 6:

e1000953. doi:10.1371/journal.ppat.1000953.
69. Okagaki LH, Nielsen K (2012) Titan cells confer protection from phagocytosis in *Cryptococcus neoformans* infections. Eukaryotic Cell 11: 820–826. doi:10.1128/EC.00121-12.
70. Tucker SC, Casadevall A (2002) Replication of *Cryptococcus neoformans* in macrophages is accompanied by phagosomal permeabilization and accumulation of vesicles containing polysaccharide in the cytoplasm. Proc Natl Acad Sci USA 99: 3165–3170. doi:10.1073/pnas.052702799.
71. Voelz K, Lammas DA, May RC (2009) Cytokine signaling regulates the outcome of intracellular macrophage parasitism by *Cryptococcus neoformans*. Infect Immun 77: 3450–3457. doi:10.1128/IAI.00297-09.
72. Levitz SM, Nong SH, Seetoo KF, Harrison TS, Speizer RA, et al. (1999) *Cryptococcus neoformans* resides in an acidic phagolysosome of human macrophages. Infect Immun 67: 885–890.
73. Wozniak KL, Levitz SM (2008) *Cryptococcus neoformans* enters the endolysosomal pathway of dendritic cells and is killed by lysosomal components. Infect Immun 76: 4764–4771. doi:10.1128/IAI.00660-08.
74. Brown SM, Campbell LT, Lodge JK (2007) *Cryptococcus neoformans*, a fungus under stress. Curr Opin Microbiol 10: 320–325. doi:10.1016/j.mib.2007.05.014.
75. Chaka W, Scharringa J, Verheul AF, Verhoef J, van Strijp AG, et al. (1995) Quantitative analysis of phagocytosis and killing of *Cryptococcus neoformans* by human peripheral blood mononuclear cells by flow cytometry. Clin Diagn Lab Immunol 2: 753–759.
76. Miller MF, Mitchell TG (1991) Killing of *Cryptococcus neoformans* strains by human neutrophils and monocytes. Infect Immun 59: 24–28.
77. Diamond RD, Root RK, Bennett JE (1972) Factors influencing killing of *Cryptococcus neoformans* by human leukocytes in vitro. J Infect Dis 125: 367–376.
78. Fairn GD, Grinstein S (2012) How nascent phagosomes mature to become phagolysosomes. Trends Immunol 33: 397–405. doi:10.1016/j.it.2012.03.003.
79. Levitz SM, DiBenedetto DJ (1989) Paradoxical role of capsule in murine bronchoalveolar macrophage-mediated killing of *Cryptococcus neoformans*. J Immunol 142: 659–665.
80. Flesch IE, Schwamberger G, Kaufmann SH (1989) Fungicidal activity of IFN-gamma-activated macrophages. Extracellular killing of *Cryptococcus neoformans*. J Immunol 142: 3219–3224.
81. Steenbergen JN, Nosanchuk JD, Malliaris SD, Casadevall A (2003) *Cryptococcus neoformans* virulence is enhanced after growth in the genetically malleable host Dictyostelium discoideum. Infect Immun 71: 4862–4872.
82. Mylonakis E, Ausubel FM, Perfect JR, Heitman J, Calderwood SB (2002) Killing of *Caenorhabditis elegans* by *Cryptococcus neoformans* as a model of yeast pathogenesis. Proc Natl Acad Sci USA 99: 15675–15680. doi:10.1073/pnas.232568599.
83. Alvarez M, Casadevall A (2006) Phagosome Extrusion and Host-Cell Survival after *Cryptococcus neoformans* Phagocytosis by Macrophages. Current Biology 16: 2161–2165. doi:10.1016/j.cub.2006.09.061.
84. Ma H, Croudace JE, Lammas DA, May RC (2006) Expulsion of live pathogenic yeast by macrophages. Curr Biol 16: 2156–2160. doi:10.1016/j.cub.2006.09.032.
85. Luo Y, Alvarez M, Xia L, Casadevall A (2008) The outcome of phagocytic cell division with infectious cargo depends on single phagosome formation. PLoS One 3: e3219. doi:10.1371/journal.pone.0003219.

86. Nicola AM, Robertson EJ, Albuquerque P, Derengowski LDS, Casadevall A (2011) Nonlytic Exocytosis of *Cryptococcus neoformans* from Macrophages Occurs In Vivo and Is Influenced by Phagosomal pH. mBio 2: e00167–11–e00167–11. doi:10.1128/mBio.00167-11.
87. Bain JM, Lewis LE, Okai B, Quinn J, Gow NAR, et al. (2012) Non-lytic expulsion/exocytosis of *Candida albicans* from macrophages. Fungal Genet Biol 49: 677–678. doi:10.1016/j.fgb.2012.01.008.
88. Johnston SA, May RC (2010) The human fungal pathogen *Cryptococcus neoformans* escapes macrophages by a phagosome emptying mechanism that is inhibited by Arp2/3 complex-mediated actin polymerisation. PLoS Pathog 6. doi:10.1371/journal.ppat.1001041.
89. Chayakulkeeree M, Johnston SA, Oei JB, Lev S, Williamson PR, et al. (2011) SEC14 is a specific requirement for secretion of phospholipase B1 and pathogenicity of *Cryptococcus neoformans*. Mol Microbiol 80: 1088–1101. doi:10.1111/j.1365-2958.2011.07632.x.
90. Alvarez M, Casadevall A (2007) Cell-to-cell spread and massive vacuole formation after *Cryptococcus neoformans* infection of murine macrophages. BMC Immunol 8: 16. doi:10.1186/1471-2172-8-16.
91. Ma H, Croudace JE, Lammas DA, May RC (2007) Direct cell-to-cell spread of a pathogenic yeast. BMC Immunol 8: 15. doi:10.1186/1471-2172-8-15.
92. Lee SC, Kress Y, Zhao ML, Dickson DW, Casadevall A (1995) *Cryptococcus neoformans* survive and replicate in human microglia. Lab Invest 73: 871–879.
93. Villena SN, Pinheiro RO, Pinheiro CS, Nunes MP, Takiya CM, et al. (2008) Capsular polysaccharides galactoxylomannan and glucuronoxylomannan from *Cryptococcus neoformans* induce macrophage apoptosis mediated by Fas ligand. Cell Microbiol 10: 1274–1285. Available: http://eutils.ncbi.nlm.nih.gov/entrez/eutils/elink.fcgi?dbfrom=pubmed&id=18284419&retmode=ref&cmd=prlinks.
94. de Jesus M, Nicola AM, Frases S, Lee IR, Mieses S, et al. (2009) Galactoxylomannan-mediated immunological paralysis results from specific B cell depletion in the context of widespread immune system damage. J Immunol 183: 3885–3894. doi:10.4049/jimmunol.0900449.
95. Davis J, Zheng WY, Glatman-Freedman A, Ng JAN, Pagcatipunan MR, et al. (2007) Serologic evidence for regional differences in pediatric cryptococcal infection. The Pediatric Infectious Disease Journal 26: 549–551. doi:10.1097/INF.0b013e318047e073.
96. Atkinson AJ, Bennett JE (1968) Experience with a new skin test antigen prepared from *Cryptococcus neoformans*. Am Rev Respir Dis 97: 637–643.
97. Saha DC, Goldman DL, Shao X, Casadevall A, Husain S, et al. (2007) Serologic evidence for reactivation of cryptococcosis in solid-organ transplant recipients. Clin Vaccine Immunol 14: 1550–1554. doi:10.1128/CVI.00242-07.
98. Fessel WJ (1993) Cryptococcal meningitis after unusual exposures to birds. N Engl J Med 328: 1354–1355. doi:10.1056/NEJM199305063281816.
99. Nosanchuk JD, Shoham S, Fries BC, Shapiro DS, Levitz SM, et al. (2000) Evidence of zoonotic transmission of *Cryptococcus neoformans* from a pet cockatoo to an immunocompromised patient. Ann Intern Med 132: 205–208.
100. Shrestha RK, Stoller JK, Honari G, Procop GW, Gordon SM (2004) Pneumonia due to *Cryptococcus neoformans* in a patient receiving infliximab: possible zoonotic transmission from a pet cockatiel. Respir Care 49: 606–608.
101. Lortholary O, Nunez H, Brauner MW, Dromer F (2004) Pulmonary cryptococcosis. Semin Respir Crit Care Med 25: 145–157. doi:10.1055/s-2004-824899.

102. Campbell GD (1966) Primary pulmonary cryptococcosis. Am Rev Respir Dis 94: 236–243.
103. Neuville S, Dromer F, Morin O, Dupont B, Ronin O, et al. (2003) Primary cutaneous cryptococcosis: a distinct clinical entity. Clin Infect Dis 36: 337–347. doi: 10.1086/345956.
104. Liechty CA, Solberg P, Were W, Ekwaru JP, Ransom RL, et al. (2007) Asymptomatic serum cryptococcal antigenemia and early mortality during antiretroviral therapy in rural Uganda. Trop Med Int Health 12: 929–935. doi:10.1111/j.1365-3156.2007.01874.x.
105. Andama AO, Boon den S, Meya D, Cattamanchi A, Worodria W, et al. (2013) Prevalence and outcomes of cryptococcal antigenemia in HIV-seropositive patients hospitalized for suspected tuberculosis in Uganda. J Acquir Immune Defic Syndr 63: 189–194. doi:10.1097/QAI.0b013e3182926f95.
106. Micol R, Lortholary O, Sar B, Laureillard D, Ngeth C, et al. (2007) Prevalence, determinants of positivity, and clinical utility of cryptococcal antigenemia in Cambodian HIV-infected patients. J Acquir Immune Defic Syndr 45: 555–559. doi: 10.1097/QAI.0b013e31811ed32c.
107. Jarvis JN, Govender N, Chiller T, Park BJ, Longley N, et al. (2012) Cryptococcal antigen screening and preemptive therapy in patients initiating antiretroviral therapy in resource-limited settings: a proposed algorithm for clinical implementation. J Int Assoc Physicians AIDS Care (Chic) 11: 374–379. doi:10.1177/1545109712459077.
108. Perfect JR, Dismukes WE, Dromer F, Goldman DL, Graybill JR, et al. (2010) Clinical practice guidelines for the management of cryptococcal disease: 2010 update by the infectious diseases society of america. Clin Infect Dis 50: 291–322. doi: 10.1086/649858.
109. Ou X-T, Wu J-Q, Zhu L-P, Guan M, Xu B, et al. (2011) Genotypes coding for mannose-binding lectin deficiency correlated with cryptococcal meningitis in HIV-uninfected Chinese patients. J Infect Dis 203: 1686–1691. doi:10.1093/infdis/jir152.
110. O'Meara TR, Alspaugh JA (2012) The *Cryptococcus neoformans* capsule: a sword and a shield. Clin Microbiol Rev 25: 387–408. doi:10.1128/CMR.00001-12.
111. Steen BR, Lian T, Zuyderduyn S, MacDonald WK, Marra M, et al. (2002) Temperature-regulated transcription in the pathogenic fungus *Cryptococcus neoformans*. Genome Res 12: 1386–1400. doi:10.1101/gr.80202.
112. Wang Y, Aisen P, Casadevall A (1995) *Cryptococcus neoformans* melanin and virulence: mechanism of action. Infect Immun 63: 3131–3136.
113. Vecchiarelli A, Pericolini E, Gabrielli E, Chow S-K, Bistoni F, et al. (2011) *Cryptococcus neoformans* galactoxylomannan is a potent negative immunomodulator, inspiring new approaches in anti-inflammatory immunotherapy. Immunotherapy 3: 997–1005. doi:10.2217/imt.11.86.
114. Cox GM, McDade HC, Chen SC, Tucker SC, Gottfredsson M, et al. (2001) Extracellular phospholipase activity is a virulence factor for *Cryptococcus neoformans*. Mol Microbiol 39: 166–175.
115. Cox GM, Mukherjee J, Cole GT, Casadevall A, Perfect JR (2000) Urease as a virulence factor in experimental cryptococcosis. Infect Immun 68: 443–448.
116. Cox GM, Harrison TS, McDade HC, Taborda CP, Heinrich G, et al. (2003) Superoxide dismutase influences the virulence of *Cryptococcus neoformans* by affecting growth within macrophages. Infect Immun 71: 173–180.
117. Syme RM, Spurrell JC, Ma LL, Green FH, Mody CH (2000) Phagocytosis and protein processing are required for presentation of *Cryptococcus neoformans* mitogen to T lymphocytes. Infect Immun 68: 6147–6153.

118. Casadevall A, Nosanchuk JD, Williamson P, Rodrigues ML (2009) Vesicular transport across the fungal cell wall. Trends Microbiol 17: 158–162. doi:10.1016/j.tim.2008.12.005.
119. Oliveira DL, Freire-de-Lima CG, Nosanchuk JD, Casadevall A, Rodrigues ML, et al. (2010) Extracellular vesicles from *Cryptococcus neoformans* modulate macrophage functions. Infect Immun 78: 1601–1609. doi:10.1128/IAI.01171-09.
120. Bunting LA, Neilson JB, Bulmer GS (1979) *Cryptococcus neoformans*: gastronomic delight of a soil ameba. Sabouraudia 17: 225–232.
121. Greub G, Raoult D (2004) Microorganisms resistant to free-living amoebae. Clin Microbiol Rev 17: 413–433.
122. Castellani A (1955) [Phagocytic and destructive action of Hartmanella castellanii (Amoeba castellanii) on pathogenic encapsulated yeast-like fungi Torulopsis *neoformans* (*Cryptococcus neoformans*)]. Ann Inst Pasteur (Paris) 89: 1–7.
123. Apidianakis Y, Rahme LG, Heitman J, Ausubel FM, Calderwood SB, et al. (2004) Challenge of Drosophila melanogaster with *Cryptococcus neoformans* and role of the innate immune response. Eukaryotic Cell 3: 413–419.
124. London R, Orozco BS, Mylonakis E (2006) The pursuit of cryptococcal pathogenesis: heterologous hosts and the study of cryptococcal host-pathogen interactions. FEMS Yeast Res 6: 567–573. doi:10.1111/j.1567-1364.2006.00056.x.
125. Goldman D, Lee SC, Casadevall A (1994) Pathogenesis of pulmonary *Cryptococcus neoformans* infection in the rat. Infect Immun 62: 4755–4761.
126. Zaragoza O, Alvarez M, Telzak A, Rivera J, Casadevall A (2007) The relative susceptibility of mouse strains to pulmonary *Cryptococcus neoformans* infection is associated with pleiotropic differences in the immune response. Infect Immun 75: 2729–2739. doi:10.1128/IAI.00094-07.
127. Neuville S, Lortholary O, Dromer F (2000) Do kinetics of the humoral response to *Cryptococcus neoformans* proteins during murine cryptococcosis reflect outcome? Infect Immun 68: 3724–3726.
128. Kronstad J, Saikia S, Nielson ED, Kretschmer M, Jung W, et al. (2012) Adaptation of *Cryptococcus neoformans* to mammalian hosts: integrated regulation of metabolism and virulence. Eukaryotic Cell 11: 109–118. doi:10.1128/EC.05273-11.
129. Goulart L, Rosa e Silva LK, Chiapello L, Silveira C, Crestani J, et al. (2010) *Cryptococcus neoformans* and *Cryptococcus gattii* genes preferentially expressed during rat macrophage infection. Med Mycol 48: 932–941. doi: 10.3109/13693781003677494.
130. Lorenz MC, Bender JA, Fink GR (2004) Transcriptional response of *Candida albicans* upon internalization by macrophages. Eukaryotic Cell 3: 1076–1087. doi:10.1128/EC.3.5.1076-1087.2004.
131. Szymczak WA, Davis MJ, Lundy SK, Dufaud C, Olszewski M, et al. (2013) X-Linked Immunodeficient Mice Exhibit Enhanced Susceptibility to *Cryptococcus neoformans* Infection. mBio 4. doi:10.1128/mBio.00265-13.
132. Dromer F, Aucouturier P, Clauvel JP, Saimot G, Yeni P (1988) *Cryptococcus neoformans* antibody levels in patients with AIDS. Scand J Infect Dis 20: 283–285.
133. McClelland EE, Nicola AM, Prados-Rosales R, Casadevall A (2010) Ab binding alters gene expression in *Cryptococcus neoformans* and directly modulates fungal metabolism. J Clin Invest 120: 1355–1361. doi:10.1172/JCI38322.
134. Li W, Averette AF, Desnos-Ollivier M, Ni M, Dromer F, et al. (2012) Genetic Diversity and Genomic Plasticity of *Cryptococcus neoformans* AD Hybrid Strains. G3 (Bethesda) 2: 83–97. doi:10.1534/g3.111.001255.
135. Xu J, Mitchell TG (2003) Comparative gene genealogical analyses of strains of

serotype AD identify recombination in populations of serotypes A and D in the human pathogenic yeast *Cryptococcus neoformans*. Microbiology 149: 2147–2154.
136. Xu J, Vilgalys R, Mitchell TG (2000) Multiple gene genealogies reveal recent dispersion and hybridization in the human pathogenic fungus *Cryptococcus neoformans*. Mol Ecol 9: 1471–1481.
137. Bovers M, Hagen F, Kuramae EE, Diaz MR, Spanjaard L, et al. (2006) Unique hybrids between the fungal pathogens *Cryptococcus neoformans* and *Cryptococcus gattii*. FEMS Yeast Res 6: 599–607. doi:10.1111/j.1567-1364.2006.00082.x.
138. Idnurm A, Bahn Y-S, Nielsen K, Lin X, Fraser JA, et al. (2005) Deciphering the model pathogenic fungus *Cryptococcus neoformans*. Nat Rev Micro 3: 753–764. doi: 10.1038/nrmicro1245.
139. Litvintseva AP, Thakur R, Vilgalys R, Mitchell TG (2006) Multilocus sequence typing reveals three genetic subpopulations of *Cryptococcus neoformans* var. grubii (serotype A), including a unique population in Botswana. Genetics 172: 2223–2238. doi:10.1534/genetics.105.046672.
140. Meyer W, Aanensen DM, Boekhout T, Cogliati M, Diaz MR, et al. (2009) Consensus multi-locus sequence typing scheme for *Cryptococcus neoformans* and *Cryptococcus gattii*. Med Mycol 47: 561–570. doi:10.1080/13693780902953886.
141. Chrisman CJ, Alvarez M, Casadevall A (2010) Phagocytosis of *Cryptococcus neoformans* by, and nonlytic exocytosis from, Acanthamoeba castellanii. Applied and Environmental Microbiology 76: 6056–6062. doi:10.1128/AEM.00812-10.
142. Mylonakis E, Moreno R, Khoury El JB, Idnurm A, Heitman J, et al. (2005) Galleria mellonella as a model system to study *Cryptococcus neoformans* pathogenesis. Infect Immun 73: 3842–3850. doi:10.1128/IAI.73.7.3842-3850.2005.
143. Sukroongreung S, Kitiniyom K, Nilakul C, Tantimavanich S (1998) Pathogenicity of basidiospores of Filobasidiella *neoformans* var. *neoformans*. Med Mycol 36: 419–424.
144. Velagapudi R, Hsueh Y-P, Geunes-Boyer S, Wright JR, Heitman J (2009) Spores as infectious propagules of *Cryptococcus neoformans*. Infect Immun 77: 4345–4355. doi:10.1128/IAI.00542-09.
145. Staib F, Mishra SK (1975) [Contributions to the strain-specific virulence of *Cryptococcus neoformans*. Animal experiments with two *C. neoformans*-strains isolated from bird manure. Preliminary report (author's transl)]. Zentralbl Bakteriol Orig A 230: 81–85.
146. Irokanulo EA, Akueshi CO (1995) Virulence of *Cryptococcus neoformans* serotypes A, B, C and D for four mouse strains. J Med Microbiol 43: 289–293.
147. Ngamskulrungroj P, Chang Y, Sionov E, Kwon-Chung KJ (2012) The Primary Target Organ of *Cryptococcus gattii* Is Different from That of *Cryptococcus neoformans* in a Murine Model. mBio 3. doi:10.1128/mBio.00103-12.
148. Byrnes EJ, Li W, Ren P, Lewit Y, Voelz K, et al. (2011) A diverse population of *Cryptococcus gattii* molecular type VGIII in southern Californian HIV/AIDS patients. PLoS Pathog 7: e1002205. doi:10.1371/journal.ppat.1002205.
149. Pal M (2005) Pathogenicity of environmental strains of *Cryptococcus neoformans* var *neoformans* in murine model. Rev Iberoam Micol 22: 129.
150. Bolaños B, Mitchell TG (1989) Phagocytosis of *Cryptococcus neoformans* by rat alveolar macrophages. J Med Vet Mycol 27: 203–217.
151. Kozel TR, Pfrommer GS, Guerlain AS, Highison BA, Highison GJ (1988) Strain variation in phagocytosis of *Cryptococcus neoformans*: dissociation of susceptibility to phagocytosis from activation and binding of opsonic fragments of C3. Infect Immun 56: 2794–2800.

152. Bolaños B, Mitchell TG (1989) Killing of *Cryptococcus neoformans* by rat alveolar macrophages. J Med Vet Mycol 27: 219–228.
153. Levitz SM, Dupont MP, Smail EH (1994) Direct activity of human T lymphocytes and natural killer cells against *Cryptococcus neoformans*. Infect Immun 62: 194–202.
154. Byrnes EJ, Li W, Lewit Y, Ma H, Voelz K, et al. (2010) Emergence and pathogenicity of highly virulent *Cryptococcus gattii* genotypes in the northwest United States. PLoS Pathog 6: e1000850. doi:10.1371/journal.ppat.1000850.
155. Voelz K, May RC (2010) Cryptococcal interactions with the host immune system. Eukaryotic Cell 9: 835–846. doi:10.1128/EC.00039-10.
156. Liu X, Hu G, Panepinto J, Williamson PR (2006) Role of a VPS41 homologue in starvation response, intracellular survival and virulence of *Cryptococcus neoformans*. Mol Microbiol 61: 1132–1146. doi:10.1111/j.1365-2958.2006.05299.x.
157. Hu G, Hacham M, Waterman SR, Panepinto J, Shin S, et al. (2008) PI3K signaling of autophagy is required for starvation tolerance and virulenceof *Cryptococcus neoformans*. J Clin Invest 118: 1186–1197. doi:10.1172/JCI32053.
158. Panepinto J, Liu L, Ramos J, Zhu X, Valyi-Nagy T, et al. (2005) The DEAD-box RNA helicase Vad1 regulates multiple virulence-associated genes in *Cryptococcus neoformans*. J Clin Invest 115: 632–641. doi:10.1172/JCI23048.
159. Luberto C, Toffaletti DL, Wills EA, Tucker SC, Casadevall A, et al. (2001) Roles for inositol-phosphoryl ceramide synthase 1 (IPC1) in pathogenesis of *C. neoformans*. Genes Dev 15: 201–212.
160. Dromer F, Salamero J, Contrepois A, Carbon C, Yeni P (1987) Production, characterization, and antibody specificity of a mouse monoclonal antibody reactive with *Cryptococcus neoformans* capsular polysaccharide. Infect Immun 55: 742–748.
161. Sebastià J, Cristòfol R, Martín M, Rodríguez-Farré E, Sanfeliu C (2003) Evaluation of fluorescent dyes for measuring intracellular glutathione content in primary cultures of human neurons and neuroblastoma SH-SY5Y. Cytometry A 51: 16–25. doi:10.1002/cyto.a.10003.
162. Markovic J, Mora NJ, Broseta AM, Gimeno A, de-la-Concepción N, et al. (2009) The depletion of nuclear glutathione impairs cell proliferation in 3t3 fibroblasts. PLoS One 4: e6413. doi:10.1371/journal.pone.0006413.
163. Ikeda R, Sawamura K (2008) Bacterial and H2O2 stress-induced apoptosis-like events in *Cryptococcus neoformans*. Research in Microbiologoy 159: 628–634. doi:10.1016/j.resmic.2008.07.006.
164. Murphy JW, Mosley RL, Cherniak R, Reyes GH, Kozel TR, et al. (1988) Serological, electrophoretic, and biological properties of *Cryptococcus neoformans* antigens. Infect Immun 56: 424–431.
165. Kwon-chung K, Bennett J (1992) Culture Media and Reagents. Medical mycology. Lippincott Williams & Wilkins. p. p.816.
166. Xue C, Tada Y, Dong X, Heitman J (2007) The human fungal pathogen *Cryptococcus* can complete its sexual cycle during a pathogenic association with plants. Cell Host Microbe 1: 263–273. doi:10.1016/j.chom.2007.05.005.
167. Xue C, Liu T, Chen L, Li W, Liu I, et al. (2010) Role of an expanded inositol transporter repertoire in *Cryptococcus neoformans* sexual reproduction and virulence. mBio 1. doi:10.1128/mBio.00084-10.
168. Pfaffl MW (2001) A new mathematical model for relative quantification in real-time RT-PCR. Nucleic Acids Res 29: e45.
169. Hellemans J, Mortier G, de Paepe A, Speleman F, Vandesompele J (2007) qBase relative quantification framework and software for management and automated analysis of real-time quantitative PCR data. Genome Biol 8: R19. doi:10.1186/

gb-2007-8-2-r19.
170. Saeed AI, Sharov V, White J, Li J, Liang W, et al. (2003) TM4: a free, open-source system for microarray data management and analysis. BioTechniques 34: 374–378.
171. López S, Prieto M, Dijkstra J, Dhanoa MS, France J (2004) Statistical evaluation of mathematical models for microbial growth. Int J Food Microbiol 96: 289–300. doi: 10.1016/j.ijfoodmicro.2004.03.026.
172. Janbon G, Maeng S, Yang D-H, Ko Y-J, Jung K-W, et al. (2010) Characterizing the role of RNA silencing components in *Cryptococcus neoformans*. Fungal Genet Biol 47: 1070–1080. doi:10.1016/j.fgb.2010.10.005.
173. Williamson PR (1997) Laccase and melanin in the pathogenesis of *Cryptococcus neoformans*. Front Biosci 2: e99–e107.
174. Toffaletti DL, del Poeta M, Rude TH, Dietrich F, Perfect JR (2003) Regulation of cytochrome c oxidase subunit 1 (COX1) expression in *Cryptococcus neoformans* by temperature and host environment. Microbiology (Reading, Engl) 149: 1041–1049.
175. Clemons KV, Stevens DA (2010) Cryptococcosis in Experimental Animals: Lessons Learned. *Cryptococcus*: From Human Pathogen to Model Yeast. ASM Press. pp. 473–488.
176. Ma LL, Wang CLC, Neely GG, Epelman S, Krensky AM, et al. (2004) NK cells use perforin rather than granulysin for anticryptococcal activity. J Immunol 173: 3357–3365.
177. Schein JE, Tangen KL, Chiu R, Shin H, Lengeler KB, et al. (2002) Physical maps for genome analysis of serotype A and D strains of the fungal pathogen *Cryptococcus neoformans*. Genome Res 12: 1445–1453. doi:10.1101/gr.81002.
178. Feldmesser M, Rivera J, Kress Y, Kozel TR, Casadevall A (2000) Antibody interactions with the capsule of *Cryptococcus neoformans*. Infect Immun 68: 3642–3650.
179. Garcia-Hermoso D, Dromer F, Janbon G (2004) *Cryptococcus neoformans* capsule structure evolution in vitro and during murine infection. Infect Immun 72: 3359–3365. doi:10.1128/IAI.72.6.3359-3365.2004.
180. Ormerod KL, Morrow CA, Chow EWL, Lee IR, Arras SDM, et al. (2013) Comparative Genomics of Serial Isolates of *Cryptococcus neoformans* Reveals Gene Associated with Carbon Utilization and Virulence. G3 (Bethesda). doi:10.1534/g3.113.005660.
181. Moore R (1998) Cytology and ultrastructure of yeasts and yeastlike fungi. The yeasts, a taxonomic study. Elsevier, Vol. 3. p. p.33.
182. Cassone A, Simonetti N, Strippoli V (1974) Wall structure and bud formation in *Cryptococcus neoformans*. Arch Microbiol 95: 205–212. doi:10.1007/BF02451762.
183. Simmons R (1989) Comparison of chitin localization in *Saccharomyces cerevisiae*, *Cryptococcus neoformans* and *Malassezia* spp. Mycologicla Research 94: 551–553.
184. LYONS A, PARISH C (1994) Determination of lymphocyte division by flow cytometry. J Immunol Methods 171: 131–137. doi:10.1016/0022-1759(94)90236-4.
185. Brodin P, Christophe T (2011) High-content screening in infectious diseases. Current Opinion in Chemical Biology 15: 534–539. doi:10.1016/j.cbpa.2011.05.023.
186. Jayaswal S, Kamal MA, Dua R, Gupta S, Majumdar T, et al. (2010) Identification of Host-Dependent Survival Factors for Intracellular Mycobacterium tuberculosis through an siRNA Screen. PLoS Pathog 6: e1000839. doi:10.1371/journal.ppat.1000839.s008.
187. Nishiuchi H, Tabira Y, Yamagishi K (2012) A combination of flow cytometry and traditional screening using chemicals to isolate high glutathione-producing yeast mutants. Biosci Biotechnol Biochem 76: 1085–1090.
188. Fortuniak A, Zadzinski R, Bilinski T, Bartosz G (1996) Glutathione depletion in the

yeast *Saccharomyces cerevisiae*. Biochem Mol Biol Int 38: 901–910.
189. Zadzinski R, Fortuniak A, Bilinski T, Grey M, Bartosz G (1998) Menadione toxicity in *Saccharomyces cerevisiae* cells: activation by conjugation with glutathione. Biochem Mol Biol Int 44: 747–759.
190. Sangalli-Leite F, Scorzoni L, Mesa-Arango AC, Casas C, Herrero E, et al. (2011) Amphotericin B mediates killing in *Cryptococcus neoformans* through the induction of a strong oxidative burst. Microbes Infect 13: 457–467. doi:10.1016/j.micinf.2011.01.015.
191. Van Peer G, Mestdagh P, Vandesompele J (2012) Accurate RT-qPCR gene expression analysis on cell culture lysates. Sci Rep 2: 222. doi:10.1038/srep00222.
192. Macura N, Zhang T, Casadevall A (2007) Dependence of macrophage phagocytic efficacy on antibody concentration. Infect Immun 75: 1904–1915. doi:10.1128/IAI.01258-06.
193. Levitz SM (2010) Innate Recognition of Fungal Cell Walls. PLoS Pathog 6: e1000758. doi:10.1371/journal.ppat.1000758.
194. Franzot SP, Mukherjee J, Cherniak R, Chen LC, Hamdan JS, et al. (1998) Microevolution of a standard strain of *Cryptococcus neoformans* resulting in differences in virulence and other phenotypes. Infect Immun 66: 89–97.
195. MacCallum DM, Castillo L, Nather K, Munro CA, Brown AJP, et al. (2009) Property differences among the four major *Candida albicans* strain clades. Eukaryotic Cell 8: 373–387. doi:10.1128/EC.00387-08.
196. Rosowski EE, Lu D, Julien L, Rodda L, Gaiser RA, et al. (2011) Strain-specific activation of the NF-kappaB pathway by GRA15, a novel *Toxoplasma gondii* dense granule protein. J Exp Med 208: 195–212. doi:10.1084/jem.20100717.
197. Kébaïer C, Louzir H, Chenik M, Ben Salah A, Dellagi K (2001) Heterogeneity of wild *Leishmania major* isolates in experimental murine pathogenicity and specific immune response. Infect Immun 69: 4906–4915. doi:10.1128/IAI.69.8.4906-4915.2001.
198. Holzmuller P, Biron DG, Courtois P, Koffi M, Bras-Gonçalves R, et al. (2008) Virulence and pathogenicity patterns of *Trypanosoma brucei gambiense* field isolates in experimentally infected mouse: differences in host immune response modulation by secretome and proteomics. Microbes Infect 10: 79–86. doi:10.1016/j.micinf.2007.10.008.
199. Lobo C-A, de Frazao K, Rodriguez M, Reid M, Zalis M, et al. (2004) Invasion profiles of Brazilian field isolates of *Plasmodium falciparum*: phenotypic and genotypic analyses. Infect Immun 72: 5886–5891. doi:10.1128/IAI.72.10.5886-5891.2004.
200. Shi M, Li SS, Zheng C, Jones GJ, Kim KS, et al. (2010) Real-time imaging of trapping and urease-dependent transmigration of *Cryptococcus neoformans* in mouse brain. J Clin Invest 120: 1683–1693. doi:10.1172/JCI41963.
201. Casadevall A (2010) Cryptococci at the brain gate: break and enter or use a Trojan horse? J Clin Invest 120: 1389–1392. doi:10.1172/JCI42949.
202. Sabiiti W, Bicanic T, May RC (2012) Investigating clinical cryptococcosis in the context of phagocyte-*Cryptococcus* interactions London.
203. Robertson EJ, Najjuka G, Rolfes MA, Akampurira A, Jain N, et al. (2013) *Cryptococcus neoformans* Ex Vivo Capsule Size Is Associated With Intracranial Pressure and Host Immune Response in HIV-associated Cryptococcal Meningitis. J Infect Dis. doi:10.1093/infdis/jit435.
204. Brouwer AE, Teparrukkul P, Pinpraphaporn S, Larsen RA, Chierakul W, et al. (2005) Baseline correlation and comparative kinetics of cerebrospinal fluid colony-forming unit counts and antigen titers in cryptococcal meningitis. J Infect Dis 192: 681–684. doi:10.1086/432073.

205. Bicanic T, Brouwer AE, Meintjes G, Rebe K, Limmathurotsakul D, et al. (2009) Relationship of cerebrospinal fluid pressure, fungal burden and outcome in patients with cryptococcal meningitis undergoing serial lumbar punctures. AIDS 23: 701–706. doi:10.1097/QAD.0b013e32832605fe.
206. Lortholary O, Improvisi L, Nicolas M, Provost F, Dupont B, et al. (1999) Fungemia during murine cryptococcosis sheds some light on pathophysiology. Med Mycol 37: 169–174.
207. Charlier C, Chrétien F, Baudrimont M, Mordelet E, Lortholary O, et al. (2005) Capsule structure changes associated with *Cryptococcus neoformans* crossing of the blood-brain barrier. Am J Pathol 166: 421–432.
208. Zaragoza O, Nielsen K (2013) Titan cells in *Cryptococcus neoformans*: cells with a giant impact. Curr Opin Microbiol. doi:10.1016/j.mib.2013.03.006.
209. Dworkin J, Shah IM (2010) Exit from dormancy in microbial organisms. Nat Rev Micro 8: 890–896. doi:10.1038/nrmicro2453.
210. Chao MC, Rubin EJ (2010) Letting sleeping dos lie: does dormancy play a role in tuberculosis? Annu Rev Microbiol 64: 293–311. doi:10.1146/annurev.micro.112408.134043.
211. Keren I, Minami S, Rubin E, Lewis K (2011) Characterization and Transcriptome Analysis of Mycobacterium tuberculosis Persisters. mBio 2: e00100–11–e00100–11. doi:10.1128/mBio.00100-11.
212. Murphy DJ, Brown JR (2007) Identification of gene targets against dormant phase Mycobacterium tuberculosis infections. BMC Infect Dis 7: 84. doi:10.1186/1471-2334-7-84.
213. Markus MB (2011) The hypnozoite concept, with particular reference to malaria. Parasitol Res 108: 247–252. doi:10.1007/s00436-010-2072-y.
214. Gray JV, Petsko GA, Johnston GC, Ringe D, Singer RA, et al. (2004) “Sleeping beauty”: quiescence in *Saccharomyces cerevisiae*. Microbiol Mol Biol Rev 68: 187–206. doi:10.1128/MMBR.68.2.187-206.2004.
215. Arcangioli B, Ben Hassine S (2009) Unrepaired oxidative DNA damage induces an ATR/ATM apoptotic-like response in quiescent fission yeast. Cell Cycle 8: 2326–2331.
216. Lamarre C, Sokol S, Debeaupuis J-P, Henry C, Lacroix C, et al. (2008) Transcriptomic analysis of the exit from dormancy of Aspergillus fumigatus conidia. BMC Genomics 9: 417. doi:10.1186/1471-2164-9-417.
217. Kasuga T, Townsend JP, Tian C, Gilbert LB, Mannhaupt G, et al. (2005) Long-oligomer microarray profiling in Neurospora crassa reveals the transcriptional program underlying biochemical and physiological events of conidial germination. Nucleic Acids Res 33: 6469–6485. doi:10.1093/nar/gki953.
218. Botts MR, Hull CM (2010) Dueling in the lung: how *Cryptococcus* spores race the host for survival. Curr Opin Microbiol 13: 437–442. doi:10.1016/j.mib.2010.05.003.
219. Valcourt JR, Lemons JMS, Haley EM, Kojima M, Demuren OO, et al. (2012) Staying alive: metabolic adaptations to quiescence. Cell Cycle 11: 1680–1696. doi:10.4161/cc.19879.
220. Aguilera J, Petit T, de Winde JH, Pronk JT (2005) Physiological and genome-wide transcriptional responses of *Saccharomyces cerevisiae* to high carbon dioxide concentrations. FEMS Yeast Res 5: 579–593. doi:10.1016/j.femsyr.2004.09.009.
221. Price MS, Betancourt-Quiroz M, Price JL, Toffaletti DL, Vora H, et al. (2011) *Cryptococcus neoformans* Requires a Functional Glycolytic Pathway for Disease but Not Persistence in the Host. mBio 2. doi:10.1128/mBio.00103-11.
222. Grahl N, Shepardson KM, Chung D, Cramer RA (2012) Hypoxia and fungal

pathogenesis: to air or not to air? Eukaryotic Cell 11: 560–570. doi:10.1128/EC.00031-12.
223. Chun CD, Liu OW, Madhani HD (2007) A link between virulence and homeostatic responses to hypoxia during infection by the human fungal pathogen *Cryptococcus neoformans*. PLoS Pathog 3: e22. doi:10.1371/journal.ppat.0030022.
224. Ingavale SS, Chang YC, Lee H, McClelland CM, Leong ML, et al. (2008) Importance of mitochondria in survival of *Cryptococcus neoformans* under low oxygen conditions and tolerance to cobalt chloride. PLoS Pathog 4: e1000155. doi:10.1371/journal.ppat.1000155.
225. Upadhya R, Campbell LT, Donlin MJ, Aurora R, Lodge JK (2013) Global transcriptome profile of *Cryptococcus neoformans* during exposure to hydrogen peroxide induced oxidative stress. PLoS One 8: e55110. doi:10.1371/journal.pone.0055110.s009.

Appended

1. Primer table 1

Primers used to study gene expression of virulence factors after macrophage interaction with 9 clinical isolates and H99 reference strain

Name	Sequence (5' to 3')	Size (bp)	Concentration (μM)	$MgCl_2$
CX49[a]	TGAGAAGGACCCTGCCAACA	197	0.5	-
CX50[a]	ACTCCGGCTTGTAGGCATCAA			
vfsa-IPC1F1	TTGCCACACCTGGGAATC	87	0.5	-
vfsa-IPC1R1	TTTGCATCGGTGCCGAG			
vfsa-VAD1F2	ATTATCCCTACCCTTAACCGAAT	91	0.5	-
vfsa-VAD1R2	ATGTTTGAAGTGCGAGTTCT			
vfsa-APP1F1	CTGTGCCAACTGTGTTGAAAT	122	0.3	2mM
vfsa-APP1R1	TGCTGAGTAACGCAGTTTGGA			
vfsa-URE1F1	CGATTCTGGCACAAATGCTAT	105	0.3	-
vfsa-URE1R1	AGAGCCCTGTCAATGACT			
vfsa-LAC1F1	AGAAGGGAAGGAAGGTGATG	101	0.3	-
vfsa-LAC1R1	TATACCTCACAACCGCCAAT			
vfsa-PLB1F1	CTGCTTTGAGGACTACCTATGAGCGA	119	0.5	-
vfsa-PLB1R1	CCTTGAGTTGTAACCACCATTGACGAA			
vfsa-COX1F1	CTGGTATGACACTACACAAGATGCCTC	92	0.5	-
vfsa-COX1R1	ACCAGCTAGAACTGGGATACATAGGA			

2. Primer table 2

Primers used to study gene expression of 37 fungal genes involved in starvation, resistance to oxidative stress, stationary phase metabolism, autophagy, and chitin and capsule formation

Primer_ID	Gene	Primer_sequence	Universal ProbeLibrary (Roche)	Tm
18_s_rRna_1	18S_rRNA			
18S_rRNA_1591P		agcgtgagtcaccagctcgc	na	68
18S_rRNA_1510F		ggcctgggtaatcttgtgaa		61
18S_rRNA_1636R		gtacaaagggcagggacgta		63
CNAG_00396	TPK3			
CNAG_00396_F484		actcaagctgcccttgaaac	27	59
CNAG_00396_R543		ggaagttgggaccctagca		60
CNAG_00483	ACT1			
CNAG_00483_F715		ctcatggagcgtggttacct	29	60
CNAG_00483_R774		aatgtctcgaacgatttctcg		59
CNAG_00570	BCY1			
CNAG_00570_F906		gctgatgcacaatgctcct	38	59
CNAG_00570_R973		ccagggcccataaagtacaa		59
CNAG_00797	ACS2			
CNAG_00797_F1455		cgatgtagagggtgttctcgt	79	59
CNAG_00797_R1518		cctgtagacagtcctggcaat		59
CNAG_01232	PMC1			
CNAG_01232_F437		gatggtcaattgggacttgg	32	60

CNAG_01232_R496		tcttcatggagtagccgtctg		60
CNAG_01445	ATG9			
CNAG_01445_F114		ttcgttgcatgttcaagacg	35	60
CNAG_01445_R173		gtcctcaatgcatcgctttc		60
CNAG_01480	RPL12A			
CNAG_01480_F412		tctgttggttgcactgttgac	79	59
CNAG_01480_R497		tactcgtcgggaacgacaat		60
CNAG_01496	PPT1			
CNAG_01496_F122		ttccttcgcctgttttgagt	54	59
CNAG_01496_R184		gctctccatcagatcccaac		59
CNAG_01722	VPS13			
CNAG_01722_F7450		aacgcaatcgacatgatgg	83	60
CNAG_01722_R7509		agcggtggaaggcacttt		60
CNAG_02503	GPX2			
CNAG_02503_F488		aatgtgttggccgatatggt	31	60
CNAG_02503_R547		tctcgatttcttccttgagctt		59
CNAG_03143	HSP12			
CNAG_03143_F138		ccaatcccagaagtcttacacc	126	59
CNAG_03143_R209		gactcctggttgtcgttcttg		59
CNAG_03202	CYR1			
CNAG_03202_F1679		tgccaggtaggattgtcctc	13	60
CNAG_03202_R1738		ccgtcccagtaaatggtgtc		60
CNAG_04217	PCK1			
CNAG_04217_F1277		gcaggtatgccaagatgctc	58	60
CNAG_04217_R1339		tgatcaaccaacaattgactctg		60
CNAG_04448	RPL19A			
CNAG_04448_F399		gaacaagcgtgtcttgatgg	7	59
CNAG_04448_R458		ttggttcggagcttctcg		60
CNAG_04485	FAA1			
CNAG_04485_F1559		aagcctttaccgaggatggt	9	59
CNAG_04485_R1619		ccgtccttattccattgtcc		59
CNAG_04621	GSY1			
CNAG_04621_F488		aagccggtttagccatcc	4	60
CNAG_04621_R550		tggtgaagattgtggtgacg		60
CNAG_05303	ICL1			
CNAG_05303_F990		acagtcgatcggcacctc	78	59
CNAG_05303_R1051		ctggcagaccgaacgatt		59
CNAG_05653	MLS1			
CNAG_05653_F649		gaagctcgactttggaacga	29	60
CNAG_05653_R708		ctgctgaacacccaaatgac		59
CNAG_06114	VPS21			
CNAG_06114_F351		tgttatcgctctcgtcggta	58	59
CNAG_06114_R425		tcggaagatgaagatgcaga		59
CNAG_06174	GCN2			
CNAG_06174_F2803		gtgcggcaacccagtatc	65	60
CNAG_06174_R2862		ttcgtttgatttgtggtttgg		60
CNAG_06642_R4725		acggaggtaagcgaagatga		59
CNAG_06668	AIM38			
CNAG_06668_F255		gtctggtgtcggtcagaagg	34	60
CNAG_06668_R326		tgtgtcattttcccccactt		60
CNAG_06699	GAPDH			
CNAG_06699_F858		cgttggcactaccgaatctt	64	60
CNAG_06699_R924		gacaaagttggcattaagagca		59

CNAG_06892	ATG3			
CNAG_06892_F564		ggcagtgaggattgtgcat	30	59
CNAG_06892_R634		tcacttgaaggaggttctttcc		59
CNAG_06908	SNZ2			
CNAG_06908_F689		ctgcgccttatcatttgttg	41	59
CNAG_06908_R749		aaggaaacgacgggcaat		60
CNAG_06917	PRX1			
CNAG_06917_F471		cgaaatcttgcgtgtcattg	78	60
CNAG_06917_R530		ggggtggtgatacggtgtt		60
CNAG_07531	SNO1			
CNAG_07531_F505		acgccaacaaagacagacg	4	59
CNAG_07531_R575		ggcggtgaagggatgtact		59
CNAG_07561	GND1			
CNAG_07561_F457		ccccacatcaaggacatctt	44	59
CNAG_07561_R519		gtcacagcagggctcacc		60
CNAG_00746	CAS35			
CNAG_00746_F274		aggcttggatttacgctgaa	69	59
CNAG_00746_R333		accaaatttgctgcccttt		59
CNAG_01164	GFA1			
CNAG_01164_F241		gcgaaggagaaggttgacat	30	59
CNAG_01164_R301		gggtatgtgccatcgaggt		60
CNAG_01019	SOD1			
CNAG_01019_P262		atccagacgaacagctgcg	na	63
CNAG_01019_F242		acgttggtgacctcggtaat		59
CNAG_01019_R306		gtcggaaaagtcgagctgag		60
CNAG_01283	CAP5			
CNAG_01283_F55		cccgcgtctacatctcatct	39	60
CNAG_01283_R114		agtgtgggtcgaaggaatgt		59
CNAG_05581	CHS4			
CNAG_05581_F1778		tgcttgtctcgtcatctcgt	10	59
CNAG_05581_R1838		tgccttctagtctcgccaac		60
CNAG_05799	CDA2			
CNAG_05799_F1320		cacttcttccagcgggtct	83	60
CNAG_05799_R1383		agcggcaagagcaatgag		60
CNAG_06016	CAP6			
CNAG_06016_F1657		gataccgttcgttgggtcaa	78	60
CNAG_06016_R1716		tgtagtctcagaagcggaagg		59
CNAG_07937	CAS1			
CNAG_07937_F327		gtttgttggggactcgacag	59	60
CNAG_07937_R394		tagatgccttgccgacctt		60
CNAG_09009	COX1			
CNAG_09009_F91		gctttctctgttcttatccgactt	50	59
CNAG_09009_R155		tggtcaccgtttagaaattgg		59

3. Article: 'Dynamics of *Cryptococcus neoformans*-Macrophage Interactions reveal that fungal background influences outcome during cryptococcal meningoencephalitis in humans', Alanio et al., mBio 2011

RESEARCH ARTICLE

Dynamics of *Cryptococcus neoformans*-Macrophage Interactions Reveal that Fungal Background Influences Outcome during Cryptococcal Meningoencephalitis in Humans

Alexandre Alanio,[a,b,c] Marie Desnos-Ollivier,[a,b] and Françoise Dromer[a,b]

Institut Pasteur, Molecular Mycology Unit, Paris, France[a]; CNRS URA3012, Institut Pasteur, Paris France[b]; and Service de Maladies Infectieuses et Tropicales, Hôpital Necker-Enfants Malades, Paris, France[c]

ABSTRACT **Cryptococcosis is a multifaceted fungal infection with variable clinical presentation and outcome. As in many infectious diseases, this variability is commonly assigned to host factors. To investigate whether the diversity of *Cryptococcus neoformans* clinical (ClinCn) isolates influences the interaction with host cells and the clinical outcome, we developed and validated new quantitative assays using flow cytometry and J774 macrophages. The phenotype of ClinCn-macrophage interactions was determined for 54 ClinCn isolates recovered from cerebrospinal fluids (CSF) from 54 unrelated patients, based on phagocytic index (PI) and 2-h and 48-h intracellular proliferation indexes (IPH2 and IPH48, respectively). Their phenotypes were highly variable. Isolates harboring low PI/low IPH2 and high PI/high IPH2 values were associated with nonsterilization of CSF at week 2 and death at month 3, respectively. A subset of 9 ClinCn isolates with different phenotypes exhibited variable virulence in mice and displayed intramacrophagic expression levels of the *LAC1*, *APP1*, *VAD1*, *IPC1*, *PLB1*, and *COX1* genes that were highly variable among the isolates and correlated with IPH48. Variation in the expression of virulence factors is thus shown here to depend on not only experimental conditions but also fungal background. These results suggest that, in addition to host factors, the patient's outcome can be related to fungal determinants. Deciphering the molecular events involved in *C. neoformans* fate inside host cells is crucial for our understanding of cryptococcosis pathogenesis.**

IMPORTANCE ***Cryptococcus neoformans* is a life-threatening human fungal pathogen that is responsible for an estimated 1 million cases of meningitis/year, predominantly in HIV-infected patients. The diversity of infecting isolates is well established, as is the importance of the host factors. Interaction with macrophages is a major step in cryptococcosis pathogenesis. How the diversity of clinical isolates influences macrophages' interactions and impacts cryptococcosis outcome in humans remains to be elucidated. Using new assays, we uncovered how yeast-macrophage interactions were highly variable among clinical isolates and found an association between specific behaviors and cryptococcosis outcome. In addition, gene expression of some virulence factors and intracellular proliferation were correlated. While many studies have established that virulence factors can be differentially expressed as a function of experimental conditions, our study demonstrates that, under the same experimental conditions, clinical isolates behaved differently, a diversity that could participate in the variable outcome of infection in humans.**

Received 12 July 2011 **Accepted** 15 July 2011 **Published** 9 August 2011

Citation Alanio A, Desnos-Ollivier M, Dromer F. 2011. Dynamics of *Cryptococcus neoformans*-macrophage interactions reveal that fungal background influences outcome during cryptococcal meningoencephalitis in humans. mBio 2(4):e00158-11. doi:10.1128/mBio.00158-11.

Editor Liise-Anne Pirofski, Albert Einstein College of Medicine

Address correspondence to Françoise Dromer, dromer@pasteur.fr.

With 1 million cases per year and 700,000 annual deaths, cryptococcosis is one of the most frequent invasive fungal infections worldwide (1). It occurs mostly in patients with immune defects, especially those with AIDS, but also non-HIV immunocompromised patients (e.g., patients with sarcoidosis, solid organ transplant patients, and patients under steroid or other immunosuppressive therapy) (2). Cryptococcosis is a multifaceted pathology in terms of clinical presentation and outcome, with meningoencephalitis being the most frequent and severe presentation. Despite undergoing 3 months of adequate antifungal treatment, 15 to 20% patients will die from cryptococcosis (3). This infection is due to the haploid yeasts *Cryptococcus neoformans*, including varieties *grubii* (serotype A) and *neoformans* (serotype D), and *Cryptococcus gattii*. *C. neoformans* propagates by budding and is also capable of sexual multiplication and same-sex mating, which contributes to the high diversity of the overall population, even if asexual expansion is the predominant feature (4). The isolates responsible for infections are serotype A or D, haploid or diploid, and mating type alpha (*MAT*α) or **a** (5). Single (one strain) or mixed (mixture of isolates belonging to various serotypes, mating types, genotypes, and/or ploidies) infections are possible, as evidenced in unpurified clinical cultures (6). Overall, haploid *C. neoformans* serotype A *MAT*α isolates represent the most prevalent clinical isolates worldwide (5).

C. neoformans is a facultative intracellular pathogen (7–9). Interaction of *C. neoformans* with host cells can lead to phagocytosis, with occasional escape to the extracellular space (vomocytosis), and possible transfer of yeast cells between phagocytic cells (10).

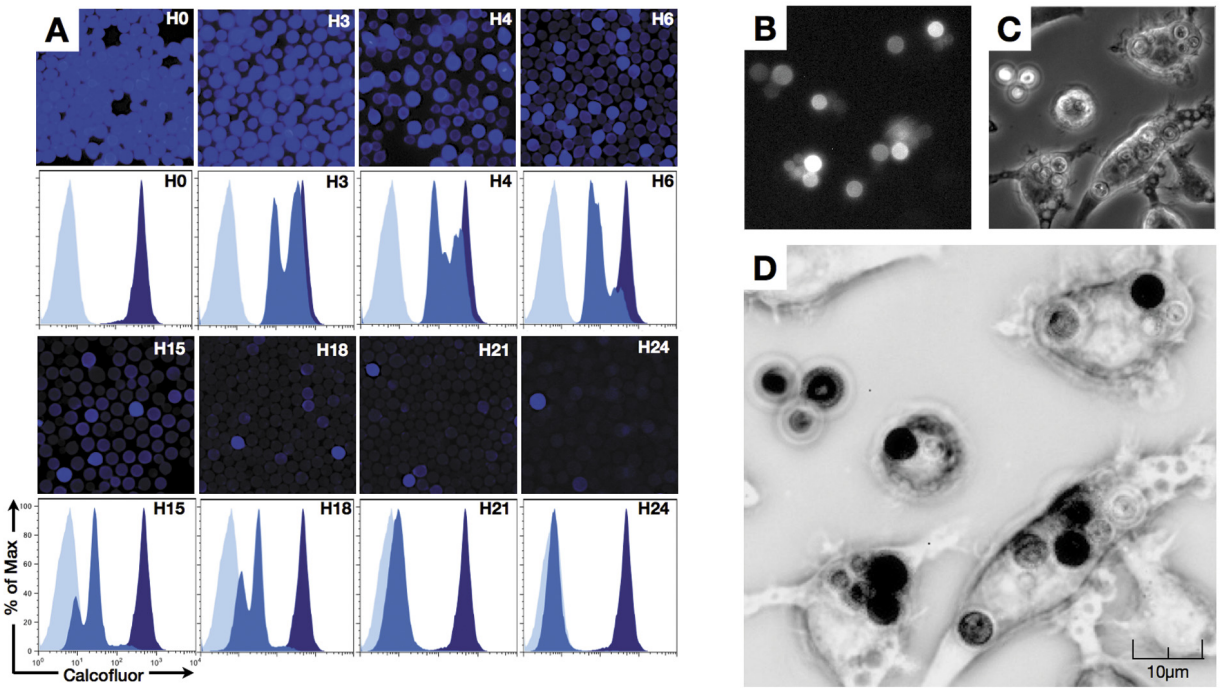

FIG 1 Decrease in fluorescence in calcofluor-labeled *C. neoformans* (reference strain H99) during multiplication. (A) *C. neoformans* multiplication *in vitro* was evaluated after staining of yeast cells with calcofluor prior to incubation at 30°C in liquid YPD for up to 24 h. Aliquots of the culture were harvested at various times (starting at 0 h of incubation [H0]), and fluorescence was assessed in parallel by microscopic observation and flow cytometry. Decreasing numbers of brightly fluorescent cells were observed from H3 to H24 after incubation, and flow cytometry revealed the appearance of cells of intermediate fluorescence intensity (daughter cells; medium blue) compared to the negative control (light blue) and the initial population (mother cells, dark blue). (B to D) Visualization of H99 multiplication inside macrophages assessed by dynamic imaging. Yeast cells were stained with calcofluor prior to incubation with the J774 cell line at a 2.5:1 ratio in the presence of E1 anticapsular polysaccharide monoclonal antibody (E1 MAb) (10^6 yeast cells/1 μg E1 MAb). Dynamic imaging using the Nikon Biostation was performed starting after 1 h of coincubation (images obtained at 16 h 45 min are shown). (B) DAPI fluorescence filter. (C) Transmitted light. (D) Decreased fluorescence of daughter cells assessed after image treatment using ImageJ software (merging panels B and C and inverting the look-up table [LUT]. Mother *C. neoformans* cells appear black, whereas daughter cells look medium to light gray. Original magnification, ×40.

C. neoformans is capable of replication within the phagolysosome, sometimes associated with host cell lysis (10). These interactions are thought to be involved in different steps of pathogenesis, such as dormancy (11), dissemination (8, 12), and blood-brain barrier crossing (8). Ma and colleagues reported that *C. gattii* genotype VGII (responsible for the Vancouver Island outbreak) was associated with increased intramacrophagic yeast proliferation and virulence in mice compared to other genotypes (13). For *C. neoformans*, the influence of genotypic/phenotypic diversity on pathogenesis and clinical outcome has not yet been established.

Our hypothesis is that the clinical outcome of cryptococcal meningoencephalitis in humans is related to fungal determinants and not only to the individual's immune status and/or genetic susceptibility to infection. We took advantage of a large prospective multicenter study on cryptococcosis (3) that collected clinical information and isolates to test this hypothesis. We thus developed a standardized model of yeast-macrophage (murine cell line J774) interactions to study *C. neoformans* clinical (ClinCn) isolates and assessed the correlation between the *in vitro* parameters characterizing the isolates and the outcome of infection in the corresponding patients.

TABLE 1 Characteristics of the 54 patients corresponding to the 54 clinical isolates of *Cryptococcus neoformans* studied

Parameter	*n* (%)
Male/female ratio	4.4:1
Born in Africa	12/54 (22.2)
HIV infected	45/54 (83.3)
Non-HIV infected	9/54 (16.7)
Abnormal neurology	24/54 (44.4)
Abnormal brain imaging	18/51 (35.3)
Disseminated infection	35/54 (64.8)
Capsular polysaccharide titer of >512 in CSF	27/49 (55.1)
Nonsterilization of CSF at wk 2	24/45 (53.3)
Death at mo 3	11/53 (20.8)

RESULTS

New flow cytometry assays are implemented to assess the dynamics of *C. neoformans*-macrophage interactions. To estimate whether the interaction between ClinCn isolates and host cells was variable, we developed original quantitative flow cytometry assays using the J774 murine macrophage cell line. Calcofluor (Calco) is a basic fluorescent dye used to stain fungal cell wall. Preliminary studies using Calco staining revealed that fluorescence is transmitted from mother to daughter cells during multiplication (Fig. 1A). Immediately after staining, mean fluorescence intensity (MFI) was high for all cells. After 3 h of culture, an emerging population with a decreased MFI was detected, while budding cells harboring decreased fluorescence were seen by fluorescence microscopy. This suggested that Calco-labeled chitin was transferred from

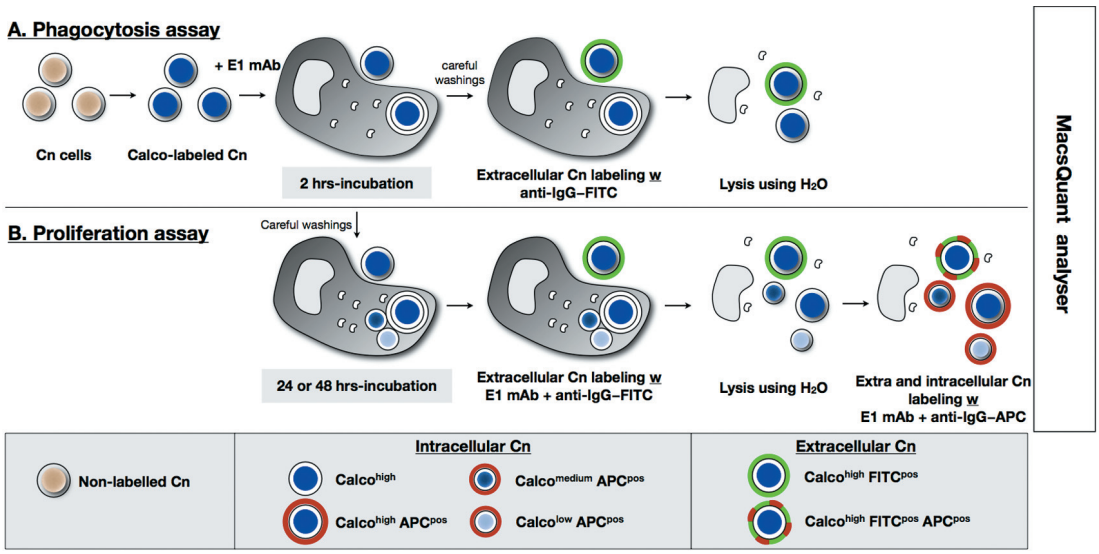

FIG 2 Schematic representation of *Cryptococcus neoformans* (Cn) labeling steps for flow cytometry analysis of yeast-macrophage interaction (FACS-YMI). Yeasts were first stained with calcofluor and then incubated with J774 cells at 37°C in the presence of E1 MAb (opsonin). After careful PBS washings, the incubation was stopped after 2 h of incubation (phagocytosis assay) (A) or prolonged incubation up to 48 h in fresh medium (proliferation assay) (B). In both assays, the remaining extracellular yeast cells were then stained with anti-IgG–FITC antibody and washed, and J774 cells were lysed using H_2O. An additional labeling step was performed in the proliferation assay with E1 MAb and anti-IgG–APC added to stain daughter yeast cells. Samples were analyzed using the MacsQuant analyzer.

mother to daughter cells during budding. During protracted incubation, several populations with decreased MFI progressively appeared, while the high-Calco-fluorescent initial population progressively disappeared over 24 h. This phenomenon was confirmed using dynamic imaging of yeast cells proliferating inside J774 cells (Fig. 1B to 1D; see Fig. S1 and Movie S1 in the supplemental material). Of note, macrophages containing yeast cells were capable of mitosis (Fig. S1B and S1C) and subsequent fusion (Fig. S1D and S1E) (14).

Based on these observations, we decided to assess the dynamics of yeast-macrophage interactions (YMI) by flow cytometry assays (using a fluorescence-activated cell sorter) using the MacsQuant analyzer (FACS-YMI, Fig. 2). Preliminary experiments using the *C. neoformans* reference strain H99 helped us define optimal opsonin quantity (monoclonal antibody [MAb] E1) and a yeast/macrophage ratio in comparison with microscopic results (see Fig. S2A in the supplemental material). In the phagocytosis assay, three distinct populations were observed on the Calco-fluorescein isothiocyanate (FITC) dot plot: the intracellular *C. neoformans* population, which was high for Calco fluorescence and FITC negative ($Calco^{high}$ $FITC^{neg}$); the extracellular *C. neoformans* population, which was $Calco^{high}$ and FITC positive ($Calco^{high}$ $FITC^{pos}$); and cell debris, which was $Calco^{neg}$ $FITC^{neg}$ (Fig. 3A). This allowed us to define a phagocytic index (PI) (103 ±7 for H99). In the proliferation assay, three distinct intracellular *C. neoformans* populations (allophycocyanin-positive [APC^{pos}] $FITC^{neg}$ gate) were observed: the mother *C. neoformans* cell population, which was $Calco^{high}$, and two populations of daughter cells that were $Calco^{medium}$ and $Calco^{low}$ (Fig. 3B), the cells with the lowest fluorescence being the smallest cells (Fig. S2B). Intracellular proliferation indexes were then calculated based on the number of $Calco^{high}$, $Calco^{medium}$, and $Calco^{low}$ populations after 2 h (IPH2) and 48 h (IPH48) of incubation (1.0 ±0.2 and 1.2 ±0.2, respectively, for H99).

Results obtained with H99 mutants validate the FACS-YMI assays. To validate the assays, mutant strains derived from H99 and known for increased phagocytosis (*app1*Δ and *lac1*Δ) and decreased proliferation (*vad1*Δ, *vps34*Δ, *ipc1*Δ, and *lac1*Δ) were screened in comparison to H99. The FACS-YMI assays allowed discrimination between mutant strains based on PI, IPH2, and IPH48 ($P < 0.0001$ each) (Fig. 4). For the mutants, the PIs were categorized into two groups (similar to H99 [ranging from 0.8 to 1.2] for *vps34*Δ, *ipc1*Δ, and *vad1*Δ or higher [from 1.5 to 1.9] for *app1*Δ and *lac1*Δ). Three categories were also delineated for IPH2 (very low [0.02 to 0.04] for *vad1*Δ and *vps34*Δ, intermediate low [0.35] for *lac1*Δ, and low [0.7] for *app1*Δ and *ipc1*Δ) and for IPH48 (very low [0.02 to 0.2] for *vps34*Δ and *vad1*Δ, low [0.8] for *lac1*Δ, and high [2.9 to 3.1] for *app1*Δ and *ipc1*Δ).

Interactions of *C. neoformans* clinical isolates with J774 macrophages are highly diverse. Based on these validated FACS-YMI assays, we then studied 54 ClinCn isolates recovered from the cerebrospinal fluid (CSF) of HIV-positive or -negative unrelated patients (Table 1). An important diversity in terms of genotypes (11 multilocus sequence types) and baseline phenotype characteristics (colony morphology, cell and capsule sizes, growth rate, E1 MAb binding level, chitin content, and urease and laccase activities) was observed (see Fig. S3 in the supplemental material). We then established the diversity of the ClinCn-macrophage interactions. A 30-fold variation in PI (Fig. 5A; Fig. S4 in the supplemental material), 50-fold variation in IPH2, and 16-fold variation in IPH48 (Fig. 5A; Fig. S5 in the supplemental material) were found. The ClinCn isolates exhibiting high (≥0.5) PI and low (<1.0) E1 MAb binding level were mostly smooth (26/30 [86.7%]), compared to those exhibiting low PI and high E1 binding, which were mostly mucous (9/10 [90%]; $P < 0.0001$) (Fig. S6 in the supplemental material). There was no significant association between genotypes and baseline phenotypes or phenotypes of ClinCn-macrophage interaction (Fig. S7 in the supplemental material).

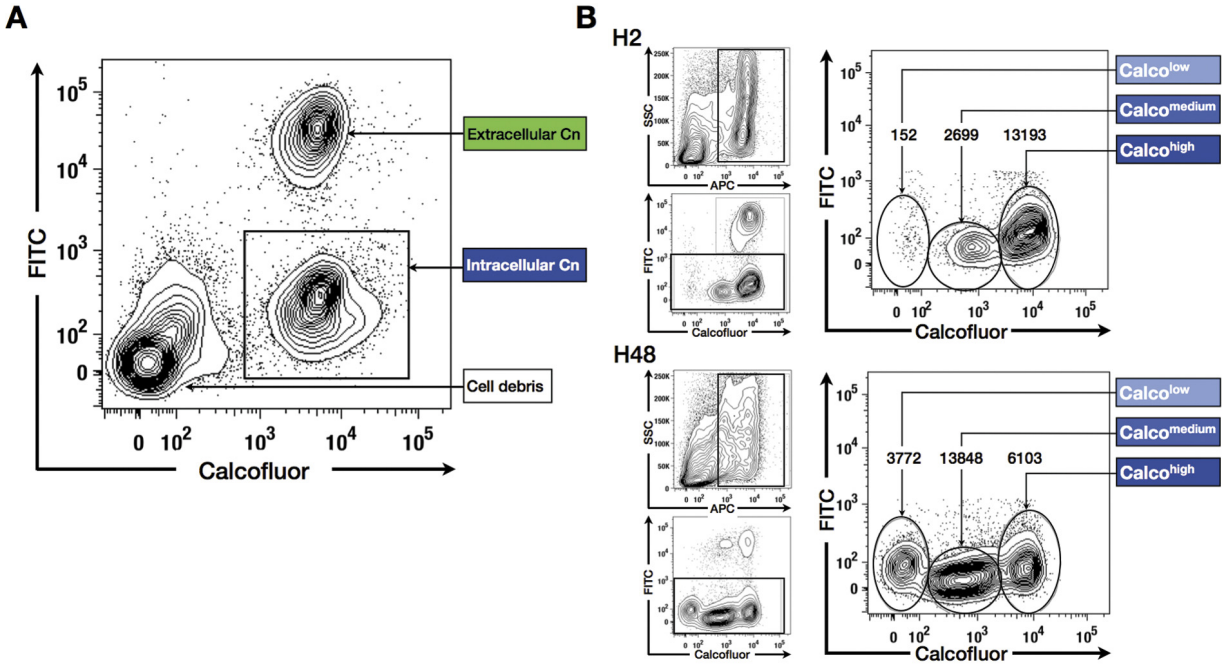

FIG 3 The FACS-YMI allowed assessment of the dynamics of yeast-macrophage interactions. (A) Determination of *C. neoformans* phagocytosis. Intracellular *C. neoformans* cells (Calco^{high} FITC^{neg}) were easily discriminated from extracellular *C. neoformans* cells (Calco^{high} FITC^{pos}) and macrophage debris (Calco^{neg} FITC^{neg}). (B) Determination of *C. neoformans* intracellular proliferation. After selection of the APC^{pos} (excluding cell debris, upper left graphs) and FITC^{neg} populations (intracellular *C. neoformans*, lower left panels), different subsets of intracellular *C. neoformans* cells corresponding to mother (Calco^{high}) and daughter (Calco^{medium} and Calco^{low}) *C. neoformans* cells were observed (right panels). A decrease of mother cells in parallel to an increase in the daughter cell population was observed between 2 h (H2) and 48 h (H48) of coincubation, asserting intracellular proliferation. (The number of events is reported above each subset.)

ClinCn-macrophage interaction phenotypes are associated with variable outcome of cryptococcal meningoencephalitis in humans. Given the high variability of ClinCn-macrophage interaction phenotypes, we then wondered if these parameters (PI, IPH2, and IPH48) correlated with outcome of infection in the corresponding patients. Four categories of isolates were defined according to PI (<0.5 and ≥ 0.5) and IPH2 (≤ 1 and >1). Based on univariate analysis, nonsterilization of CSF despite 2 weeks of antifungal therapy was associated with a population of isolates harboring decreased PI and IPH2 (Fig. 5B; Table 2). The proportions of parameters previously (3) associated with nonsterilization of CSF (gender, dissemination, or high CSF antigen titer) did not significantly differ among the four categories of isolates. Death at months 3 was significantly associated with a population of isolates harboring high PI and IPH2 (Fig. 5B). Parameters previously (3) associated with death at month 3 (abnormal neurology or brain imaging) did not significantly differ among the four categories. In the multivariate analysis, the risk of nonsterilization of the CSF at week 2 was independently associated with low PI and IPH2 (odds ratio [OR], 15.5; 95% confidence interval [95% CI], 1.3 to 184.4; $P = 0.030$) and with HIV infection (OR, 25.2; 95% CI, 1.8 to 348.6; $P = 0.016$) (Table 2).

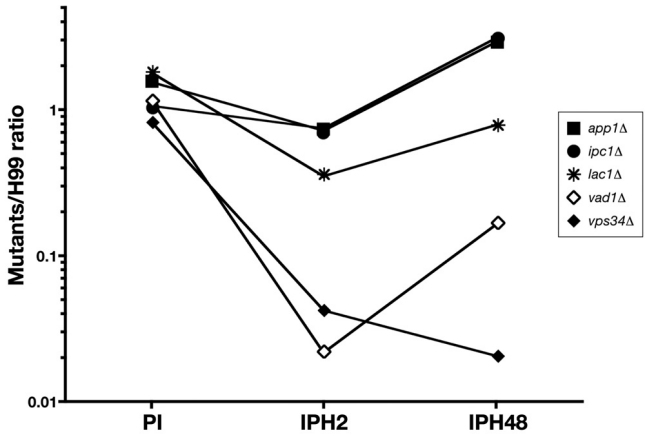

FIG 4 Screening of well-characterized mutant strains compared to H99 using the FACS-YMI assay. Dot plots presenting the corresponding values for phagocytosis (PI) and intramacrophagic proliferation at H2 (IPH2) and H48 (IPH48) for each mutant linked by a solid line ($\log_{10}$ scale). PIs were categorized in two groups: similar to H99 (*vps34*Δ, *ipc1*Δ, and *vad1*Δ mutants) and higher than H99 (*app1*Δ and *lac1*Δ mutants). Three categories were also delineated for IPH2 (very low for *vad1*Δ and *vps34*Δ, intermediate low for *lac1*Δ, and low for *app1*Δ and *ipc1*Δ), and for IPH48 (very low for *vps34*Δ and *vad1*Δ, low for *lac1*Δ, and high for *app1*Δ and *ipc1*Δ).

Expression of some virulence factors correlates with ClinCn-macrophage interaction phenotypes. Considering that in a standardized *in vitro* model, variations in ClinCn-macrophage interaction phenotypes were associated with different outcomes in humans, we further explored known virulence factors in relation to these phenotypes. We selected nine ClinCn isolates (s9-ClinCn) based on various combinations of their ClinCn-macrophage interaction phenotypes (Fig. 6A), genotypes, and related patient outcomes. All s9-ClinCn isolates were fertile (data not shown), with variable virulence in mice, as shown by median survival rates

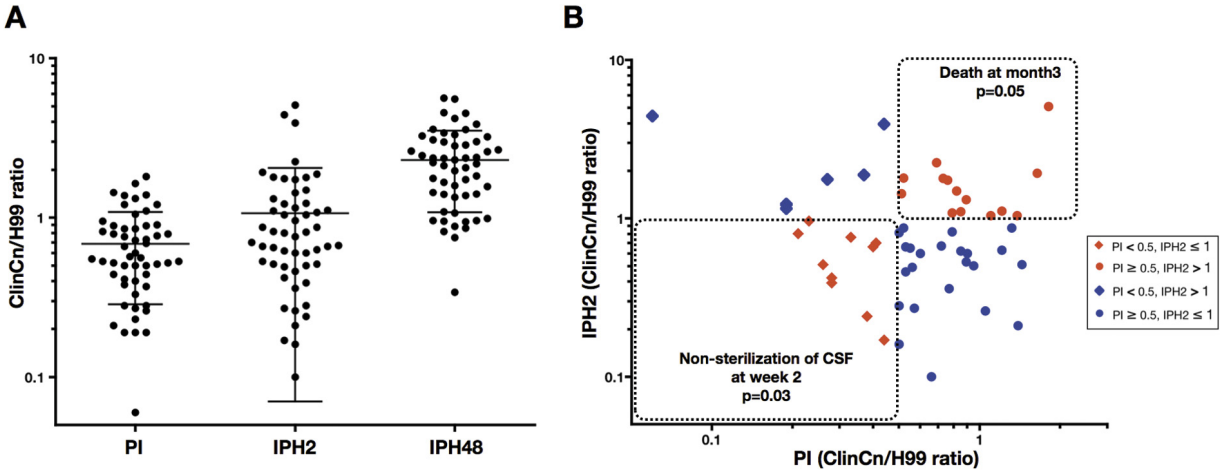

FIG 5 The 54 *C. neoformans* clinical isolates (ClinCn) (serotype A, MATα, haploid) harbored variable interactions with macrophages (phagocytosis and intracellular proliferation). (A) Compared to H99, the distribution of phagocytic (PI), 2-h proliferation (IPH2), and 48-h proliferation (IPH48) indexes showed 30-fold, 50-fold, and 16-fold variations, respectively ($\log_{10}$ scale). Each circle represents the mean of duplicates for a given ClinCn isolate obtained from two independent experiments. Bars represent means ± standard deviations (SD) for the 54 ClinCn isolates. (B) Scatter plots presenting PI versus IPH2. Four categories of isolates were defined according to PI (<0.5 and ≥0.5) and IPH2 (≤1 and >1). The population of isolates harboring a PI of <0.5 and an IPH2 of ≤1 was significantly associated with nonsterilization of CSF at week 2 ($P = 0.03$), and that harboring a PI of ≥0.5 and an IPH2 of >1 was significantly associated with death at month 3 ($P = 0.05$).

(expressed as a ratio for each s9-ClinCn isolate to H99) ranging from 0.57 (AD2-82a) to 3.3 (AD1-07a) (Fig. 6B; P < 0.0001). The 2-h intracellular (iH2) and baseline (BsH2) relative expressions of six virulence factors (*LAC1*, *URE1*, *APP1*, *VAD1*, *IPC1*, and *PLB1* genes) (15–20) and one mitochondrial gene (*COX1*, coding for cytochrome oxidase 1) (13, 21) were quantified with *GAPDH* (coding for glyceraldehyde-3-phosphate dehydrogenase) as the reference gene and H99 as the control. High BsH2 *APP1* expression (>5-fold) was significantly associated with low PI ($P = 0.028$). IPH48 expression and iH2 expression were significantly correlated for *IPC1* ($R^2 = 0.73$, $P = 0.003$), *APP1* ($R^2 = 0.66$, $P = 0.008$), *COX1* ($R^2 = 0.66$, $P = 0.008$), *VAD1* ($R^2 = 0.65$, $P = 0.009$) (Fig. 6C), and *PLB1* ($R^2 = 0.55$, $P = 0.021$). Levels of PI and iH2 expression of *LAC1* ($R^2 = 0.59$, $P = 0.016$) were also correlated. Hierarchical clustering of iH2 and BsH2 expression levels for the six genes together with PI, IPH2, and IPH48 generated four clusters, confirming the previous correlations (see Fig. S8 in the supplemental material). No correlation was found for *URE1* gene expression.

DISCUSSION

In order to assess the correlation between *C. neoformans*-macrophage interactions and clinical parameters, we designed new standardized assays. Since *C. neoformans* strains have been shown to behave similarly in various host cells (murine and human macrophages or amoeba) (22–24), we chose J774 cells for the assays. The use of this cell line and flow cytometry allowed quantification of large samples (more than 10^6 yeast cells and 10^5 macrophages) and accurate discrimination of intra- versus extracellular and mother versus daughter yeast cells. The FACS-YMI assays

TABLE 2 Patients' outcomes are significantly associated with the phenotypes of interaction with J774 macrophages of the clinical isolates for which the corresponding outcome was available[a]

Outcome[a]	Parameter	No. (%) of patients with: Failure ($n = 24$) or death ($n = 11$)	Success ($n = 21$) or survival ($n = 42$)	Univariate analysis OR	95% CI	*P*	Multivariate analysis OR	95% CI	*P*
Yeast eradication from CSF at wk 2	PI ≥ 0.5, IPH2 ≤ 1	7 (36.8)	12 (63.2)	Reference					
	PI < 0.5, IPH2 > 1	4 (80.0)	1 (20.0)	6.86	0.63–74.19	0.113	5.79	0.53–63.37	0.150
	PI ≥ 0.5, IPH2 > 1	6 (50.0)	6 (50.0)	1.71	0.40–7.43	0.471	3.48	0.61–19.78	0.159
	PI < 0.5, IPH2 ≤ 1[c]	**7 (77.8)**	**2 (22.2)**	**6.00**	**0.97–37.30**	**0.055**	**15.51**	**1.30–184.43**	**0.030**
	HIV positive[b]	**23 (95.8)**	**14 (66.7)**	**1.64**	**0.85–3.19**	**0.012**	**25.16**	**1.84–348.63**	**0.016**
	HIV negative	1 (4.2)	7 (33.3)	0.14	0.02–1.16				
Death at mo 3	PI ≥ 0.5, IPH2 ≤ 1	3 (13.0)	20 (87.0)	Reference					
	PI < 0.5, IPH2 > 1	1 (16.7)	5 (83.3)	1.34	0.11–15.70	0.819			
	PI ≥ 0.5, IPH2 > 1	**6 (42.9)**	**8 (57.1)**	**5**	**1.00–25.02**	**0.050**			
	PI < 0.5, IPH2 ≤ 1	1 (10.0)	9 (90.0)	0.74	0.07–8.13	0.806			

[a] Patients' outcomes are represented by nonsterilization of CSF at week 2 (i.e., failure or success at yeast eradication from CSF) and death at month 3 (i.e., death or survival).
[b] Only two variables were added to the model due to the small number of events recorded ($n = 24$).
[c] Parameters appearing in bold are statistically significant.

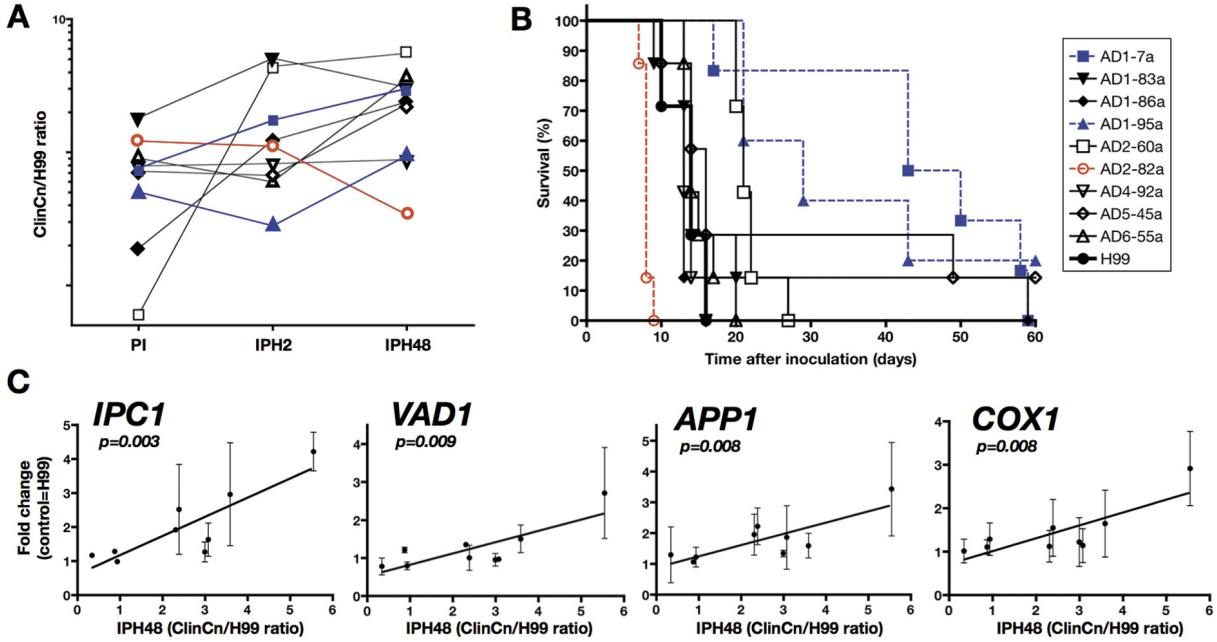

FIG 6 The *in vivo* behavior (virulence in mice) of the s9-ClinCn isolates is heterogeneous and the intracellular (J774 cells) expression levels of known virulence factors correlate with the 48-h proliferation index. (A) Dot plots presenting the corresponding PI, IPH2, and IPH48 values for each of the s9-ClinCn isolates. The values corresponding to a given isolate are linked by a solid line ($\log_{10}$ scale). (B) Outbred male mice were intravenously inoculated with 10^5 yeast cells, and death was recorded over 60 days. Compared to H99 (black circle, thick line), AD2-82a (open red circle, red dotted line) is more virulent (median survival ratio of 0.57), whereas AD1-95a (blue triangle, blue dotted line) and AD1-7a (blue square, blue dotted line) are less virulent (median survival ratios of 2.1 and 3.3, respectively). (C) Compared to H99, IPH48 of the s9-ClinCn isolates correlated with the intracellular expression of the *IPC1*, *VAD1*, *APP1*, and *COX1* genes. Bars represent means ± standard deviations (SD) of duplicates from 2 independent experiments for each s9-ClinCn isolate. The linear regression curve is shown.

were based on Calco staining and its ability to be sparsely transmitted to daughter cells during budding. Indeed, bud formation in basidiomycetous yeasts is enteroblastic (25). The inner layer of the parental multilamellar cell wall is in direct continuation with the outer layer of the bud (26). Given that chitin (~9% of the cell wall) is distributed throughout the cell wall (27, 28), the Calco-labeled chitin of the mother cell wall could contribute to the fluorescence of the daughter cells. The FACS-YMI assays represent a promising alternative to current studies dealing with microscopic or colony-forming unit enumeration and have potential wide applications. The FACS-YMI assay could become, like the carboxyfluorescein diacetate succinimidyl ester (CFSE) assay in immunology (29), an easy and reliable test to study dynamics of fungal cell proliferation.

Up to now, *C. neoformans*-host cell interactions have mostly been studied using reference or mutant strains. Few reports discuss the variability of *C. neoformans* clinical isolates (30), and only a few dealt with parasites (31–34) and other fungal species (13, 35), and none have analyzed correlation with clinical outcome. Using a large collection of ClinCn isolates, we uncovered highly variable phenotypes of *C. neoformans*-macrophage interaction without correlation with genotypes, in contrast with what was demonstrated for the clonal hypervirulent VGII *C. gattii* isolates (13). This could be explained by differences in the pathophysiology of infections due to *C. gattii* and *C. neoformans*, the first being more frequently responsible for primary infection rather than reactivation, in contrast to *C. neoformans*-related diseases (36). As a consequence, the virulence of these two pathogenic fungi in humans could be different in terms of host adaptation and immunological escape mechanisms. One may also wonder if the phenotypic intraspecies diversity reported for eukaryotes, as opposed to prokaryotes, could be explained by their complex genomes and potential recombination events during mating. This is especially true for *C. neoformans*, known for its complex sexual reproduction (4).

Since yeast-macrophage interactions are involved in the pathogenesis, we assessed whether the phenotypes determined *in vitro* were associated with a specific outcome in humans. We found that isolates harboring low PI and low IPH2 were significantly associated with nonsterilization of CSF at weeks 2, whereas those harboring high PI and high IPH2 were associated with death at month 3. Our results suggest that fungal determinants are involved, as are host factors (genetic background and type of immunosuppression) in the outcome of cryptococcal meningoencephalitis. These results highlight the monocyte/macrophage lineage as a major key player in the pathophysiology of the infection in humans, as already suggested by studies on blood-brain barrier crossing and dissemination in mice (8, 37, 38). Additional experiments are needed to assess the relevance of these data in different clinical settings, such as infections with other serotypes, mixed infections, and extrameningeal cryptococcosis.

The fate of *C. neoformans* cells in contact with host cells is dependent on multiple and yet partially unknown factors. The first one is phagocytosis. Unexpectedly, E1 binding level inversely correlated with PI. This suggests that, in addition to Fcγ and complement receptors (39), other receptors involved in innate immunity, such as mannose receptors, CD14, and Toll-like receptor 4 (TLR-4) (40), or factors modulating phagocytosis, such as the

secreted protein App1p (20), the pleiotropic transcription factor Gat201p, or the Gat201-bound gene product Gat204p (41), play a role in the phagocytosis process. After phagocytosis, *C. neoformans* intracellular persistence and proliferation are key steps of the pathogenesis process. We found a relationship between intramacrophagic *COX1*, as shown in *C. gattii* (13), but also *IPC1*, *VAD1*, *APP1*, and *PLB1* gene expression and ClinCn intracellular proliferation. This validates the FACS-YMI assays as innovative means to study virulence factors and potentially decipher the mechanisms by which *C. neoformans* cells escape or survive phagocytosis. Dissociation between early (IPH2) and late (IPH48) intracellular proliferation indexes was observed for some ClinCn isolates as well as for the *lac1*Δ mutant. We also found that a variable proportion of the intracellular yeast cells were still Calco-^{high} after 48 h of incubation, suggesting that they could either be dead or in a low replicative stage or dormancy. Altogether, this suggests that adaptation inside macrophage occurs. Some strains may have "ready-made" virulence (42) (high IPH2 and high IPH48), whereas, for others (low IPH2 and high IPH48), a longer period of metabolic adaptation to hypoxia or starvation inside macrophages could be needed to express virulence factors as described *in vivo* (43). Overall, these various phenotypes could reflect different patterns of pathogenicity. Given the complex biological processes that lead to survival or multiplication inside the phagolysosome, other studies are needed to decipher the precise mechanisms and molecular events involved.

In conclusion, while many studies established that host susceptibility to infection is crucial and that virulence factors of the pathogens can be differentially expressed as a function of environmental conditions (medium, intracellular versus free yeasts, etc.), our study demonstrates that, under the same experimental conditions, clinical isolates of *C. neoformans* behaved differently, a diversity that could participate in the variable outcome of meningoencephalitis in humans.

MATERIALS AND METHODS

Cell line. The J774.16 cell line (hereafter J774) was purchased from the American Type Culture Collection (ATCC) to study the interaction of *C. neoformans* clinical isolates with macrophages. J774 is a murine macrophage-like cell line derived from a reticulum sarcoma. Cells were maintained at 37°C in the presence of 5% CO_2 in Dulbecco's modified Eagle's medium (DMEM) supplemented with 10% heat-inactivated fetal calf serum (FCS) and 1% penicillin–streptomycin (fresh medium) (all from Invitrogen). Cells were used between 10 and 35 passages.

***C. neoformans* strains.** A panel of 54 *C. neoformans* clinical isolates was selected. All isolates were recovered from cerebrospinal fluids and responsible for single infections (one isolate/one genotype/one infection), as opposed to mixed infections (6). All isolates were collected during the CryptoA/D prospective study (3). This study was approved and reported to the French Ministry of Health (registration no. DGS970089). For each isolate, the patient's background, clinical presentation, outcome of infection, and various biological parameters were available (Table 1). Single colonies (ClinCn) from each clinical isolate were frozen in 40% glycerol at −80°C and used thereafter. All ClinCn isolates were characterized as haploid, serotype A, *MAT*α using previously described methods (6). Before each experiment, yeasts were first cultured on Sabouraud agar (SA) medium and then subcultured in liquid yeast extract-peptone-glucose medium (YPD) at 30°C at 150 rpm for 22 h (standard YPD culture). All isolates were tested blind to the clinical parameters.

Mutant strains (all derived from H99) with the genotypes *lac1*Δ (lacking laccase 1 [Lac1p]) (44), *vps34*Δ (lacking the phosphatidylinositol 3-kinase [PI3-kinase] Vps34p) (45), *vad1*Δ (lacking the DEAD-box RNA helicase Vad1p) (18) (kindly donated by P. Williamson, NIH, Bethesda, MD), *app1*Δ (lacking the antiphagocytic protein App1p [20], which binds the CR3 and CR2 receptors on phagocytic cells) (46), and *ipc1*Δ (in which inositol-phosphoryl ceramide synthase, Ipc1p, is downregulated) (19) (kindly donated by M. Del Poeta, Charleston, SC), were also used. Strain H99 (serotype A, *MAT*α, haploid) (kindly donated by J. Heitman, Duke University, NC) was used as the reference strain in all experiments.

Reagents and *C. neoformans* labeling. Calcofluor white dye (Calco) (fluorescent brightener 28; Sigma) specifically stains chitin contained in the cell wall of some eukaryote microorganisms and was used to label *C. neoformans*. Yeast cells were collected from standard YPD culture, washed twice, and resuspended in phosphate-buffered saline (PBS) (Invitrogen) at 5×10^6 to 2×10^7/ml. The cells were then incubated with Calco at 10 μg/ml in PBS for 10 min in the dark at room temperature and then washed twice in PBS. In preliminary experiments, we checked that the *in vitro* growth curves of strains were similar (identical slopes) for Calco-stained and unstained *C. neoformans* strains, except for the *lac1*Δ mutant, for which growth decreased after Calco staining (data not shown). To assess the evolution of Calco fluorescence during multiplication, Calco-stained *C. neoformans* cells (10^6/ml) cultured in standard YPD were analyzed using fluorescence microscopy (Zeiss Axioscope A1 with a 4′,6-diamidino-2-phenylindole [DAPI] filter) and flow cytometry at various incubation times. E1, a murine IgG1 monoclonal anticapsular polysaccharide antibody (E1 MAb) was used as an opsonin (47). Fluorescein isothiocyanate-labeled horse anti-mouse IgG (anti-IgG–FITC) (Vector Laboratories) and allophycocyanin-labeled goat anti-mouse IgG (anti-IgG–APC) (BD Pharmingen) were used at 1:100 for a 20-min incubation.

Baseline genotypes and phenotypes characterization of the ClinCn isolates. The genotype of each ClinCn isolate was determined by multilocus sequence typing (MLST) of seven loci, as previously described (48). The morphological aspect (smooth or mucous) was assessed after 72 h of culture on SA at 30°C. Growth curves were determined in 96-well plates starting at 10^6/ml without agitation in liquid YPD at 30°C (triplicate wells). The optical density at 600 nm (OD_{600}) was recorded up to 140 h of incubation (Labsystems Multiskan). The regression line ($y = ax + b$) was determined, and the results were expressed as the ratio between the slopes ("a" value) for the ClinCn isolates compared to that for H99. Cell and capsule sizes were determined after standard YPD culture. Cell suspensions were made at 10^6/ml in PBS. An aliquot was observed in India ink suspension, using an Axioscan microscope (Carl Zeiss, Germany) and the AxioCam ICc1 camera (Carl Zeiss, Germany). Cell size, delineated by the cell wall, and capsulated cell size, delineated by the white exclusion zone around the cells, were measured for 10 cells randomly selected from each ClinCn isolate and H99 using the Zeiss AxioVision software (Carl Zeiss, Germany). Results were expressed as the average size ratio for ClinCn versus H99 cells. The binding of E1 MAb to the capsule surface was determined. Yeast cells were cultured on SA for 24 h at 30°C for each ClinCn isolate, washed in PBS, and suspended at a concentration equivalent to an OD_{600} of 0.1. Then, 300 μl of the suspension was centrifuged and pellets were resuspended in 100 μl of PBS containing E1 MAb (0.5 μg/ml) and FITC-labeled anti-IgG for 20 min in the dark at room temperature. Then, 400 μl of PBS–1% paraformaldehyde (PFA) was added to fix cells before cytometry analysis. The results were expressed as the ratio between the geometric mean of the FITC fluorescence intensity for the ClinCn isolates and H99. The chitin content was determined after standard YPD culture and standard calcofluor staining by quantification of the geometric mean of the calcofluor fluorescence intensity for the ClinCn isolates and H99 using flow cytometry (see below).

To study the variability of the s9-ClinCn, urease and laccase activities were quantified using urea agar base medium (49) and asparagine agar containing 1 mM L-3,4-dihydroxyphenylalanine (L-Dopa) (50). Urease and laccase activities of 10^5 to 10^7 *C. neoformans* cells after 24 h of incubation at 37°C and 72 h of culture at 30°C, respectively, were quantified by measuring the diameter of the pink halo (urease), and the RGB content of colonies (laccase), using ImageJ software. The mating assay used

Murashige and Skoog medium (51), and fertility was assessed after 7 days of incubation at room temperature in the dark with KN99a (serotype A, mating type **a**), KN99α (serotype A, mating type α), and JEC20 (serotype D, mating type **a**).

Interaction with macrophages. J774 cell suspensions (10^5 in fresh medium per well of a 24-well culture plate) were incubated at 37°C in 5% CO_2 for 48 h. The day of the experiment, E1 MAb (250 μl) and Calco-stained *C. neoformans* suspension (250 μl), both in fresh medium at the desired concentrations, were added to the J774 cell monolayer and incubated at 37°C and 5% CO_2 for 2 h (phagocytosis assay, *C. neoformans*/J774 ratio, 5:1). Nonadherent extracellular yeast cells were then removed by PBS washings, and incubation was stopped to assess phagocytosis or extended to determine intracellular proliferation. Phagocytosis was determined after staining residual extracellular yeasts using anti-IgG–FITC, additional PBS washings, and macrophage lysis with distilled water (Fig. 2A). The samples were then centrifuged, resuspended in 1% paraformaldehyde in PBS (PFA-PBS), vortexed, and sonicated for 3 min before analysis.

To assess intracellular proliferation of ClinCn using flow cytometry (proliferation assay, *C. neoformans*/J774 ratio, 2.5:1), the incubation was protracted in fresh medium for 48 h. Residual extracellular yeast cells were stained by addition of E1 MAb (0.5 μg/ml) and anti-IgG–FITC and washed in PBS, and J774 cells were lysed by water (Fig. 2B). In order to differentiate potentially unstained *C. neoformans* cells from cell debris, an additional step was done using E1 MAb and APC–anti-IgG. All yeast cells were APC^{pos}, while only extracellular yeast cells were APC^{pos} $FITC^{pos}$.

Intracellular proliferation was determined for each ClinCn isolate at the end of the phagocytosis step (H2) and at 48 h (H48). Phagocytosis and proliferation were analyzed in two independent experiments.

Flow cytometry analysis of yeast-macrophage interaction (FACSYMI). Flow cytometry analyses were performed using MacsQuant analyzer and MacsQuantify software 2.0 (Milteniy BioTeC) to provide absolute quantification. Samples were analyzed using FlowJo 8.7 software (Tree Star, Inc.). Aggregates were excluded by gating relevant events in the forward scatter/side scatter (FSC/SSC) contour plot. Three parameters were calculated: (i) the phagocytic index (PI) as the number of events in the $Calco^{high}$ $FITC^{neg}$ gate at H2, (ii) intracellular proliferation at H2 (IPH2) as the ratio between daughter cells ($Calco^{low}$ + $Calco^{medium}$) and mother cells ($Calco^{high}$) at H2, and (iii) intracellular proliferation at H48 (IPH48) as the ratio between daughter cells ($Calco^{low}$ + $Calco^{medium}$) at H48 and mother cells ($Calco^{high}$) at H2.

Results were expressed as the ratio of the given parameter for the ClinCn/mutant strains compared to the H99 parameter determined in the same run. We assessed that results obtained during the two independent experiments were reproducible for PI, IPH2, and IPH48 ($P < 0.0001$ for each parameter), and means of replicates were then used for subsequent analyses.

Dynamic imaging. The evolution of fluorescence intensity from mother to daughter intracellular yeasts was assessed by dynamic imaging (Nikon Biostation). J774 cells were cultured and incubated with Calco-stained *C. neoformans* cells (2.5:1) in dishes (Hi-Q4 35-mm diameter; Nikon) at 37°C and 5% CO_2. Series of images were taken by phase-contrast and fluorescence microscopy (DAPI filter) every 5 min for 24 h at ×40 magnification. Merging and inverting the look-up table (LUT) were done using ImageJ software (http://rsb.info.nih.gov/ij/). The movie was generated from the 289 modified pictures using iMovie software v8.0.6 (Apple, Inc.).

Virulence in mice. Outbred OF1 male mice (ages 6 to 8 weeks) (Charles Rivers Laboratories) were housed 7 per cage in our animal facilities and received food and water *ad libitum*. The inoculum was prepared in sterile saline from standard YPD culture. The *C. neoformans* cell suspension (10^5/mouse) was inoculated intravenously into 7 mice. Survival was recorded once daily until day 60 after inoculation. Animals about to die (unable to reach their food) were systematically euthanized by CO_2 inhalation. Animal studies were approved by the Institut Pasteur Animal Care Committee (03/144).

Real-time PCR. RNA extraction was performed on the s9-ClinCn isolates and H99 cells coincubated with J774 cells (intracellular condition [iH2]) or in fresh medium (baseline condition [BsH2]) for 2 h at 37°C in 5% CO_2. For iH2, J774 cells were washed twice with PBS, scraped, lysed in 2 ml 0.05% SDS–ice-cold water, and vortexed, and the pellet was collected after 3 min of centrifugation at 2,000 relative centrifugal force (RCF). RTL lysis buffer (500 μl; Qiagen) and 1:100 β-mercaptoethanol (Sigma) were added to the *C. neoformans* pellets. The suspensions were transferred to Ceramique Magna Lyser green bead tubes (Roche Diagnostics), homogenized three times with the Magna Lyser instrument (30 s at 7,000 rpm), and centrifuged (3 min at 10,000 RCF). RNA extraction was performed on 350 μl supernatant using the RNeasy minikit (Qiagen). RNAs were quantified and qualified using the Nanodrop spectrometer (ThermoFisher Scientific, Inc.).

cDNA was generated from Turbo DNase (Ambion)-treated RNA using the Transcriptor first-strand cDNA synthesis kit (Roche Diagnostics). Quantitative reverse transcription-PCR (RT-PCR) using 10 μl of LightCycler 480 SYBR green I master, 2 μl of cDNA, and specific primers (see Table S1 in the supplemental material) in a LightCycler 480 (Roche Diagnostics) consisted of a denaturation step at 95°C, 45 cycles of amplification (95°C for 5 s, 60°C for 5 s, and 72°C for 5 s). Each cDNA was analyzed in duplicate and normalized with the corresponding *GAPDH* gene expression (52) and was variable in different experimental conditions. Fold changes for each s9-ClinCn isolate (iH2 and BsH2 conditions) were assessed compared to H99 under the same conditions, according to Pfaffl (53). Two independent RNA extractions for each condition were analyzed blindly, and an internal calibrator consisting of an iH2 cDNA of H99 was used in each RT-PCR run as recommended (54).

Statistical analysis. Graph and Pearson's index (R^2) calculation, exact Fisher's test, and one-way analysis of variance (ANOVA) were performed using Prism 4.0 (GraphPad Software). Stata 10.0 software (Stata Corporation) was used to compare the ClinCn-macrophage interaction phenotypes with clinical outcome for the corresponding patients. For the multivariate analysis, logistic regression was used to determine factors independently associated with nonsterilization of CSF at week 2 (45 patients with available information). Only two variables were entered in the model because of the limited number of events ($n = 24$). Odds ratios (ORs) and their 95% confidence intervals (95% CIs) were determined.

Schematic representation of fold changes was performed using the open-source genomic analysis software MeV v4.6.1 (The TM4 Development Group) obtained from http://mev.tm4.org (55). Complete linkage clustering and Pearson's correlation were chosen to perform hierarchical clustering. The principal component analysis (PCA) was performed based on three interaction parameters (PI, IPH2, and IPH48) and five mycological parameters (cell and capsule size, E1 binding, growth, and chitin content) using MeV v4.6.1 (Manhattan distance, mean centering mode, and 10 neighbors for KNN imputation). Variables were compared using the Student *t* test. *P* values of ≤0.05 were considered significant.

ACKNOWLEDGMENTS

We thank Frederique Vernel-Pauillac and Dea Garcia-Hermoso (Molecular Mycology Unit) for the experimental infections, Emmanuel Perret (Imagopole) for expertise in dynamic imaging, and Laure Diancourt (Genotyping and Public Health Facility) for the MLST.

A.A. is a recipient of a "Poste d'Accueil CNRS-CEA/APHP." This work was supported by Institut Pasteur. The authors have no conflicts of interest.

SUPPLEMENTAL MATERIAL

Supplemental material for this article may be found at http://mbio.asm.org/lookup/suppl/doi:10.1128/mBio.00158-11/-/DCSupplemental.

Figure S1, PDF file, 0.943 MB.

Figure S2, PDF file, 0.881 MB.

Figure S3, PDF file, 0.866 MB.
Figure S4, PDF file, 0.844 MB.
Figure S5, PDF file, 0.903 MB.
Figure S6, PDF file, 0.792 MB.
Figure S7, PDF file, 0.807 MB.
Figure S8, PDF file, 0.830 MB.
Table S1, DOC file, 0.05 MB.
Movie S1, MOV file, 6.458 MB.

REFERENCES

1. **Park BJ, et al.** 2009. Estimation of the current global burden of cryptococcal meningitis among persons living with HIV/AIDS. AIDS **23**: 525–530.
2. **Casadevall A, Perfect J.** 1998. Cryptococcus neoformans, p. 407–456. ASM Press, Washington, DC.
3. **Dromer F, Mathoulin-Pélissier S, Launay O, Lortholary O, Cryptococcosis Study Group, French.** 2007. Determinants of disease presentation and outcome during cryptococcosis: the CryptoA/D study. Plos Med **4**:e21.
4. **Hsueh Y, Lin X, Kwon-Chung K, Heitman J.** 2010. Sexual reproduction of *Cryptococcus*, p. 81–96. In Heitman J, Kozel TR, Kwon-Chung KJ, Perfect JR, Casadevall A (ed), Cryptococcus: from human pathogen to model yeast. ASM Press, Washington, DC.
5. **Lin X, Heitman J.** 2006. The biology of the *Cryptococcus neoformans* species complex. Annu. Rev. Microbiol. **60**:69–105.
6. **Desnos-Ollivier M, et al.** 2010. Mixed infections and *in vivo* evolution in the human fungal pathogen *Cryptococcus neoformans*. mBio **1**(1):e00091-10.
7. **Feldmesser M, Kress Y, Novikoff P, Casadevall A.** 2000. *Cryptococcus neoformans* is a facultative intracellular pathogen in murine pulmonary infection. Infect. Immun. **68**:4225–4237.
8. **Charlier C, et al.** 2009. Evidence of a role for monocytes in dissemination and brain invasion by *Cryptococcus neoformans*. Infect. Immun. **77**: 120–127.
9. **Chrétien F, et al.** 2002. Pathogenesis of cerebral *Cryptococcus neoformans* infection after fungemia. J. Infect. Dis. **186**:522–530.
10. **Bliska JB, Casadevall A.** 2009. Intracellular pathogenic bacteria and fungi—a case of convergent evolution? Nat. Rev. Microbiol. **7**:165–171.
11. **Del Poeta M.** 2004. Role of phagocytosis in the virulence of *Cryptococcus neoformans*. Eukaryot. Cell **3**:1067–1075.
12. **Santangelo R, et al.** 2004. Role of extracellular phospholipases and mononuclear phagocytes in dissemination of cryptococcosis in a murine model. Infect. Immun. **72**:2229–2239.
13. **Ma H, et al.** 2009. The fatal fungal outbreak on Vancouver Island is characterized by enhanced intracellular parasitism driven by mitochondrial regulation. Proc. Natl. Acad. Sci. U. S. A. **106**:12980–12985.
14. **Luo Y, Alvarez M, Xia L, Casadevall A.** 2008. The outcome of phagocytic cell division with infectious cargo depends on single phagosome formation. PLoS One **3**:e3219.
15. **Cox GM, et al.** 2001. Extracellular phospholipase activity is a virulence factor for *Cryptococcus neoformans*. Mol. Microbiol. **39**:166–175.
16. **Cox GM, Mukherjee J, Cole GT, Casadevall A, Perfect JR.** 2000. Urease as a virulence factor in experimental cryptococcosis. Infect. Immun. **68**: 443–448.
17. **Williamson PR.** 1997. Laccase and melanin in the pathogenesis of *Cryptococcus neoformans*. Front. Biosci. **2**:e99–e107.
18. **Panepinto J, et al.** 2005. The DEAD-box RNA helicase Vad1 regulates multiple virulence-associated genes in *Cryptococcus neoformans*. J. Clin. Invest. **115**:632–641.
19. **Luberto C, et al.** 2001. Roles for inositol-phosphoryl ceramide synthase 1 (IPC1) in pathogenesis of *C. neoformans*. Genes Dev. **15**:201–212.
20. **Luberto C, et al.** 2003. Identification of App1 as a regulator of phagocytosis and virulence of *Cryptococcus neoformans*. J. Clin. Invest. **112**: 1080–1094.
21. **Toffaletti DL, Del Poeta M, Rude TH, Dietrich F, Perfect JR.** 2003. Regulation of cytochrome c oxidase subunit 1 (COX1) expression in *Cryptococcus neoformans* by temperature and host environment. Microbiology **149**:1041–1049.
22. **Steenbergen JN, Shuman HA, Casadevall A.** 2001. *Cryptococcus neoformans* interactions with amoebae suggest an explanation for its virulence and intracellular pathogenic strategy in macrophages. Proc. Natl. Acad. Sci. U. S. A. **98**:15245–15250.
23. **Chrisman CJ, Alvarez M, Casadevall A.** 2010. Phagocytosis of *Cryptococcus neoformans* by, and nonlytic exocytosis from, *Acanthamoeba castellanii*. Appl. Environ. Microbiol. **76**:6056–6062.
24. **Fries BC, Taborda CP, Serfass E, Casadevall A.** 2001. Phenotypic switching of *Cryptococcus neoformans* occurs *in vivo* and influences the outcome of infection. J. Clin. Invest. **108**:1639–1648.
25. **Moore R.** 1998.Cytology and ultrastructure of yeasts and yeastlike fungi, p. 33–44. In Kurtzman CP, Fell JW (ed), The yeasts, a taxonomic study. Elsevier, Philadelphia, PA.
26. **Cassone A, Simonetti N, Strippoli V.** 1974. Wall structure and bud formation in *Cryptococcus neoformans*. Arch. Microbiol. **95**:205–212.
27. **Simmons R.** 1989. Comparison of chitin localization in *Saccharomyces cerevisiae*, *Cryptococcus neoformans* and *Malassezia* spp. Mycol. Res. **94**: 551–553.
28. **Gilbert N, Lodge J, Specht C.** 2010. The cell wall of *Cryptococcus*, p. 67–80. In Heitman J, Kozel TR, Kwon-Chung KJ, Perfect JR, Casadevall A (ed),Cryptococcus: from human pathogen to model yeast. ASM Press, Washington, DC.
29. **Lyons AB, Parish CR.** 1994. Determination of lymphocyte division by flow cytometry. J. Immunol. Methods **171**:131–137.
30. **Kozel TR, Pfrommer GS, Guerlain AS, Highison BA, Highison GJ.** 1988. Strain variation in phagocytosis of *Cryptococcus neoformans*: dissociation of susceptibility to phagocytosis from activation and binding of opsonic fragments of C3. Infect. Immun. **56**:2794–2800.
31. **Rosowski EE, et al.** 2011. Strain-specific activation of the NF-kappaB pathway by GRA15, a novel *Toxoplasma gondii* dense granule protein. J. Exp. Med. **208**:195–212.
32. **Kébaïer C, Louzir H, Chenik M, Ben Salah A, Dellagi K.** 2001. Heterogeneity of wild *Leishmania major* isolates in experimental murine pathogenicity and specific immune response. Infect. Immun. **69**:4906–4915.
33. **Holzmuller P, et al.** 2008. Virulence and pathogenicity patterns of *Trypanosoma brucei gambiense* field isolates in experimentally infected mouse: differences in host immune response modulation by secretome and proteomics. Microbes Infect. **10**:79–86.
34. **Lobo C-A, et al.** 2004. Invasion profiles of Brazilian field isolates of *Plasmodium falciparum*: phenotypic and genotypic analyses. Infect. Immun. **72**:5886–5891.
35. **MacCallum DM, et al.** 2009. Property differences among the four major *Candida albicans* strain clades. Eukaryot. Cell **8**:373–387.
36. **Dromer F, Casadevall A, Perfect J, Sorrell T.** 2010. *Cryptococcus neoformans*: latency and disease, p. 429–430. In Heitman J, Kozel TR, Kwon-Chung KJ, Perfect JR, Casadevall A (ed),Cryptococcus: from human pathogen to model yeast. ASM Press, Washington, DC.
37. **Shi M, et al.** 2010. Real-time imaging of trapping and urease-dependent transmigration of *Cryptococcus neoformans* in mouse brain. J. Clin. Invest. **120**:1683–1693.
38. **Casadevall A.** 2010. Cryptococci at the brain gate: break and enter or use a Trojan horse? J. Clin. Invest. **120**:1389–1392.
39. **Macura N, Zhang T, Casadevall A.** 2007. Dependence of macrophage phagocytic efficacy on antibody concentration. Infect. Immun. **75**: 1904–1915.
40. **Levitz SM.** 2010. Innate recognition of fungal cell walls. PLoS Pathog. **6**:e1000758.
41. **Chun CD, Brown JCS, Madhani HD.** 2011. A major role for capsule-independent phagocytosis-inhibitory mechanisms in mammalian infection by *Cryptococcus neoformans*. Cell Host Microbe **9**:243–251.
42. **Casadevall A, Steenbergen JN, Nosanchuk JD.** 2003. "Ready made" virulence and "dual use" virulence factors in pathogenic environmental fungi—the *Cryptococcus neoformans* paradigm. Curr. Opin. Microbiol. **6**:332–337.
43. **Hu G, Cheng P-Y, Sham A, Perfect JR, Kronstad JW.** 2008. Metabolic adaptation in *Cryptococcus neoformans* during early murine pulmonary infection. Mol. Microbiol. **69**:1456–1475.
44. **Liu X, Hu G, Panepinto J, Williamson PR.** 2006. Role of a VPS41 homologue in starvation response, intracellular survival and virulence of *Cryptococcus neoformans*. Mol. Microbiol. **61**:1132–1146.
45. **Hu G, et al.** 2008. PI3K signaling of autophagy is required for starvation tolerance and virulence of *Cryptococcus neoformans*. J. Clin. Invest. **118**: 1186–1197.
46. **Stano P, et al.** 2009. App1: an antiphagocytic protein that binds to complement receptors 3 and 2. J. Immunol. **182**:84–91.
47. **Dromer F, Salamero J, Contrepois A, Carbon C, Yeni P.** 1987. Production, characterization, and antibody specificity of a mouse monoclonal antibody reactive with *Cryptococcus neoformans* capsular polysaccharide. Infect. Immun. **55**:742–748.

48. **Meyer W, et al.** 2009. Consensus multi-locus sequence typing scheme for *Cryptococcus neoformans* and *Cryptococcus gattii*. Med. Mycol. **47**: 561–570.
49. **Kwon-Chung K, Bennett J (ed).** 1992. Medical mycology, p. 816–826. Lippincott Williams & Wilkins, Philadelphia, PA.
50. **Fan W, Kraus PR, Boily M-J, Heitman J.** 2005. *Cryptococcus neoformans* gene expression during murine macrophage infection. Eukaryot. Cell **4**:1420–1433.
51. **Xue C, Tada Y, Dong X, Heitman J.** 2007. The human fungal pathogen *Cryptococcus* can complete its sexual cycle during a pathogenic association with plants. Cell Host Microbe **1**:263–273.
52. **Xue C, et al.** 2010. Role of an expanded inositol transporter repertoire in *Cryptococcus neoformans* sexual reproduction and virulence. mBio **1**(1): e00084-10.
53. **Pfaffl MW.** 2001. A new mathematical model for relative quantification in real-time RT-PCR. Nucleic Acids Res. **29**:e45.
54. **Hellemans J, Mortier G, de Paepe A, Speleman F, Vandesompele J.** 2007. qBase relative quantification framework and software for management and automated analysis of real-time quantitative PCR data. Genome Biol. **8**:R19.
55. **Saeed AI, et al.** 2003. TM4: a free, open-source system for microarray data management and analysis. Biotechniques **34**:374–378.

4. Commentary: 'Dynamic virulence: real-time assessment of intracellular pathogenesis links *Cryptococcus neoformans* phenotype with clinical outcome', Mansour et al., mBio 2011

Dynamic Virulence: Real-Time Assessment of Intracellular Pathogenesis Links *Cryptococcus neoformans* Phenotype with Clinical Outcome

Michael K. Mansour,[a] Jatin M. Vyas,[a] and Stuart M. Levitz[b]

Department of Medicine, Division of Infectious Diseases, Massachusetts General Hospital, Boston, Massachusetts, USA,[a] and Department of Medicine, Division of Infectious Diseases and Immunology, University of Massachusetts Medical Center, Worcester, Massachusetts, USA[b]

ABSTRACT While a myriad of studies have examined host factors that predispose persons to infection with the opportunistic fungal pathogen *Cryptococcus neoformans*, comparatively little has been done to examine how virulence factor differences among cryptococcal isolates may impact outcome. In the recent report by Alanio et al. (A. Alanio, M. Desnos-Ollivier, and F. Dromer, mBio 2:e00158-11, 2011), novel flow cytometry-based techniques were employed to demonstrate an association between the phenotype of *C. neoformans*-macrophage interactions, as measured by phagocytosis and intracellular replication, and patient outcomes, as determined by positive cultures on therapy and survival. These experiments establish that the prognosis of patients with cryptococcosis is influenced by the phenotypic properties of the infecting fungal isolate.

Cryptococcus neoformans is an encapsulated opportunistic yeast which is responsible for approximately 1 million infections and over 600,000 deaths per year worldwide (1). The patient populations most affected are those with adaptive immunity dysfunction, specifically T-cell defects. Individuals suffering from AIDS or lymphoma or recipients of chronic immunosuppressive medication are at highest risk for developing cryptococcal infection (2). *C. neoformans* is ubiquitous, but a higher rate of infection is observed in sub-Saharan countries, which suggests that either there are host factors that result in a more susceptible phenotype or there are differences in the virulence of the fungal strains found in these niches. More recently, hypervirulent strains of the closely related species *Cryptococcus gattii* have caused epidemic infections in predominantly immunocompetent individuals (3).

C. neoformans can exist as a haploid or diploid organism and divides using either an asexual budding cycle or a sexual stage with conidial forms. *Cryptococcus* has a complete and intact life cycle in the environment but has clearly found a niche as a mammalian pathogen. The ability of *C. neoformans* to survive in the human phagocyte may have evolved through the interactions of the fungal cells with free-living amoebae (4).

Exposure to *C. neoformans* is thought to typically occur following inhalation of airborne organisms. Once the organisms are in the lungs, professional phagocyte populations (e.g., dendritic cells, macrophages, and polymorphonuclear leukocytes) clear the majority of the organism burden and potently influence the nature and outcome of adaptive immune responses. The strong association of $CD4^+$ T-cell depletion or dysfunction with cryptococcosis is testimony to the particular importance of this immune cell to cryptococcal host defenses. For these reasons, studies aimed at understanding the interaction between professional antigen-presenting cells such as macrophages and *Cryptococcus* will help define the steps leading to lasting immunity and correlate clinical outcome.

In a recent issue of *mBio*, Alanio et al. (5) show that the interaction of *Cryptococcus* with host innate immunity is more complex than previously thought. Using a large panel of *C. neoformans* organisms isolated from cerebrospinal fluid (CSF) of patients with cryptococcal meningoencephalitis, clinical outcome was shown to rely not only on host immune factors but also on specific virulence properties of the organism. To accomplish this task, Alanio et al. (5) devised an ingenious flow cytometry-based standardized macrophage assay that allowed quantification of both *C. neoformans* phagocytosis and intracellular replication. Using a reference strain and a macrophage-like cell line, indices were then generated reflecting rates of phagocytosis and intracellular proliferation. Remarkably, based on these two metrics, the authors were able to segregate the cryptococcal isolates into distinct macrophage phenotypes that correlated with clinical and microbiological outcomes (Fig. 1). Patients with isolates that had both a high phagocytic index and high intracellular proliferation experienced a 5-fold-increased risk of death. On the other hand, patients with isolates exhibiting both a low phagocytic index and low intracellular proliferation had a 15-fold-increased risk of having positive CSF cultures after 2 weeks of antifungal therapy. Interestingly, phenotypic characteristics that have been associated with virulence in animal studies (including capsule size, growth rate, chitin content, and urease and laccase activities) did not correlate with clinical outcome.

It is important to remember that because all the isolates in the study by Alanio et al. (5) came from patients who had cryptococcal meningitis, they possess some degree of virulence. Thus, rather than looking at virulence in the traditional sense, the authors have taken a fresh approach by looking at how the interaction of *C. neoformans* with macrophages *in vitro* correlates with outcomes in patients who are already infected and receiving antifungal drugs. The results suggest that a dynamic interplay between host innate cells and *Cryptococcus* continues well after phagocytosis. In support of this concept, Alanio et al. (5) also demonstrated that *Cryp-*

Published 27 September 2011

Citation Mansour MK, Vyas JM, Levitz SM. 2011. Dynamic virulence: real-time assessment of intracellular pathogenesis links *Cryptococcus neoformans* phenotype with clinical outcome. mBio 2(5):e00217-11. doi:10.1128/mBio.00217-11.

Address correspondence to Stuart M. Levitz, stuart.levitz@umassmed.edu.

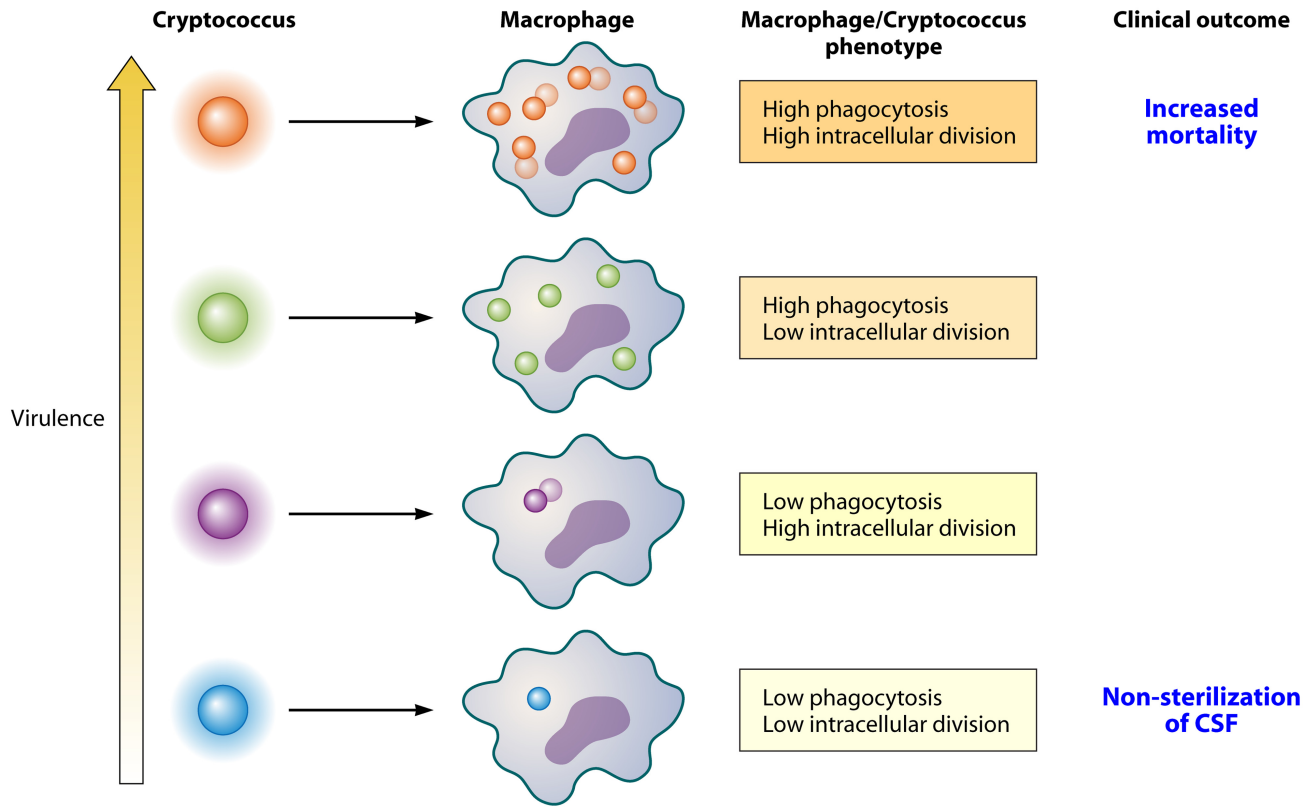

FIG 1 The intrinsic virulence of clinical isolates of *Cryptococcus neoformans* was assessed by flow cytometry following interaction with macrophages. Patients with isolates that had high phagocytic indices and increased cellular division had significantly increased mortality at 3 months. Conversely, patients with isolates exhibiting low phagocytic indices and reduced cellular division were more likely to fail to sterilize their cerebrospinal fluid at 2 weeks.

tococcus changes its gene expression profile within the macrophage phagolysosome.

Similarly to other intracellular pathogens, *C. neoformans* undergoes phenotypic and perhaps genotypic change as it adapts to life within the cell. One implication of the work of Alanio et al. (5) is that these intracellular changes have significant clinical ramifications. The receptor-ligand interactions leading to phagocytosis, antifungal activity, and cytokine responses have been well characterized (6). However, we are just beginning to understand the subsequent intracellular events occurring in the phagolysosomal compartment and the consequences of these events. It is clear that this period is not quiescent, and evidence is mounting that there is continued sampling of the pathogens by the innate immune cell. Recent studies have shown that the toll-like receptors (TLR), such as TLR 9, continue to engage the fungal phagolysosome well beyond the initial surface events leading to phagocytosis (7). Data also suggest that the fungal surface evolves within the phagosomal compartment, presenting new and distinct antigens. This fact was highlighted in a study of *Aspergillus fumigatus* conidia and hyphae where each morphotype was found to elicit a unique immune response (8).

How can we frame these data? The study by Alanio et al. (5) suggests that fungal pathogenesis is dependent not only on host response but also on the dynamic adaptations by the pathogen. Other studies have also supported fungus-specific intracellular virulence factors. *C. gattii* isolated from the Vancouver Island outbreak has enhanced intracellular survival and proliferation in macrophages. In this example, microarray analysis identified the majority of the gene expression differences, as compared to control, to be centered on mitochondrial genes, which are thought to promote a better-fit state of survival in a phagolysosome (9). Our ability to understand how fungi sense and adapt to intracellular compartments will be important for deciphering the nature of the host-pathogen interaction. In order to answer these questions, new techniques will need to be developed to assess the activities within the phagosomal compartments of professional phagocytes. The work by Alanio et al. (5) is an excellent example of the ingenuity required to advance the field of fungal pathogenesis. Moreover, the authors' successful ability to correlate the macrophage phenotype of clinical isolates with patient outcomes has "to-the-bedside" implications. In the future, therapy for cryptococcosis may very well be individualized based on the phenotypic and genotypic characteristics of both the host and pathogen.

ACKNOWLEDGMENTS

M.K.M. is supported by NIAID, NIH (T32-AI007061-34), and in part by internal funds from the MGH Department of Medicine. J.M.V. is supported by NIAID, NIH (1R01AI092084-01A1), and S.M.L. is supported by NIAID, NIH (5R01AI025780-26 and 1R21AI093302-01).

REFERENCES

1. **Park BJ, et al.** 2009. Estimation of the current global burden of cryptococcal meningitis among persons living with HIV/AIDS. AIDS **23**:525–530.
2. **Perfect JR, et al.** 2010. Clinical practice guidelines for the management of

cryptococcal disease: 2010 update by the Infectious Diseases Society of America. Clin. Infect. Dis. **50**:291–322.
3. **Kidd SE, et al.** 2004. A rare genotype of *Cryptococcus gattii* caused the cryptococcosis outbreak on Vancouver Island (British Columbia, Canada). Proc. Natl. Acad. Sci. U. S. A. **101**:17258–17263.
4. **Steenbergen JN, Shuman HA, Casadevall A.** 2001. *Cryptococcus neoformans* interactions with amoebae suggest an explanation for its virulence and intracellular pathogenic strategy in macrophages. Proc. Natl. Acad. Sci. U. S. A. **98**:15245–15250.
5. **Alanio A, Desnos-Ollivier M, Dromer F.** 2011. Dynamics of *Cryptococcus neoformans*-macrophage interactions reveal that fungal background influences outcome during cryptococcal meningoencephalitis in humans. mBio **2**:e00158-11.
6. **Levitz SM.** 2010. Innate recognition of fungal cell walls. PLoS Pathog. **6**:e1000758.
7. **Kasperkovitz PV, Cardenas ML, Vyas JM.** 2010. TLR9 is actively recruited to *Aspergillus fumigatus* phagosomes and requires the N-terminal proteolytic cleavage domain for proper intracellular trafficking. J. Immunol. **185**: 7614–7622.
8. **Bozza S, et al.** 2002. Dendritic cells transport conidia and hyphae of *Aspergillus fumigatus* from the airways to the draining lymph nodes and initiate disparate Th responses to the fungus. J. Immunol. **168**: 1362–1371.
9. **Ma H, et al.** 2009. The fatal fungal outbreak on Vancouver Island is characterized by enhanced intracellular parasitism driven by mitochondrial regulation. Proc. Natl. Acad. Sci. U. S. A. **106**:12980–12985.

Abstract

Cryptococcosis is an opportunistic infection due to the ubiquitous yeast *Cryptococcus neoformans*. This pathogen is a facultative intracellular organism. Interaction with immune cells including monocytes/macrophages lineage and dendritic cells are of major importance in the natural history of the infection. In humans, the pathophysiology of the infection evolves in three steps (i) primoinfection in childhood, (ii) dormancy, demonstrated from epidemiological and genotypic data in the lab few years ago (Garcia-Hermoso et al. 1999), (iii) reactivation upon immunosuppression. In terms of disease, clinical presentation and outcome of cryptococcosis are known to be diverse among individuals even those sharing the same underlying diseases.

To address the question of the impact of fungal diversity on the natural course of the infection at the macrophage-level (standardized model of yeasts/J774 macrophages in vitro interaction), murine model-level (murine model of cryptococcosis in OF1 outbred mice) and human-level (CryptoA/D database), we studied (i) the diversity of *C. neoformans*/macrophages interactions using well characterized clinical isolates (ii) the correlation between in vitro phenotype of the isolate and clinical outcome in humans (iii) the diversity of adaptation to the host. We developed new assays and new tools using flow cytometry (quantitative flow cytometry, multispectral imaging flow cytometry, sorting), microscopy (dynamic imaging), gene expression analysis (single-cell quantitative real time PCR) to overcome technical issues.

We found high variation in phagocytic, 2 hours-, 48hours-intracellular proliferation indexes among the 54 ClinCn compared to H99. No correlation with the genotype was observed. The lack of sterilization at week 2 despite active antifungal therapy was significantly associated with a lower phagocytic index, whereas treatment failure at month 3 and death from cryptococcosis were significantly related to a higher 2 hours-intracellular proliferation. Among 9 selected clinical isolates compared to H99, (i) the virulence in mice was significantly different, intracellular expression of some virulence factors correlated with (ii) intracellular proliferation and (iii) phagocytic indexes. With a focus on multiplication and stress response and considering the H99 reference strain, we observed the appearance of various populations of yeasts during mice and macrophage infections. After sorting yeasts populations, we observed that a specific one was less prone and dependent of serum to grow compared to the other populations. Gene expression analysis revealed that this population had specific metabolic characteristics that could reflect dormancy.

We found a high diversity of *C. neoformans* upon interaction with macrophages considering 54 clinical isolates in correlation with clinical outcome in humans, but also a considerable adaptation to host in our two models considering the reference strains H99. We observed also even more diversity of fungal adaptation to host when clinical isolates were considered. All together, these data suggest that cryptococcosis and fungal disease in general could be more complex diseases since diversity, plasticity and adaptation of the fungal organism to hosts is high and heterogeneous.